THÈSE

En vue de l'obtention du

DOCTORAT DE L'UNIVERSITÉ DE TOULOUSE

Délivré par :

Institut National Polytechnique de Toulouse (INP Toulouse)

Discipline ou spécialité :

Génie Électrique

Présentée et soutenue par :

M. TIANYI LIU

le vendredi 15 décembre 2017

Titre :

Control strategy for a mono-inverter multi-PMSM system - Stability and efficiency

---

Ecole doctorale :

Génie Electrique, Electronique, Télécommunications (GEET)

Unité de recherche :

Laboratoire Plasma et Conversion d'Energie (LAPLACE)

Directeur(s) de Thèse :

M. MAURICE FADEL

Rapporteurs :

M. DEMBA DIALLO, UNIVERSITE PARIS 11

M. MICKAEL HILAIRET, UNIVERSITE DE FRANCHE COMTE

Membre(s) du jury :

M. GEORGES BARAKAT, UNIVERSITE DU HAVRE, Président

M. GAEL PONS, MIDI INGENIERIE, Membre

M. MAURICE FADEL, INP TOULOUSE, Membre

Mme MARIA PIETRZAK-DAVID, INP TOULOUSE, Membre

Abstract

During these decades, Permanent Magnet Synchronous Motor (PMSM) has become a vital part of military, industry and civil applications due to the advantages of high power density, high efficiency, high reliability and simple structure, small volume and light weight. Sometimes, multiple PMSMs are used to carry out cooperative functions. For example, the bogie of a locomotive, the flight control surface of an airplane. These PMSMs usually operates at the same speed. To reduce the volume and weight, an idea of sharing the static power conversion devices, which is called Mono-Inverter Multi-PMSM system (MIMPMSM), is raised. Although many researchers have given different controller solutions for the MIMPMSM system, most of them are not clear in the aspects of system stability and efficiency issues. This has become the biggest obstacle to the practical use of MIMPMSM.

Oriented with these problems, starting with a MIMPMSM system with 2 motors, in the first step, we have tested some control strategies by an experiment to verify the feasibility and performance of them. In final, based on the experiment data, we have figured that the over-constraint problem exists in some control strategies. Then, an analysis and controller design based on steady-state model of a Mono-Inverter Dual-PMSM (MIDPMSM) system are carried out. By studying the solution existence problem of the steady-state model, we give out the design guideline to the controller structure. Combining the open-loop stability and steady-state solution, the region of controllability and stability is obtained. Lagrange Multiplier is used develop the expression of efficiency-optimal steady-state related to torque and speed. The experiment has shown that the efficiency of the new controller has improved significantly.

Meanwhile, we have explored the influence of parameter variation in system stability and efficiency-optimization. The variation will influence the stability region. But its influence can be eliminated by using Master-Slave strategy. On the other hand, in the aspect of efficiency optimization, the simulation results have shown that parameter mismatch, especially the permeant flux, can cause high efficiency loss.

In the last step, this controller is also adapted to a MIMPMSM system with more than two motors. The simulation results demonstrate the effectiveness.

Key Words:

- Multi-motor system
- Shared structure
- Permanent Magnet Synchronous Motor
- Efficiency
- Stability

Résumé

Durant ces dernières décennies, le moteur synchrone à aimants permanents (MSAP) est devenu un actionneur essentiel pour les applications militaires, industrielles et civiles grâce à ses avantages de haute densité de puissance, de rendement élevé, de grande fiabilité avec une structure simple, un faible volume et un poids réduit. Parfois, plusieurs MSAP sont utilisés pour effectuer des tâches coopératives. Par exemple le boggie d'une locomotive ou encore les surfaces de vol d'un avion. Ces MSAP fonctionnent généralement à la même vitesse. Pour réduire le volume et le poids, une idée de mutualisation des dispositifs de conversion statique, appelée système Multi-MSAP Mono-Convertisseur (MIMSAPMC), est proposée. Bien que de nombreux chercheurs aient déjà proposé différentes solutions de contrôle pour le système MIMSAPMC, la plupart d'entre eux ne garantissent pas la stabilité et l'efficacité énergétique du système. Ceci est devenu le plus grand obstacle à l'utilisation pratique du MIMSAPMC.

A cet effet et en commençant par un système MIMSAPMC avec 2 moteurs nous avons testé expérimentalement quelques stratégies de commande pour en vérifier la faisabilité et les performances. Sur la base des données mesurées, nous avons constaté que le problème de sur-contraintes existe dans certaines stratégies de contrôle. Ensuite, la synthèse d'une commande basée sur un modèle en régime permanent d'un système MIMSAPMC est réalisée. En étudiant le problème d'existence du régime permanent, nous formulons une procédure de conception de la structure de la loi de commande. En combinant la stabilité en boucle ouverte et la solution en régime permanent, nous définissons alors la région de contrôlabilité et de stabilité. La méthode des multiplieurs de Lagrange est ensuite utilisée pour formuler l'expression de l'état d'équilibre optimal en fonction du couple et de la vitesse. L'expérience a montré que l'efficacité avec cette nouvelle loi de commande s'est considérablement améliorée.

Dans le même temps, nous avons exploré l'influence de la variation des paramètres pour la stabilité du système et pour l'optimisation de l'efficacité. Ainsi, nous montrons que la variation paramétrique influence la zone de stabilité. Mais son influence peut être éliminée en utilisant la stratégie Maitre-Esclave. Par ailleurs, en ce qui concerne l'optimisation de l'efficacité énergétique, les résultats de simulation ont montré que la non-concordance des paramètres, en particulier le flux de l'aimant, peut entraîner une perte d'efficacité élevée.

Dans la dernière étape, ce contrôleur est également adapté à un système MIMSAPMC avec un nombre de moteurs supérieurs à 2. Les résultats de la simulation démontrent alors l'efficacité de la proposition.

Mots Clés:

- Système Multimachine
- Mutualisation
- Machine Synchrone à Aimant
- Efficacité énergétique
- Stabilité

Acknowledgements

The works presented in this thesis have been realized in **LAboratoire PLAsma et Conversion d'Energie** (LAPLACE) in **Nationale Supérieure d'Electrotechnique, d'Electronique, d'Informatique, d'Hydraulique et des Télécommunications** (ENSEEIHT) of the **Institut National Polytechnique de Toulouse** within the group COmmande et DIAgnostic des Systèmes Electriques (CODIASE).

I would first thank the China Scholarship Council (CSC), who has given the financial support to me during the Phd studying so that I have the possibility to come to France to realize my Phd study.

I wish to express my deep gratitude to my supervisor, Prof. Maurice FADEL, for the confidence, guidance, encouragement and suppor he has given me, even in the most tough times, during all these years of thesis. His knowledge and experience have given me great help in my research and have made me avoid many detours.

I would like to thank Professor Maria DAVID for her critical support in administrative issue of the Universite de Toulouse and Doctoral school.

I am also grateful to Dr. Abdelkader BOUARFA for his kind advices and significant help for the research and the writing of the thesis.

And last, but most importantly, I'm very deeply indebted to my family for bearing with me during these years of studying.

List of symbols

N	Number of motors
M_k	Motor with the index k, $1 \leq k \leq N$
ω_e	Electrical speed of motor (rad/s)
ω_{eM_k}	Electrical speed of the motor k (rad/s)
ω_m	Mechanical speed of motor (rad/s)
ω_{mM_k}	Mechanical speed of the motor k (rad/s)
T_e	Electromagnetic torque (N.M.)
T_{eM_k}	Electromagnetic torque of the motor k(N.M.)
P_m	Mechanical power of motor (W)
N_p	Number of poles of stator
φ_p	Permanent magnet flux (Wb)
L_s	Inductance of stator's coil (H)
R_s	Stator resistance (Ω)
I_d	d-axis stator current in d-q frame (A)
I_{dM_k}	d-axis stator current of motor k (A)
I_q	q-axis stator current in d-q frame (A)
I_{qM_k}	q-axis stator current of motor k (A)
$\overrightarrow{I_{dq}}$	Stator current vector in d-q frame (A)
$\overrightarrow{\varphi_{dq}}$	Rotor flux vector in d-q frame (A)
θ_e	Electrical angle of the rotor in $\alpha - \beta$ frame (rad)
θ_{eM_k}	Electrical angle of motor k (rad)
θ_d	Electrical angle difference between motor 1 and motor 2 (rad)
$\theta_d^{M_1,M_k}$	Electrical angle difference between motor 1 and motor k (rad)
V_{abc}	Three phase voltage of a motor (A)
I_{abc}	Three phase current of a motor (A)

V_p	Peak phase voltage (V)
I_p	Peak phase current (A)
V_O	Voltage of the reference point O (V)
V_N	Voltage of the neutral point N (V)
V_{AN}, V_{BN}, V_{CN}	Phase voltage of phase A, B, C (V)
V_{AO}, V_{BO}, V_{CO}	Voltage between line and reference point O (V)
V_{DC}	DC bus voltage (V)
ΔV_{DC}	Voltage offset of the DC bus (V)
V_α, V_β	Voltage components in α-β frame (V)
φ	Power factor angle (rad)
S_A, S_B, S_C	Switch state of the legs A B C of a 2-level 3-phase inverter
T_s	Sampling time interval
$\mathbb{M}$	A set representing all machines involved in a MIMPMSM system

List of abbreviations

BLDC	Brushless DC
BLAC	Brushless AC
DTC	Direct Torque Control
FCS-MPC	Finite Control Set-Model Predictive Control
IGBT	Insulated-Gate Bipolar Transistor
IM	Induction Machine
IPMSM	Interior mounted PMSM
MTPA	Maximum Torque Per Ampere
MPC	Model Predictive Control
MIMPMSM	Mono-Inverter Multi-PMSM
MIDPMSM	Mono-Inverter Dual-PMSM
MIMO	Multi-Input Multi-Output
PM	Permanent Magnet
PMSM	Permanent Magnet Synchronous Machine
OPTC	Optimal Predictive Torque Control
PTC	Predictive Torque Control
PTCSS	Predictive Torque Control Split & Seek
SVPWM	Space Vector Pulse Width Modulation
SPMSM	Surface mounted PMSM

List of publication

1. T. LIU and M. FADEL, "**An Efficiency-Optimal Control Method for Mono-Inverter Dual-PMSM Systems**," in *IEEE Transactions on Industry Applications*, vol. PP, no. 99, pp. 1-1.
2. Tianyi liu, Maurice fadel, **A Controller Proposed for Mono-Inverter Multiple-PMSM system**, In IFAC-PapersOnLine, Volume 50, Issue 1, 2017, Pages 14800-14805, ISSN 2405-8963
3. T. Liu and M. Fadel, "**An efficiency optimizing controller design method for Mono-Inverter Dual-PMSM system**," 2016 IEEE International Conference on Power Electronics, Drives and Energy Systems (PEDES), Trivandrum, 2016, pp. 1-6.
4. T. Liu and M. Fadel, "**Performance comparison of control strategies for mono-inverter Dual-PMSM system**," 2016 IEEE International Power Electronics and Motion Control Conference (PEMC), Varna, 2016, pp. 637-642.
5. T. Liu and M. Fadel, "**Comparative study of different predictive torque control strategies for mono-inverter dual-PMSM system**," 2016 18th Mediterranean Electrotechnical Conference (MELECON), Lemesos, 2016, pp. 1-6.

Résumé en français

Au cours de ces dernières décennies, la machine électrique est devenue un élément essentiel pour les applications militaires, industrielles et civiles en tant qu'actionneur ou encore pour la génération d'énergie. Avec le développement technologique actuel, plusieurs types de machines deviennent candidates comme la machine à courant continu (MCC), la machine asynchrone (MAS), la machine synchrone (MS) ou la machine à réluctance (MRV) …. Parmi celles-ci, la machine synchrone à aimants permanents (MSAP) est attractive en raison de sa forte densité de puissance (faible volume et faible poids), de son rendement élevé, de sa grande fiabilité associée à une simplicité structurelle native. Elle constitue ainsi un actionneur à hautes performances et de par son fonctionnement la MSAP surpasse les défauts congénitaux de la MCC en utilisant un convertisseur statique pour alimenter le stator au lieu d'un collecteur pour atteindre le rotor. Le bénéfice se trouve aussi sur le plan thermique car les pertes Joule se trouvent alors en périphérie de la machine ce qui facilite le refroidissement. Par conséquent, la MSAP bénéficie de la simplicité de commande de la MCC et des performances augmentées liées au fait que le flux est structurellement installé au rotor par l'aimant permanent. Par rapport à la MAS, il n'y a pas de courant dans le rotor, ce qui fait que la MSAP a un rendement plus élevé et des capacités dynamiques accrues. La vitesse de rotation est directement liée à la fréquence électrique des courants statoriques, ce qui facilite le pilotage aussi bien en vitesse qu'en position.

Système multi-machine synchrone à aimants

Afin de contrôler une MSAP, un onduleur doit être utilisé pour convertir une tension continue en un système de tensions triphasées sinusoïdales. En général, chaque MSAP doit être alimentée par son propre onduleur. Mais parfois, plusieurs MSAP sont employées dans un même système multi-machine. On peut envisager de mettre en commun une partie de la structure de pilotage pour toutes les machines de sorte que le poids et la complexité du système entier soient réduits. La Figure 1.1 montre l'architecture la plus simple dans laquelle toutes les MSAP sont connectées en parallèle.

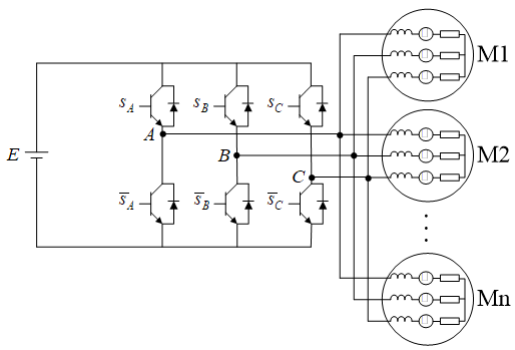

Figure 1.1 Structure de mise en parallèle

Pour un système électrique, il est souvent bénéfique de réduire le nombre de

composants et notamment pour les systèmes embarqués. En effet, plus on utilise de composants, plus la probabilité de défaillance est élevée. Bien que la demande de courant puisse croître avec l'augmentation du nombre de machines, la complexité et le poids d'un même onduleur n'augmentent pas nécessairement avec la puissance requise. Ainsi, avec une l'idée de mutualisation de l'onduleur pour l'ensemble des machines, nous pouvons grandement réduire le poids et la complexité de l'ensemble du système et augmenter ainsi sa disponibilité.

Applications multi-MSAP

Nous donnons ci-après quelques applications connues ou ambitionnées pour la mise l'usage de systèmes multi-machines.

1) Portes d'ascenseur

Un système de portes d'ascenseur classique voit ses deux portes entraînées par une liaison mécanique complexe. Une machine entraîne ce système mécanique et, par conséquent, les deux portes s'ouvrent et se ferment ensemble. Ce système de liaison mécanique est évidemment complexe et sujet à défaillances. Considérant que la vitesse d'une MSAP est toujours synchrone à la fréquence d'alimentation, nous pouvons envisager de mettre en parallèle plusieurs machines pour mutualiser l'onduleur afin que de pouvoir éliminer le système de liaison mécanique complexe. Le synchronisme des actions reposera sur la définition de la loi commande.

2) Transport ferroviaire

Dans un système de traction d'un véhicule ferroviaire, étant donné les contraintes mécaniques (largeur de voie, diamètre de roue, garde au sol, ..) l'espace est limité et un système de traction distribué (Figure 1.2 (a)) est généralement utilisé. Chaque roue du bogie est alors équipée d'une machine répondant aux exigences de puissance de traction totale. Cela rend cette application idéale pour une structure partagée.

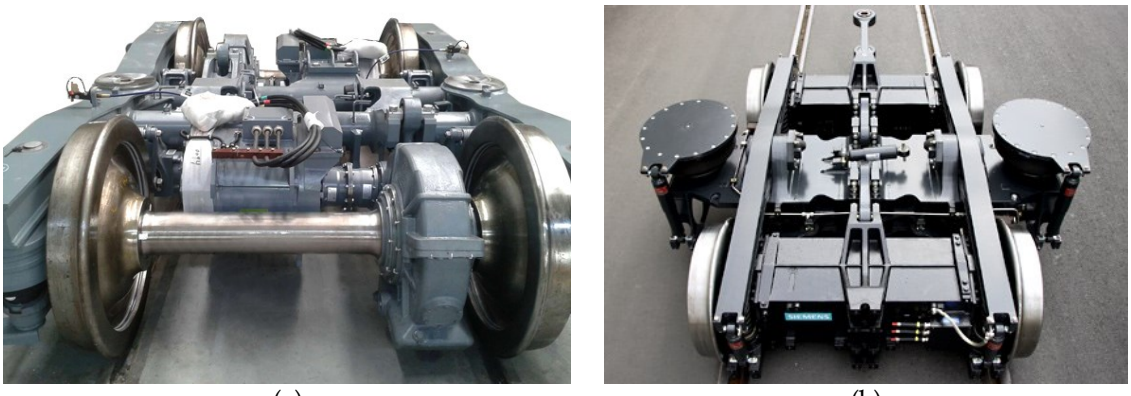

(a) (b)

Figure 1.2 Structure de Bogie (a) avec réduction ; (b) entrainement direct (Syntegra from Siemens).

Au cours des dernières années, l'idée d'utiliser la MSAP comme base d'un système de

traction a été développée pour le métro, les trains de banlieue et pour des applications de train à grande vitesse. Le couple massique élevé d'une MSAP rend possible la fabrication d'un tel système d'entraînement de traction sans engrenage (Figure 1.8 (b)). Il est prévisible que l'architecture partagée basée sur la MSAP offre un grand potentiel pour la traction ferroviaire.

3) Aéronautique

Motivé par le concept « d'avion plus électrique », le domaine de l'aéronautique s'intéresse au remplacement de la puissance mécanique ou hydraulique à bord par l'énergie électrique. Dans cette voie, l'architecture partagée est très utile dans l'électrification du système notamment pour les commandes de vol.

Tout d'abord, les applications aéronautiques nécessitent une tolérance aux pannes très généralement obtenue par redondance matérielle. Ainsi chaque actionneur est équipé de plusieurs systèmes d'entraînement redondants. Cela rend tout le système de contrôle complexe et lourd. Dans l'architecture partagée utilisant un même onduleur pour piloter plusieurs actionneurs, la redondance n'est nécessaire que pour cet onduleur.

Figure 1.3 Système de spoiler pour un avion commercial.

Deuxièmement, plusieurs actionneurs sont souvent assignés au pilotage d'un même système, tel qu'un ascenseur, un spoiler ou un volet (Figure 1.3). Cela répartit uniformément la force motrice sur une surface de contrôle longue et mince, augmentant ainsi la force aérodynamique effective et réduisant le poids de la structure. Ces actionneurs sont entièrement synchrones, de sorte que l'idée de connexion des MSAP en parallèle se révèle pertinente ici.

Différentes structures de partage

Il existe plusieurs types de structures de partage, chacune ayant leurs avantages et inconvénients. Les solutions classiques sont présentées sur la Figure 1.4.

La Figure 1.4 (a) illustre la structure de mise en commun de phases entre N machines avec 2N bras d'onduleur. Dans cette structure, deux phases des machines sont mises en communs via l'onduleur. Les phases restantes se connectent individuellement à leur propre bras. Dans ce cas, deux machines doivent fonctionner dans la même direction ou

dans des directions opposées avec la même vitesse.

La Figure 1.4 (b) montre la structure de mise en commun de phases entre N machines avec 2N+1 bras d'onduleur. Une seule phase de chaque machine est mise en commun. Toutes les machines peuvent fonctionner indépendamment.

La Figure 1.4 (c) montre le partage de la structure à point milieu. Dans cette configuration, une phase de chaque machine sera connectée au point milieu du bus DC alimentant l'onduleur. Les deux autres phases de chaque machine se connectent à leurs propres bras. Chaque machine peut fonctionner à sa propre vitesse. Cette architecture présente un inconvénient assez évident, car la tension du point milieu n'est pas nécessairement constamment égale à la moitié du bus continu. En conséquence il est nécessaire d'équilibrer le point milieu ce qui n'est pas forcément chose évidente.

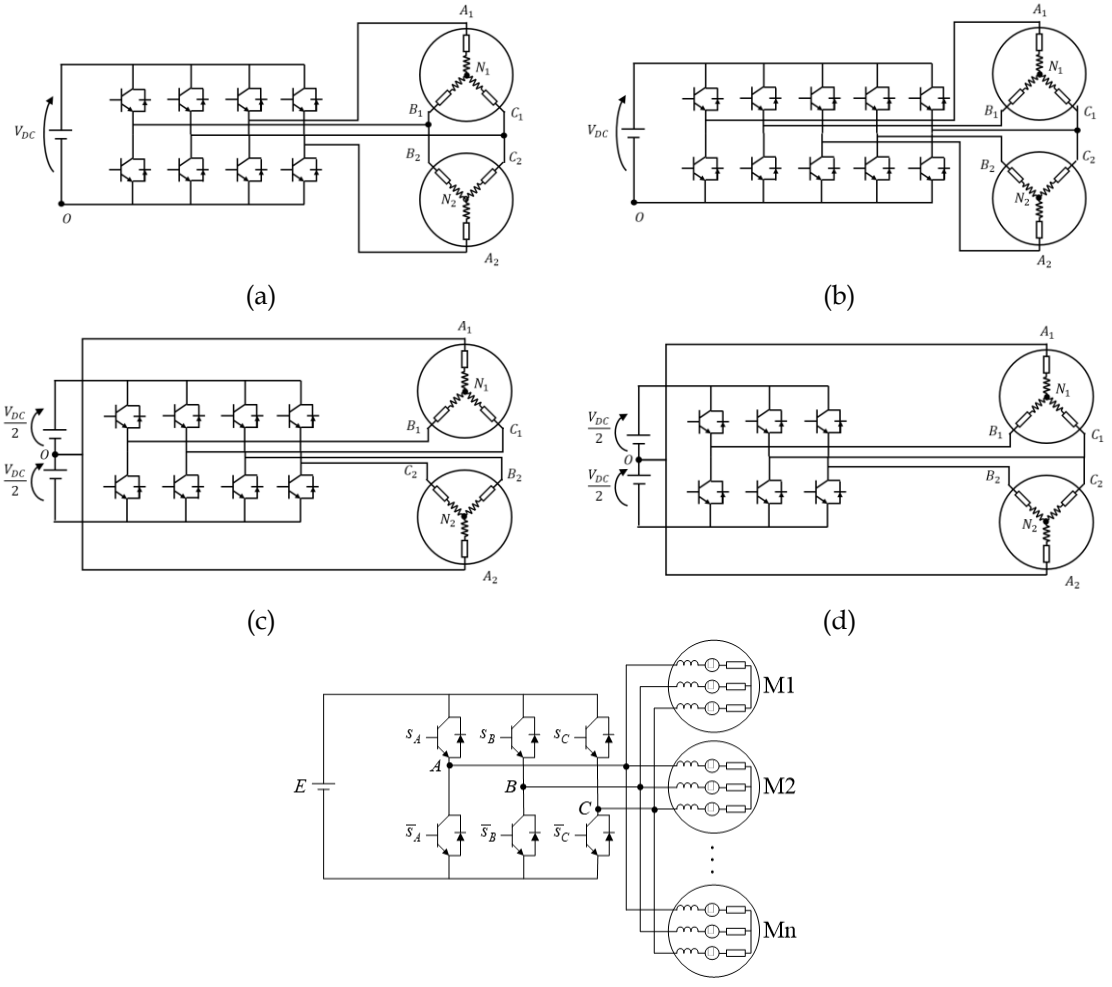

Figure 1.4 Plusieurs structures de partage : (a) bras en commun : N machines avec 2N bras ; (b) bras en commun : N machines avec 2N+1 bras ; (c) structure à point milieu ; (d) structure mixte ; (e) structure en parallèle.

La Figure 1.4 (d) montre la structure hybride. C'est une combinaison des deux

premières structures mentionnées ci-avant. Selon cette structure, un onduleur à trois bras est utilisé pour entraîner deux machines. D'une part, similairement à la structure de mise en commun de bras, une phase de chaque machine (phase C_1 et C_2) sera connectée à un même bras de l'onduleur. D'autre part, similairement à la structure à point milieu, une autre phase de chaque machine (phase A_1 et A_2) sera connectée au point milieu O du bus continu. La troisième phase est connectée à son propre bras d'onduleur. Tout comme pour la structure à mise en commun de bras, dans une telle configuration, toutes les machines doivent fonctionner dans des directions identiques ou opposées avec la même vitesse.

A noter que toutes ces solutions se caractérisent par une limitation de la tension disponible pour chaque machine ce qui limite la zone de fonctionnement notamment en vitesse maximale.

La Figure 1.4 (e) montre la structure parallèle. C'est la plus simple en configuration matérielle. Dans cette configuration, un onduleur classique à 3 bras 2 niveaux est utilisé et les 3 phases de chaque machine sont connectées en parallèle aux 3 bras de l'onduleur. Aucune modification ne doit être effectuée sur les machines. Toutes les machines reçoivent exactement la même tension en fréquence et en amplitude. Mais les inconvénients de cette proposition sont également clairs : toutes les machines connectées en parallèle doivent fonctionner à la même vitesse. Par rapport à la structure précédente, le problème de stabilité doit être pris en compte lors de la conception du contrôleur en définissant la loi d'autopilotage adaptée.

Comparaison de ces différentes structures

Nom de la structure	Nombre de bras pour N machines	Conditions de fonctionnement (degrés de liberté)	Avantages	Inconvénients
Bras communs : N machine avec 2N bras	2N	$\Omega_1 = \Omega_2$ ou $\Omega_1 = -\Omega_2$	Facile à mettre en œuvre	Sur-courant dans les bras communs
Bras communs : N machines avec 2N + 1 bras	2N+1	Indépendantes	Fonctionnement indépendant de la vitesse	Sur-courant dans les bras communs
Point milieu	2N	Indépendantes	Fonctionnement indépendant de la vitesse	L'accès au point milieu est nécessaire
Mixte	N+1	$\Omega_1 = \Omega_2$ ou $\Omega_1 = -\Omega_2$	Moins de bras nécessaires par rapport à la précédente	L'accès au point milieu est nécessaire
Parallèle	3	$\Omega_1 = \Omega_2$	Facile à mettre en œuvre Aucune modification matérielle requise	Pas facile à contrôler

Table 1 Résumé des structures évoquées

Les avantages et les inconvénients des différentes structures sont résumés dans la Table 1. Nous devons choisir la structure la plus appropriée en fonction de l'application. En comparaison, nous pouvons voir que l'architecture parallèle est la moins contraignante par rapport aux autres architectures. Dans nos applications, tous les MSAP fonctionnent

à la même vitesse. La structure à bras communs fournit plus de liberté de fonctionnement, mais cela n'a pas d'intérêt particulier dans notre cas et cette structure induit un poids supplémentaire. L'architecture à point milieu permet aux deux machines de fonctionner indépendamment en utilisant seulement un onduleur à quatre bras, mais elle exige que la tension du point milieu O soit constamment égale à la moitié de la tension continue. En pratique, le contrôle du point milieu n'est pas toujours chose aisée et quelque fois prohibé (aéronautique, ..).

État de l'art des stratégies de pilotage d'un système mono-onduleur alimentant deux MSAP en parallèle

Dans la structure parallèle, bien que les machines aient la même vitesse elles peuvent subir des couples de charge différents. Comme il n'y a qu'une seule source de tension, le contrôleur de couple doit pouvoir trouver le meilleur compromis en respectant la référence de couple et assurer la stabilité de toutes les machines. Dans la littérature scientifique, le cas simple de 2 machines est souvent utilisé pour explorer les possibilités de commande de ce type de système. On parle de système mono-onduleur à double MSAP en parallèle (MODMSAP).

La première étude du système MODMSAP est proposée par John Chiasson en 2002. Dans cet article, deux machines sont mécaniquement liées, ce qui n'est pas exactement le même cas que nous avons traité dans notre travail. Mais il a obtenu une conclusion importante en étudiant le problème d'existence de la solution aux équations de commande en régime permanent : la possibilité de contrôler le couple de chaque machine de manière indépendante provient du déplacement de l'angle électrique interne entre les deux machines. Cette conclusion constitue le critère de faisabilité et de contrôlabilité de ce système.

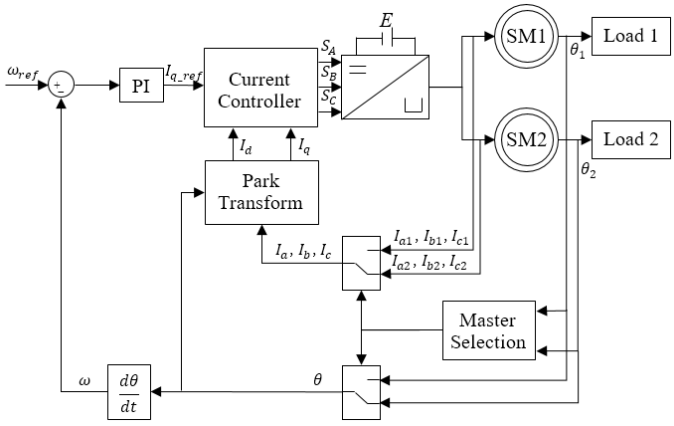

Figure 1.5 Schéma du contrôleur de Maître-Esclave

En 2011, le laboratoire LAPLACE à Toulouse a proposé la stratégie maître-esclave (Figure 1.5). Cette solution gère le système MODMSAP en élisant, à chaque période de commande, une machine maître et l'autre esclave. L'autopilotage est effectué sur la machine maître, tandis que la machine esclave fonctionne en boucle ouverte. La sélection

du maître n'est pas permanente mais basée sur la notion de stabilité, qui est reste un indicateur important du système MODMSAP. Selon ce critère, à chaque instant, la stratégie Maître-Esclave sélectionne la machine la plus chargée comme maître, de sorte que la stabilité du système soit alors préservée.

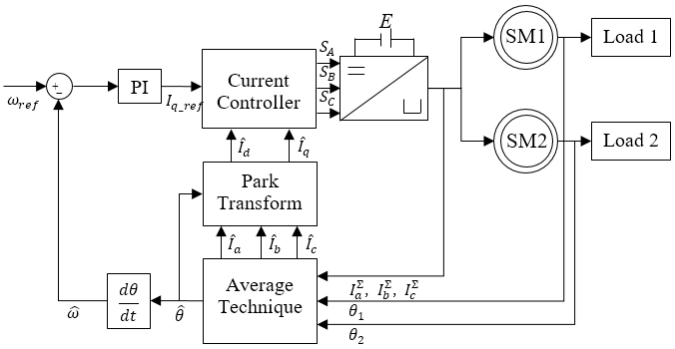

Figure 1.6 Schéma du contrôleur de la stratégie basée sur les valeurs de algébrique moyennes

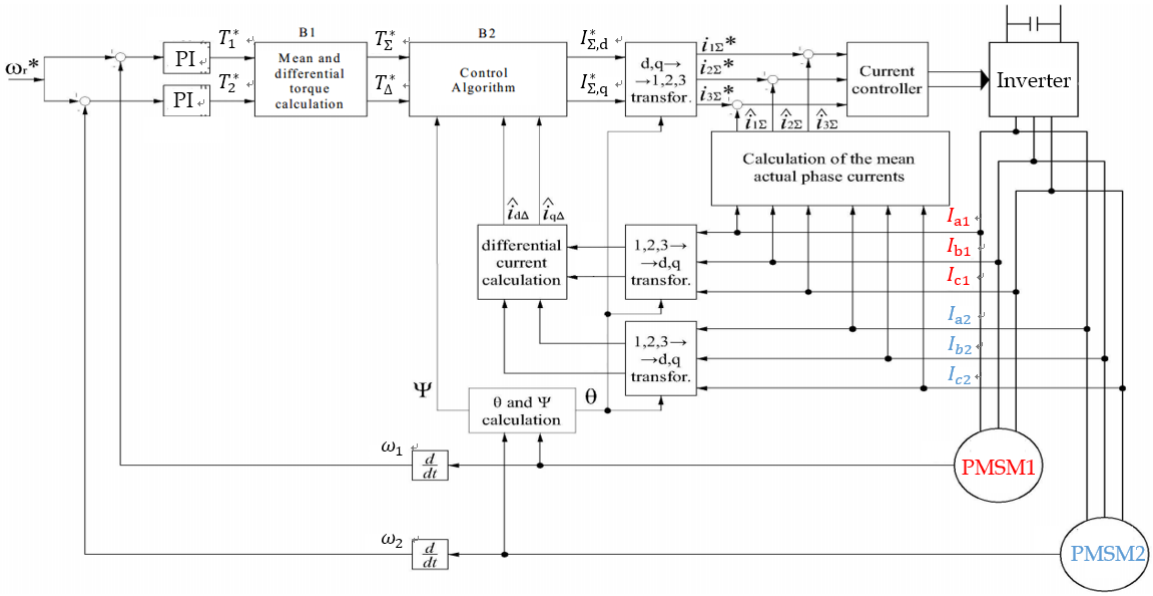

Figure 1.7 Schéma du contrôleur de $\Sigma - \Delta$

La stratégie basée sur les valeurs moyennes est une classe importante de stratégies de contrôle existantes pour ce type de système. C'est très intuitif mais les déclinaisons sont nombreuses. La première catégorie de stratégie (Figure 1.6) en valeur moyenne utilise la moyenne algébrique des courants et de la position du rotor. Une seconde catégorie, également appelée stratégie Σ-Δ (Figure 1.7), utilise la somme vectorielle (Σ) et la différence (Δ) des vecteurs courants dans le repère d-q afin d'améliorer les performances en régime transitoire et en régime permanent. Le processus en valeur moyenne peut également être appliqué à l'étage de sortie, qui utilise deux boucles de régulation indépendantes pour deux machines et applique la valeur moyenne de leur sortie à l'onduleur. Le problème majeur est que ces stratégies de contrôle ne fonctionnent correctement que lorsque la différence d'angle entre les deux machines reste faible. Ceci induit une contrainte sur la différence de couple de charge appliqué aux deux machines qui pour le coup doit rester faible. Par ailleurs le problème de stabilité peut devenir plus

critique pour des fonctionnements à basse vitesse où la résistance statorique n'est plus forcément négligeable devant la réactance synchrone.

La commande directe de couple, initialement proposée dans le cas d'une MSAP, a été également étendue au système MODMSAP. Elle divise l'hexagone de tension de l'onduleur triphasé en 12 secteurs de 30°. Quatre valeurs d'entrée sont considérées : deux liées au flux de chaque machine et deux liées au couple. Sur la base des 16 combinaisons possibles dans les 12 secteurs différents, une table de commutation est proposée pour déterminer le meilleur vecteur de tension à appliquer par l'onduleur en fonction de la situation courante. L'inconvénient de cette solution pour un système MODMSAP est la grande taille de la table de commutation et la difficulté d'un choix pertinent dans cette configuration de charge.

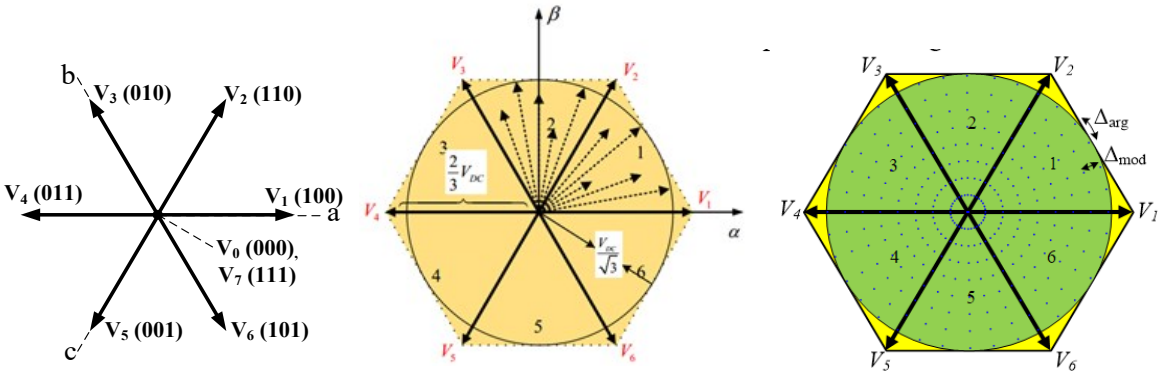

Figure 1.8 Espace vectoriel de tension utilisé dans l'optimisation pour (a) PTC. (b) PTCSS. (c) OPTC.

Similairement, les méthodes de commande prédictive à base de modèle (MPC) ont été également adaptées au système MODMSAP. On transforme le problème de contrôle en un problème d'optimisation qui utilise une prédiction du comportement futur d'un système et détermine la solution de commande optimale qui minimise un critère donné. Trois stratégies différentes sont connues : Predictive Torque Control (PTC), Predictive Torque Control Split & Seek (PTCSS) et Optimal Predictive Torque Control (OPTC). Parmi elles, la stratégie PTC proposée initialement pour une MSAP est étendue au cas MODMSAP en remplaçant la fonction coût par la somme des fonctions de coût associées à chaque machine (Figure 1.8 (a)). Avec la stratégie PTCSS, le nombre de vecteur de commande candidat est augmenté ce qui affine l'erreur sur la fonction coût (Figure 1.8 (b)). La stratégie OPTC, basée sur une approche en valeur moyenne, a prouvé que le vecteur de tension optimal pour deux machines correspond à la valeur moyenne des vecteurs de tension optimaux de chaque machine. Sur la base de cette conclusion, un contrôleur à réponse pile est proposé (Figure 1.8 (c)). La différence majeure entre ces deux dernières stratégies est l'utilisation de la SVPWM, car elle permet de réaliser le vecteur de tension optimal, i.e. qui minimise (voire annule) la fonction coût. Plus le vecteur de tension utilisé est proche du vecteur de tension optimal, plus la fonction coût est faible.

Expérimentation et analyse comparative des stratégies de contrôle existantes

Dans cette partie, une expérience impliquant les stratégies maitre-esclave, PTC, PTCSS et OPTC est menée en vue comparer ces méthodes en termes de performances. Ces stratégies sont testées sous le même environnement d'expérimentation pour éliminer au maximum les facteurs non algorithmiques. Dans l'expérience, deux facteurs considérés : la stabilité et la performance. Plusieurs critères de performances propres à un tel système sont évalués.

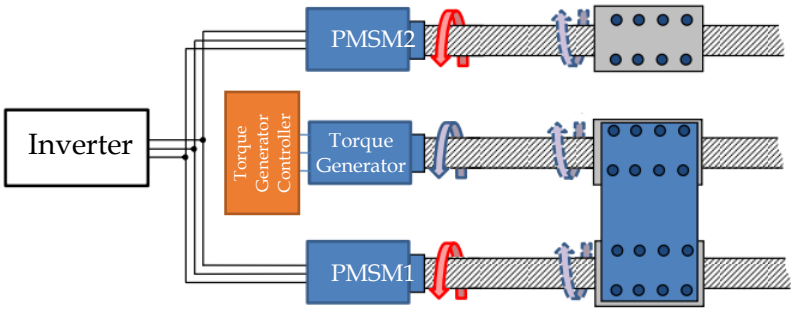

Figure 1.9 Illustration du montage expérimental

La Figure 1.9 présente le schéma du banc expérimental. Trois MSAP ont été utilisés. Les MSAP 1 et MSAP 2 sont les machines principales et possèdent des caractéristiques identiques. Chacune d'elles est équipée d'un codeur de position pour mesurer la position du rotor et de capteurs de courant. La machine située entre elles est utilisée comme générateur de couple de charge contrôlable. Chacune des trois MSAP est connectée à un actionneur à vis à billes linéaire et entraîne son propre axe. Dans cette expérience, l'axe de MSAP 1 était rigidement relié à l'axe du générateur.

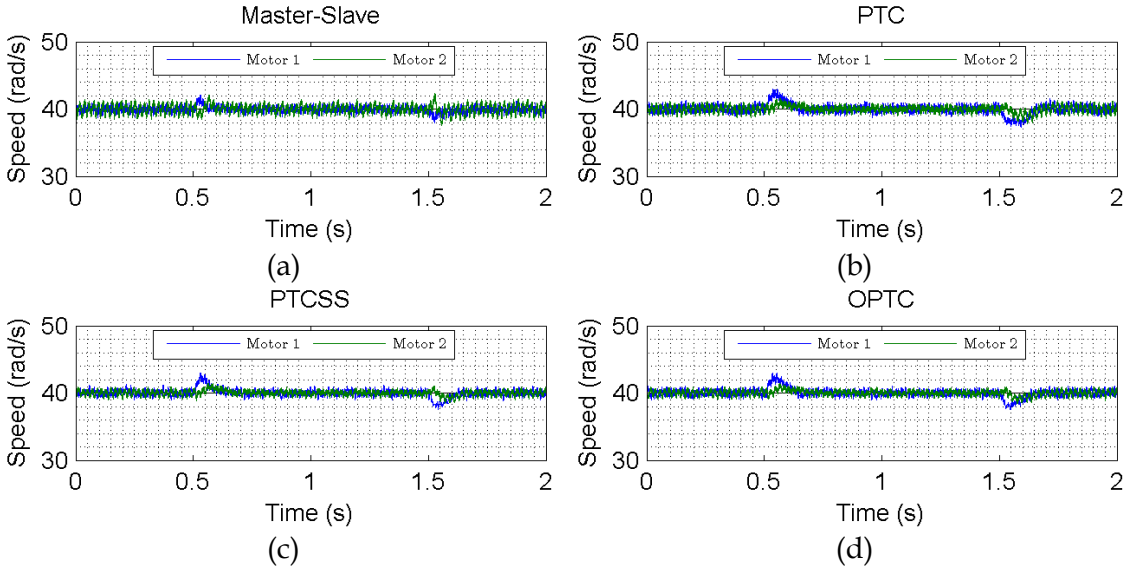

Figure 1.10 Courbes expérimentales de réponse en vitesse

La Figure 1.10 et la Figure 1.12 montrent respectivement la réponse en vitesse, la réponse en courant. La réponse en courant montre clairement qu'avec les stratégies PTCSS et OPTC, il y a moins d'ondulation de courant qu'avec la stratégie PTC. Toutes les stratégies de contrôle peuvent fonctionner correctement dans des conditions de couples

de charge déséquilibrés. Les valeurs des indicateurs de performance sont disponibles dans la Figure 2.36.

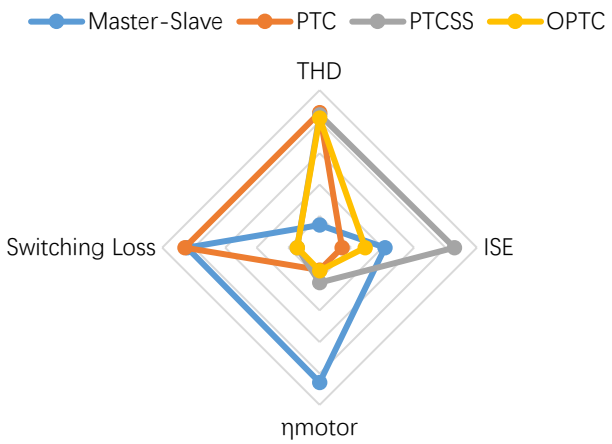

Figure 1.11 Comparaison des performances de toutes les lois de contrôle (le meilleur est à la frontière)

En résumé, l'utilisation de la SVPWM est la plus bénéfique pour l'ondulation de courant. Grâce à l'augmentation du nombre de vecteurs de tension réalisables permise par la modulation, l'ondulation de courant peut être fortement atténuée vis-à-vis des autres méthodes. Mais la restriction à un petit nombre de vecteurs de tension réalisables peut permettre de réduire les pertes de commutation de l'onduleur, pour une fréquence de commutation donnée. En pratique, il y a un compromis à faire. La stratégie maitre-esclave propose la meilleure qualité de contrôle car elle peut mieux compenser la variation du couple de charge externe. Ceci est dû à la prise en compte des positions des 2 machines ce qui donne instantanément une information sur le couple de charge appliqué.

Le plus important est que les résultats expérimentaux ont montré que l'efficacité énergétique d'une fonction coût unique est inférieure à celle d'une solution maître-esclave. L'analyse a montré que cela est dû au caractère surdéterminé du problème de commande. Orienté à partir d'un MODMSAP, il s'agit d'une découverte importante pour la conception du contrôleur et pour l'optimisation du rendement. En fait la méthode maitre-esclave garantie la stabilité pour les 2 machines mais le contrôle peut ne pas être optimal pour aucune des deux machines.

Conception d'une structure de commande pour un système MODMSAP

Un système MODMSAP est un système multi sortie multi-entrée. Avec un nombre d'entrées limité, le système est sous-actionné ou sous-déterminé traduisant le fait qu'il y a plus de contraintes que de paramètres de commande, il peut y avoir donc un conflit entre

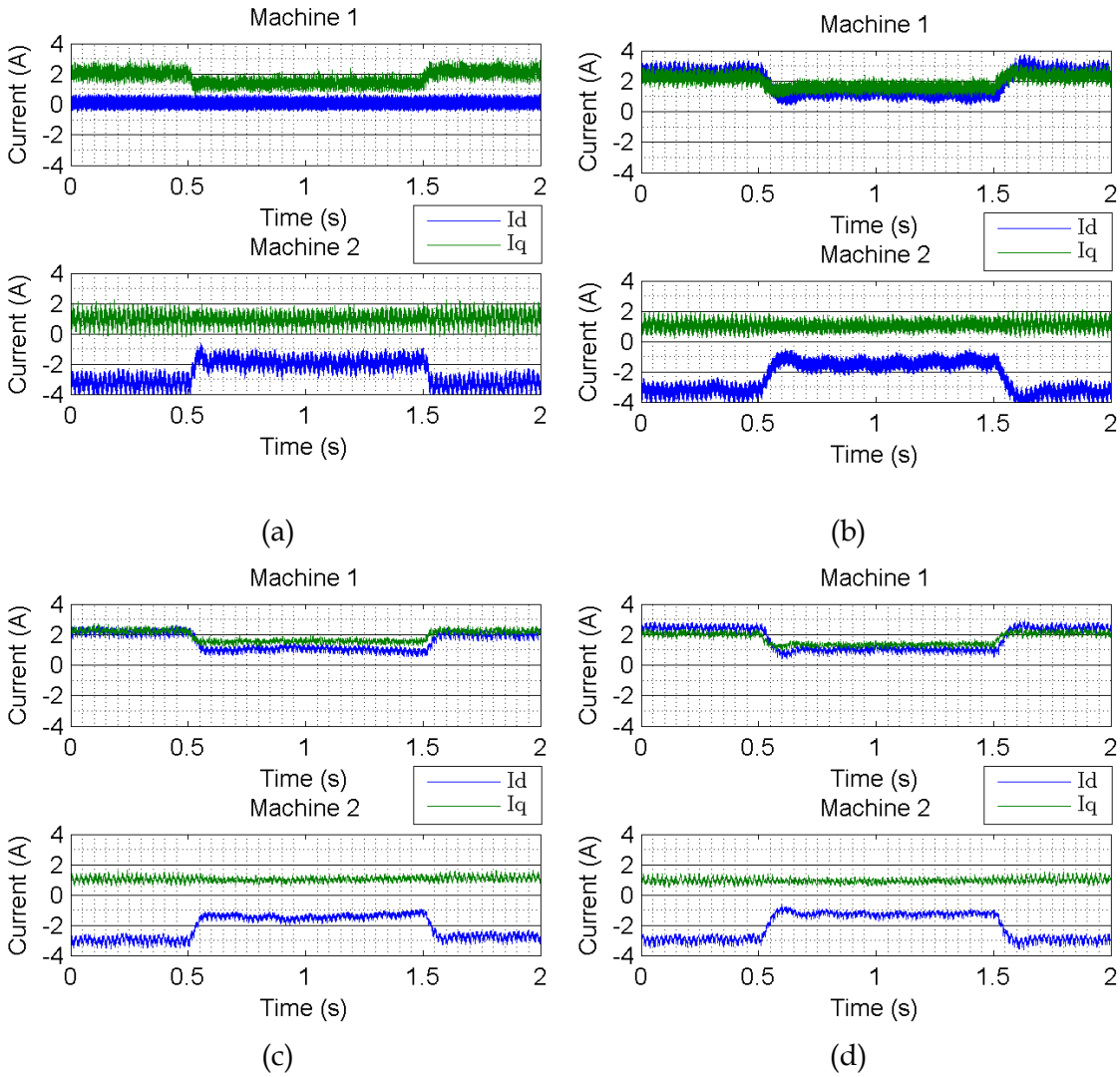

Figure 1.12 Evolution du courant – Essais Expérimentaux

les différentes contraintes à satisfaire. En effet pour une machine synchrone à pôles lisses la stratégie de contrôle de type MTPA (Maximum Torque per Ampere) conduit à imposer un courant Id nul pour la machine pilotée. Cependant dans ce cas de figure la seconde machine se voit pénalisée et globalement l'efficacité est réduite. Malheureusement avec un seul onduleur il n'est pas possible de garantir un fonctionnement MTPA simultanément pour les deux machines car la tension d'alimentation est commune.

Le modèle à l'état à l'équilibre du système MODMSAP est représenté par (1)

$$\begin{bmatrix} 1 & 0 \\ 0 & 1 \\ cos\,\theta_d & sin\,\theta_d \\ -sin\,\theta_d & cos\,\theta_d \end{bmatrix} \begin{bmatrix} V_{dM_1} \\ V_{qM_1} \end{bmatrix} = \begin{bmatrix} R_s & -L_s\omega_e & 0 & 0 \\ L_s\omega_e & R_s & 0 & 0 \\ 0 & 0 & R_s & -L_s\omega_e \\ 0 & 0 & L_s\omega_e & R_s \end{bmatrix} \begin{bmatrix} I_{dM_1} \\ I_{qM_1} \\ I_{dM_2} \\ I_{qM_2} \end{bmatrix} + \begin{bmatrix} 0 \\ \omega_e\varphi_p \\ 0 \\ \omega_e\varphi_p \end{bmatrix} \quad (1)$$

A partir de l'équation (3.16), nous pouvons voir que le système MODMSAP a deux variables d'entrée (V_{dM_1}, V_{qM_1}) et six variables d'état (I_{qM_1}, I_{qM_2}, I_{dM_1}, I_{dM_2}, θ_d, ω_e). Parmi elles, le couple et la vitesse (I_{qM_1},I_{qM_2},ω_e) sont régulés pour satisfaire à des

références désirées. Elles doivent être considérées comme des variables connues dans (1). Alors, dans (1), il reste 5 variables inconnues à gauche (I_{dM_1}, I_{dM_2}, θ_d, V_{dM_1}, V_{qM_1}) mais seulement 4 équations disponibles. Si un contrôleur est conçu pour réguler seulement la vitesse et le couple, évidemment, il y a une variable inconnue de plus que d'équations. Le système est sous-déterminé : il y a une infinité de solutions. Au contraire, si un contrôleur essaie de contraindre plus de 4 variables à leurs valeurs de références, le système devient surdéterminé : il n'existe aucune solution. Pour que le système MODMSAP fonctionne correctement, en premier lieu, le contrôleur doit définir une contrainte supplémentaire parmi I_{dM_1}, I_{dM_2} or θ_d de sorte que le système MODMSAP soit bien déterminé. Ensuite, le contrôleur calcule une valeur de référence pour cette variable contrainte supplémentaire par une procédure d'optimisation du rendement. Il est possible de réécrire (1) sous la forme d'une équation linéaire non homogène (donnée en (2)).

$$\begin{bmatrix} -R_s & 0 & 1 & 0 \\ -\omega_e L_s & 0 & 0 & 1 \\ 0 & -R_s & cos\,\theta_d & sin\,\theta_d \\ 0 & -\omega_e L_s & -sin\,\theta_d & cos\,\theta_d \end{bmatrix} \begin{bmatrix} I_{dM_1} \\ I_{dM_2} \\ V_{dM_1} \\ V_{qM_1} \end{bmatrix} = \begin{bmatrix} -\omega_e L_s I_{qM_1} \\ R_s I_{qM_1} + \omega_e \varphi_p \\ -\omega_e L_s I_{qM_2} \\ R_s I_{qM_2} + \omega_e \varphi_p \end{bmatrix} \tag{2}$$

La solution correspondante est:

$$\begin{cases} I_{dM_1} = \dfrac{Ay - B}{Z^2 x} - \dfrac{C}{Z^2} \\ I_{dM_2} = \dfrac{A - By}{Z^2 x} - \dfrac{C}{Z^2} \\ V_{dM_1} = y\left(R_s I_{dM_2} - \omega_e L_s I_{qM_2}\right) - x\left(R_s I_{qM_2} + \omega_e L_s I_{dM_2} + \omega_e \varphi_p\right) \\ V_{qM_1} = x\left(R_s I_{dM_2} - \omega_e L_s I_{qM_2}\right) + y\left(R_s I_{qM_2} + \omega_e L_s I_{dM_2} + \omega_e \varphi_p\right) \end{cases} \tag{3}$$

Que

$$\begin{aligned} Z &= \sqrt{{R_s}^2 + (\omega_e L_s)^2} \\ A &= Z^2 I_{qM_1} + R_s \omega_e \varphi_p \\ B &= Z^2 I_{qM_2} + R_s \omega_e \varphi_p \\ C &= L_s {\omega_e}^2 \varphi_p \\ x &= sin\,\theta_d \\ y &= cos\,\theta_d \end{aligned} \tag{4}$$

Conception d'un contrôleur pour le système MODMSAP

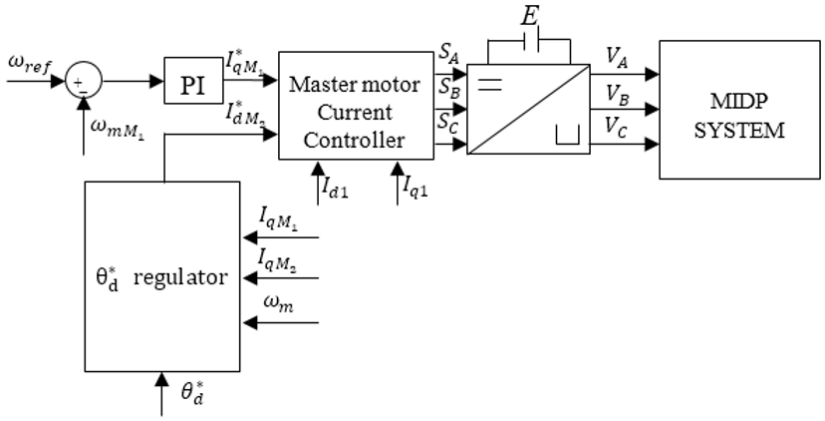

Figure 1.13 Diagramme du contrôleur proposé

La Figure 1.13 montre le schéma fonctionnel du contrôleur proposé. Le contrôleur se compose de deux blocs : le contrôleur du moteur maître et le régulateur de θ_d. Le contrôleur du moteur maître régule uniquement le moteur M_1. Le moteur M_2 est laissé en boucle ouverte. Pour la commande du moteur maître, un contrôle vectoriel est utilisé à l'aide d'une commande SVM pour l'onduleur. La référence I_{qM_1} est donnée par le régulateur de vitesse de type PI. La référence I_{dM_1} est donnée par le régulateur de θ_d. Le principe de la commande est le suivant :

1) Calculer l'état stable optimal pour θ_d

2) En déduite l'état optimal du système par (4).

3) Définissez I^*_{d1} correspondant à l'état optimal.

Les étapes 2 et 3 sont traitées par le régulateur θ_d. Cette méthode utilise θ_d pour calculer l'état optimal du système car prendre θ_d comme variable connue rend la solution d'état de (2) linéaire et unique. Cette propriété simplifie grandement l'analyse et les résultats. De plus, l'état est défini par I_{dM_1}, ce qui est plus facile à implémenter

Stabilité du contrôleur

La stabilité de M_2 doit être étudiée car cette machine fonctionne en boucle ouverte. Sa stabilité est définie par son angle de charge δ. Sa région stable est définie par :

$$\begin{cases} \left(-cos^{-1}\left(\frac{A}{B}\right),0\right) \cup \left(cos^{-1}\left(\frac{A}{B}\right),\frac{\pi}{2}\right) & A < B \\ \left(0,\frac{\pi}{2}\right) & A \geq B \end{cases} \quad (5)$$

La Figure 1.14 (a) montre l'angle δ de chaque moteur par rapport à θ_d lorsque M_1 est plus chargé (A> B). La ligne pointillée rouge représente l'angle α critique. Si le focus est sur M_2, sa stabilité est atteinte lorsque δ_{M_2} est en dessous de la ligne pointillée rouge. Il est représenté comme l'espace vert dans les différentes figures. Cette situation est similaire

à la stratégie Maître-Esclave selon laquelle un moteur moins chargé avance dans l'angle électrique ($\theta_d > 0$).

La Figure 1.14 (b) montre la courbe lorsque M_2 est plus chargé (A <B). Ici, nous devons faire attention à la partie droite de la région stable. Parce que dans cette région, M_1 est instable en boucle ouverte. Le contrôleur pour M_1 doit être capable de manipuler le moteur maître dans des conditions instables. Sinon, cette partie ne doit pas être considérée comme une région stable valide.

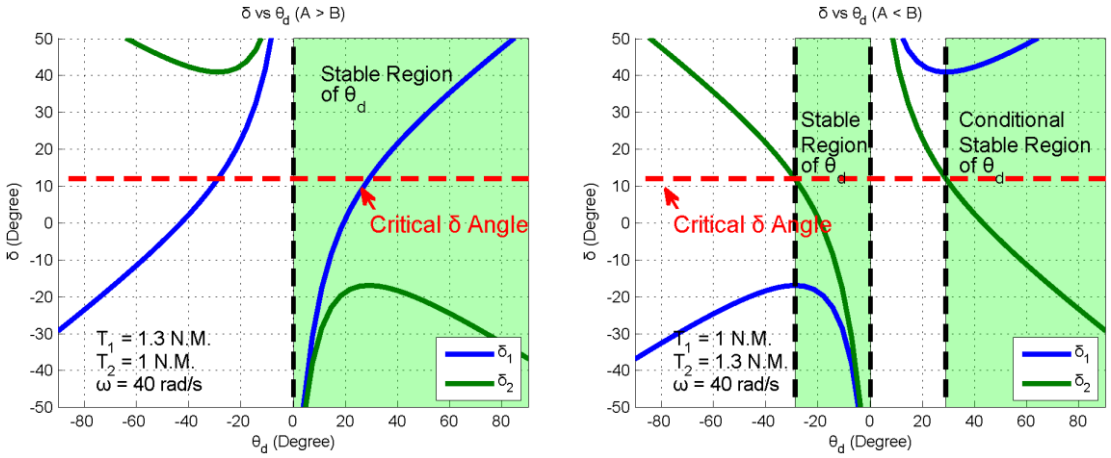

(a) (b)

Figure 1.14 Courbe typique pour δ en réponse d'un θ_d

Optimisation de l'efficacité pour le système MODMSAP

L'efficacité est optimisée en minimisant les pertes Joule des machines. La fonction coût est:

$$g = {I_{dM_1}}^2 + {I_{dM_2}}^2 \tag{6}$$

En insérant (3) dans (6), une fonction coût par rapport à θ_d est obtenue.

$$f(x,y) = \left(\frac{Ay - B}{Z^2 x} - \frac{C}{Z^2}\right)^2 + \left(\frac{A - By}{Z^2 x} - \frac{C}{Z^2}\right)^2 \tag{7}$$

θ_d est le seul degré de liberté qui minimise cette fonction de coût. Comme $\sin\theta_d = x$ et $\cos\theta_d = y$, cette fonction coût doit répondre à une contrainte (8).

$$g(x,y) = x^2 + y^2 = 1 \tag{8}$$

La solution analytique de l'optimum θ_d, qui est le point extrême de (7), peut être obtenue en utilisant la méthode du multiplicateur de Lagrange.

$$L(x,y,\lambda) = f(x,y) + \lambda(g(x,y) - 1) \tag{9}$$

A partir des dérivées partielles de (9), données ci-dessous,

$$\frac{\partial L(x,y,\lambda)}{\partial x} = 2\lambda x + 2\left(\frac{C}{Z^2} + \frac{B-Ay}{Z^2 x}\right)\frac{Ay-B}{Z^2x^2} + 2\left(\frac{C}{Z^2} + \frac{By-A}{Z^2 x}\right)\frac{A-By}{Z^2x^2} = 0 \quad (10)$$

$$\frac{\partial L(x,y,\lambda)}{\partial y} = 2\lambda y - 2A\left(\frac{C}{Z^2} + \frac{B-Ay}{Z^2 x}\right)\frac{1}{Z^2 x} + 2B\left(\frac{C}{Z^2} + \frac{By-A}{Z^2 x}\right)\frac{1}{Z^2 x} = 0 \quad (11)$$

$$\frac{\partial L(x,y,\lambda)}{\partial \lambda} = x^2 + y^2 - 1 = 0 \quad (12)$$

L'optimum θ_d est l'une des solutions de l'ensemble d'équations ci-dessus. Finalement, une équation quartique par rapport à x est obtenue.

$$x^4 + \alpha x^3 + \beta x^2 + \gamma x - \beta = 0 \quad (13)$$

avec

$$\begin{cases} \alpha = \dfrac{4C(B^3 - A^3)}{4A^2B^2 + (BC - AC)^2} \\ \beta = \dfrac{4(B^2 - A^2)^2}{4A^2B^2 + (BC - AC)^2} \\ \gamma = \dfrac{4C(A^3 - B^3 + A^2B - AB^2)}{4A^2B^2 + (BC - AC)^2} \end{cases} \quad (14)$$

Cette équation peut être résolue en utilisant la méthode Ferrari. On peut conclure que, parmi ces quatre solutions, il existe deux solutions réelles et deux solutions complexes. Les solutions réelles sont liées aux deux points extrêmes. La procédure d'optimisation est alors définie comme suit:

1) Calculer A, B, C en utilisant (4).

2) Calculer α, β, γ en utilisant (14)

3) Calculer les solutions de (13).

4) En ignorant les deux solutions complexes, les deux solutions réelles sont mises à jour et assurent via (3) le calcul du courant I_d correspondant.

5) L'angle optimal $\theta_d^{optimal} = \sin^{-1} x$ est alors définit. Il faut ensuite vérifier s'il se trouve dans la région stable en utilisant la relation (5).

6) Nous pouvons finalement définir $I_{dM_1}^*$ calculé par (3).

Etude de sensibilité du point d'équilibre.

Les paramètres d'une MSAP sont soumis à des modifications pendant le fonctionnement. Notamment la résistance de l'enroulement du stator (R_s) et le flux magnétique permanent (φ_p). Comme démontré ci-dessus, les critères de stabilité du système (5) et d'optimisation de l'efficacité énergétique (14) dépendent fortement de la précision des paramètres. Dans cette étude, R_s, L_s et φ_p sont uniquement pris en compte. La plage de variation de ces paramètres est comprise entre 50% et 150% par

rapport à leur valeur nominale.

L'équation (5) détermine la stabilité du système MODMSAP. Ainsi, lorsque la non-concordance des paramètres existe, le contrôleur ne peut pas garantir la stabilité car θ_d^* est peut-être en dehors de la région stable. La relation (15) montre la valeur critique de l'angle $\theta_d^{critical}$ qui au final dépend aussi de la vitesse comme le montre les figures 15, 16, 17 .

$$\theta_d^{critical} = f(R_s, L_s, \varphi_p) = -cos^{-1}\left(\frac{A}{B}\right) \tag{15}$$

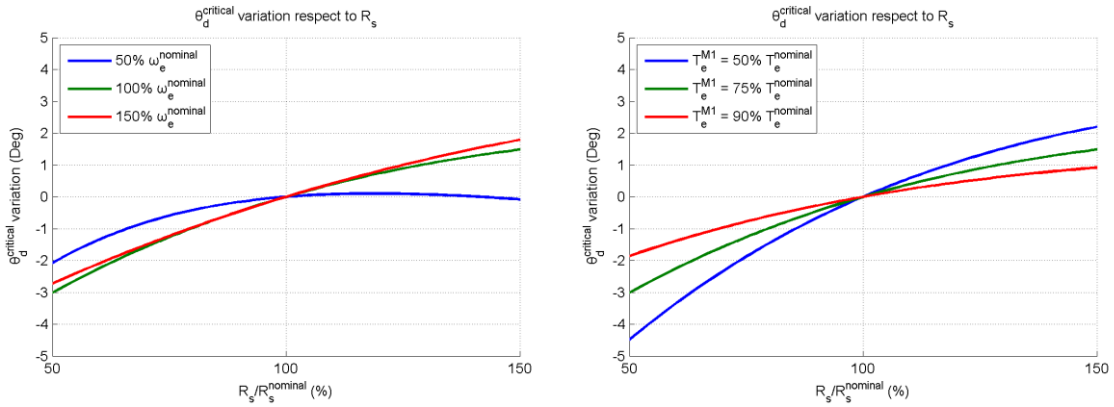

(a) (b)

Figure 1.15 $\theta_d^{critical}$ en fonction de (a) Rs et ω. (b) Rs et le Couple.

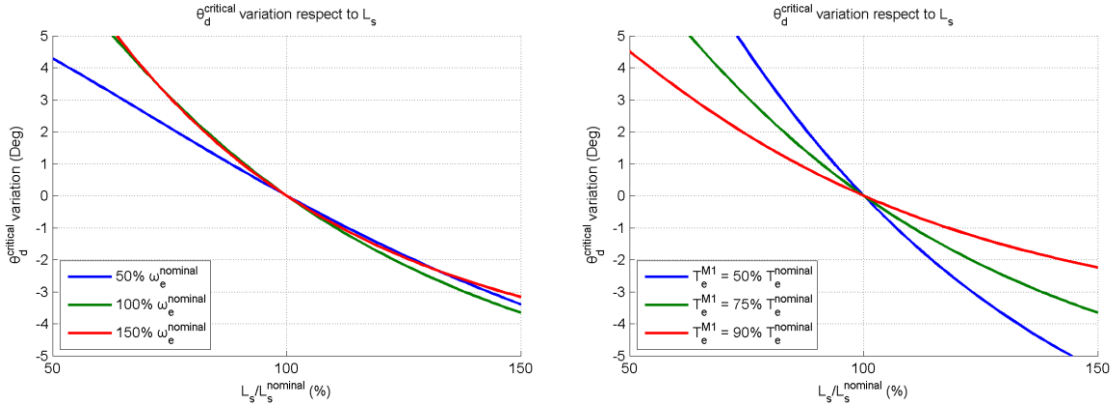

(a) (b)

Figure 1.16 $\theta_d^{critical}$ en fonction de (a) Ls et ω. (b) Ls et le Couple.

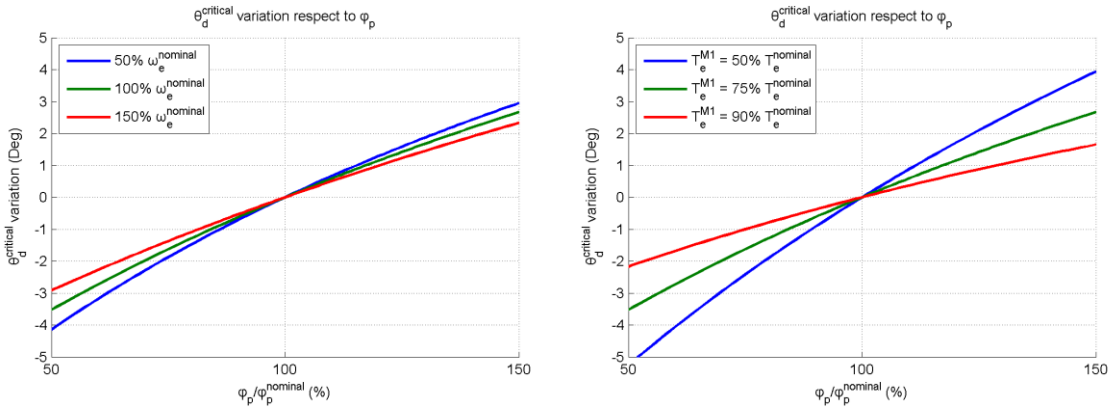

(a) (b)

Figure 1.17 $\theta_d^{critical}$ *en fonction de (a)* φ_p *et ω. (b)* φ_p *et le Couple.*

Ces figurent montrent la variation $\theta_d^{critical}$ par rapport à R_s , L_s et φ_p respectivement. On peut conclure que la limite de stabilité est sensible à la variation des paramètres. En fonction de l'état de fonctionnement, une modification de 20% d'un paramètre peut entraîner une limite de stabilité de 2 à 3 degrés en fonction de l'état de fonctionnement. De plus, ces changements sont cumulatifs. Ceci est très dangereux car si la procédure d'optimisation de l'efficacité donne un $\theta_d^{optimal}$ proche de cette limite, le contrôleur peut penser qu'il est stable mais en fait il ne l'est pas. Le système perdra immédiatement sa stabilité.

Cependant, il existe une solution simple pour stabiliser le système. Reportez-vous à (5), la région stable est indépendante des paramètres lorsque M_1 est la machine la plus chargée (A> B). Un mécanisme maître-esclave qui sélectionne toujours le moteur le plus chargé en tant que M_1 peut être introduit. Cela rend A> B toujours satisfait et par conséquent sa région stable est toujours $\left(0, \frac{\pi}{2}\right)$.

Sensibilité paramétrique de l'optimum d'efficacité énérgétique

La méthode d'optimisation proposée dépend fortement de la précision des paramètres. Ainsi, il est nécessaire de voir à quel point l'efficacité de l'optimisation sera influencée. Afin d'évaluer quantitativement l'influence et d'éliminer l'impact sur l'efficacité causé par les changements de paramètres, deux θ_ds optimaux sont calculés en fonction de différents paramètres du système. Le premier utilise les paramètres nominaux même lorsque la valeur réelle est en mouvement pour simuler une situation d'optimisation non adaptée. Le second utilise la valeur réelle (optimisation parfaite)

La Figure 1.18 (a) - (c) montre l'influence de R_s, L_s, et φ_p respectivement. L'efficacité de l'optimisation diminue lorsque le paramètre n'est pas parfaitement adapté. Mais la différence varie d'un paramètre à l'autre. Pour R_s et L_s, leur influence est relativement faible. Une diminution maximale de 4% peut être provoquée par une variation de ± 50%

de L_s. Mais la situation change quand il s'agit de φ_p, 25% d'efficacité sera perdue si elle est modifiée de 50%. Ainsi il est fortement recommandé d'implémenter un observateur de φ_p dans une application réelle.

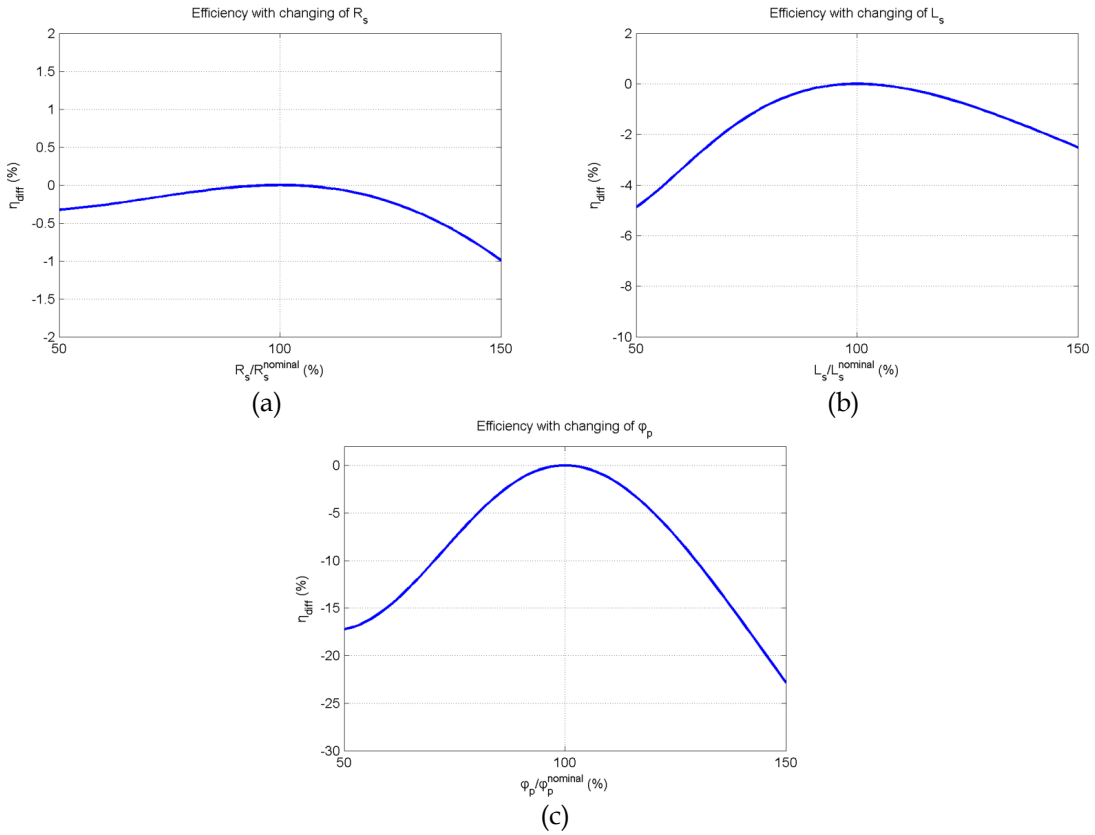

Figure 1.18 Résultat de la simulation pour l'influence des paramètres sur l'efficacité

Résultats expérimentaux du contrôleur pour le système MODMSAP

Un montage expérimental a été réalisé pour vérifier la faisabilité et illustrer les performances du contrôleur proposé. La Figure 1.18 montre les résultats obtenus. Au cours de l'expérience, les deux machines ont d'abord été sollicitées à vitesse constante. Ensuite, un couple de charge externe a été appliqué à M_1 afin de tester le régime transitoire du système, sa robustesse et son efficacité dans le cas d'un couple de charge différent.

La Figure 1.18 montre la réponse θ_d correspondante (courbe verte). La courbe bleue représente la référence optimale $de\ \theta_d$ calculée en temps réel. La valeur réelle θ_d suit la valeur de référence confirmant ainsi l'efficacité du régulateur θ_d.

La Figure 1.19 illustre la comparaison des performances expérimentales entre différents contrôleurs. La courbe bleue représente l'efficacité maximale estimée obtenue par la procédure d'optimisation. La courbe rouge montre l'efficacité de la nouvelle stratégie. La courbe noire est celle de la stratégie maitre-esclave. On peut conclure que la nouvelle stratégie de contrôle fournit une efficacité encore plus élevée, en particulier qand la différence de couple de charge est grande. Pendant ce temps, l'efficacité de la nouvelle

stratégie est presque la même que l'efficacité théorique estimée. Cela prouve l'exactitude du processus d'optimisation et de la compatibilité des paramètres.

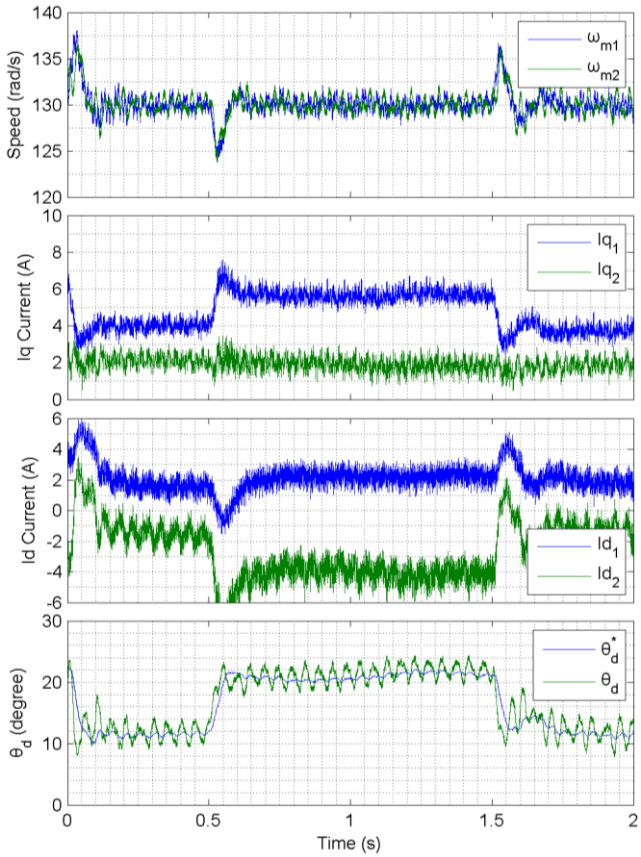

Figure 1.19 Résultats expérimentaux du test d'efficacité

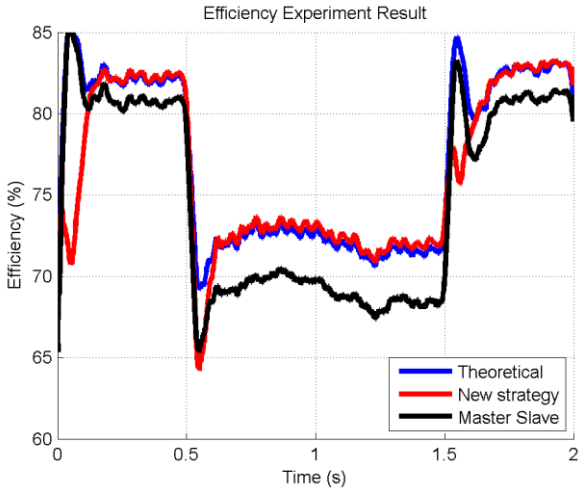

Figure 1.20 Comparaison des performances expérimentales entre différents contrôleurs

Conception d'un contrôleur pour le système Mono-Onduleur Multi-MSAP

En utilisant la méthode d'analyse des contraintes proposée dans la section précédente, il est prouvé que le système MOMMSAP est réalisable. Dans un système MOMMSAP, il y a 2N + 1 variables inconnues incluant $\underbrace{V_{dM_1}, V_{qM_1}}_{2}$, $\underbrace{I_{dM_1} \dots I_{dM_N}}_{N}$, $\underbrace{\theta_{dM_1,M_2} \dots \theta_{dM_1,M_N}}_{N-1}$. Alors

que les contraintes 2N sont disponibles. Une loi de commande garantissant la stabilité pour MOMMSAP est réalisable du point de vue de la contrôlabilité. Cependant la définition d'une valeur optimale pour θ_d s'avère plus compliquée alors I_{dM_1} est utilisé comme variable de commande.

A l'image du paragraphe précédent la stabilité du système MOMMSAP est équivalente à l'existence d'une solution du régime permanent. Par conséquent, nous établissons le critère d'existence de la solution en régime permanent de chaque machine par rapport à I_{dM_1}, qui devient:

$$\mathbb{I}_{M_k} = \begin{cases} (-\infty, -\frac{\alpha}{2Z^2} - \sqrt{f(I_{qM_k}, \omega_e) - f(I_{qM_1}, \omega_e)}] \cup [-\frac{\alpha}{2Z^2} + \sqrt{f(I_{qM_k}, \omega_e) - f(I_{qM_1}, \omega_e)}, +\infty) & f(I_{qM_k}, \omega_e) \geq f(I_{qM_1}, \omega_e) \\ (-\infty, +\infty) & f(I_{qM_k}, \omega_e) < f(I_{qM_1}, \omega_e) \end{cases} \quad (16)$$

que

$$f(I_q, \omega_e) = {I_q}^2 + \frac{2R_s \omega_e \varphi_p}{Z^2} I_q \quad (17)$$

(16) représente la plage contrainte de I_{dM_1} déterminée par M_k. Ainsi, pour tout le système composé de N moteurs, I_{dM_1} doit être réglé dans la plage déterminée par $= \mathbb{I}_{M_2} \cap \ldots \cap \mathbb{I}_{M_N}$. Cette contrainte sur I_{dM_1} conduit à deux stratégies de contrôle différentes. Leurs schémas de contrôle sont représentés sur la Figure 1.21 et la Figure 1.22.

- ***Fonctionnement sans sélection d'une machine maitre***

Un bloc dédié au calcul de la référence du courant I_{dM_1} est utilisé. À chaque instant, il évaluera $f(I_{qM_1}, \omega_e)$ et $f(I_{qM_k}, \omega_e)$ puis calculera $\mathbb{I}_{M_k}$ par (16). Au final, la référence peut être obtenue. $I^*_{dM_1}$ est réglée sur la valeur d'amplitude minimale dans $\mathbb{I}$ sous la loi MTPA (Maximum Torque Per Ampere).

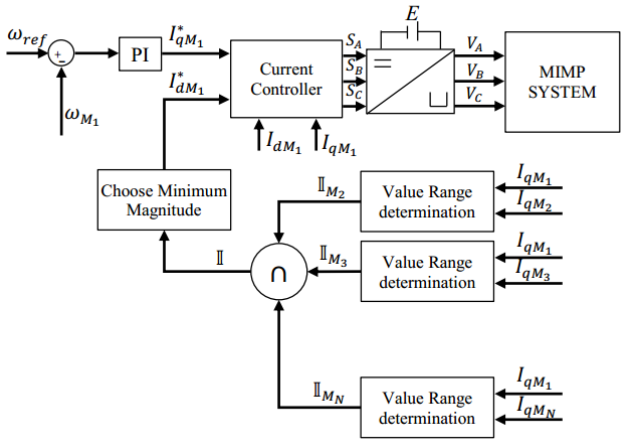

Figure 1.21 Schéma fonctionnel du contrôleur de sélection sans maître

- ***Fonctionnement avec sélection d'un maître***

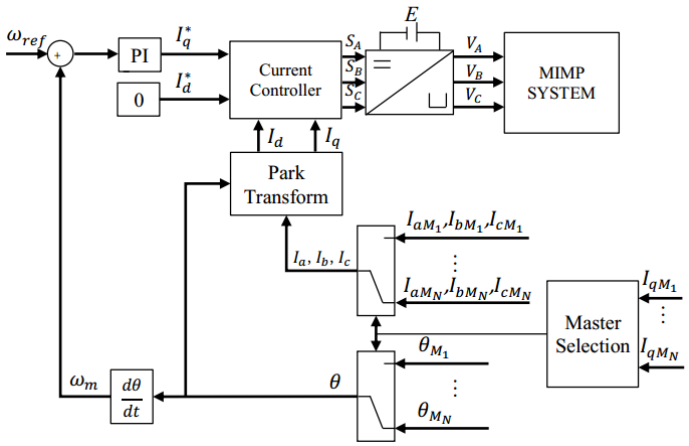

Figure 1.22 Schéma de principe du contrôleur de sélection principal

D'autre part, il est possible que non seulement I_{dM_1} soit régulé passivement sous les contraintes mais aussi que la machine soit choisie comme M_1 qui satisfait $f(I_{qM_1}, \omega_e) > f(I_{qM_k}, \omega_e)$. Par conséquent, la plage de contraintes I est toujours $(-\infty, +\infty)$ dans un tel cas. $I^*_{dM_1}$ peut-être arbitraire vis-à-vis de la stabilité.

Extension de la stratégie maître-esclave

Il y a une différence entre la stratégie de sélection principale et la stratégie conventionnelle maître-esclave. La stratégie classique compare l'angle électrique des deux machines pour déterminer la machine maître. Mais quand une ou deux machines deviennent génératrices, ce critère n'est plus valable.

Reportons-nous à (17), si nous définissons

$$I_q^{critical} = -\frac{R_s \omega_e \varphi_p}{Z^2} \tag{18}$$

La relation entre le courant I_q et la valeur de la fonction est symétrique à $I_q^{critical}$.

$$\Phi_A = \left[-\frac{R_s \omega_e \varphi_p}{Z^2}, +\infty\right] \tag{19}$$

$I_{qM_1} > I_{qM_k} \Leftrightarrow f(I_{qM_1}, \omega_e) > f(I_{qM_k}, \omega_e)$, alors que dans la région

$$\Phi_B = \left[-\infty, -\frac{R_s \omega_e \varphi_p}{Z^2},\right] \tag{20}$$

$I_{qM_1} < I_{qM_k} \Leftrightarrow f(I_{qM_1}, \omega_e) > f(I_{qM_k}, \omega_e)$. Si on considère la courbe reliant le couple à l'angle de calage δ décrite en fonction de l'amplitude de la tension différente nous obtenons une évolution sinusoïdale. Ici, nous utilisons le courant I_q pour représenter le couple directement. Nous pouvons trouver que la courbe de couple est également symétrique à $I_q^{critical}$. Comme seul le moteur maître est sous contrôle, le régulateur de courant adaptera l'amplitude de la tension en conséquence l'amplitude de la courbe pour répondre à son couple de référence.

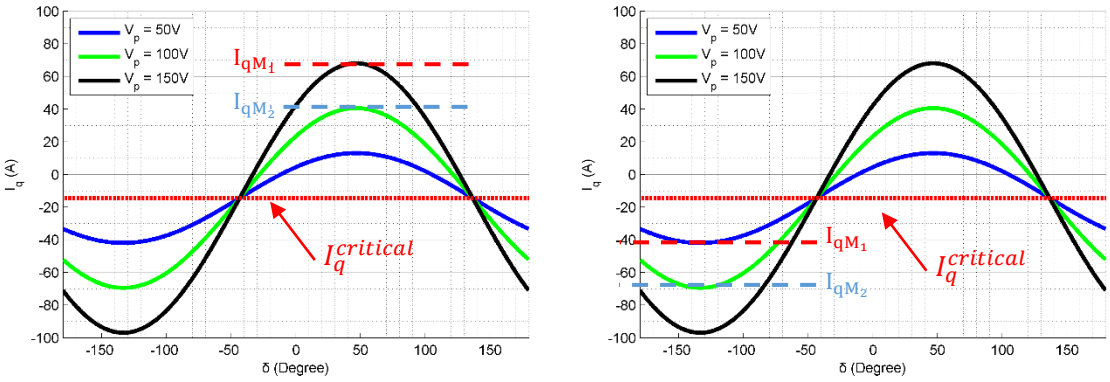

(a) (b)

Figure 1.23 Visualisation de la stabilité du MOMMSAP.

La stratégie maître-esclave conventionnelle ne fonctionne que dans la situation de la figure 18. Si le couple requis du moteur maître est I_{qM_1} (représenté par une ligne rouge), le contrôleur de courant génère la tension autour de la courbe noire. Pendant ce temps, le couple requis du moteur esclave (représenté par la ligne bleue) est également satisfait. Mais à la Figure 1.23 (b), lorsque deux machines sont en mode générateur, le Maître-Esclave conventionnel choisira toujours M_1 comme machine maître en raison de $\theta_{eM_1} < \theta_{eM_1} \Leftrightarrow I_{qM_1} > I_{qM_2}$. Mais évidemment, la tension générée ne peut pas répondre à l'exigence de couple de M_2. Ceci induira une perte de stabilité immédiatement. Pour garantir la stabilité dans toute la plage de fonctionnement, la valeur de la fonction (17) doit être privilégiée.

Simulation de la stratégie de contrôle pour le système MOMMSAP

Nous avons utilisé une simulation impliquant 4 machines menées dans MATLAB / Simulink pour vérifier le contrôleur proposé. La Figure 1.24 a montré les résultats de la simulation de la stratégie de fonctionnement sans machine maitre. La Figure 1.24 (a) montre la réponse en vitesse alors que la Figure 1.24 (b) montre l'évolution des courants dans les 4 machines. De même, la Figure 1.25 illustre le résultat de la stratégie avec sélection d'une machine maitre.

Nous notons que le contrôleur défini pour le système MIDPMSM obtenu initialement peut être étendu au mode générateur en utilisant les courants sur l'axe q pour chaque machine. Le contrôle est alors assuré par la valeur Id et nous pouvons définir une stratégie avec une sélection de machine maitre ou bien sans sélection de la machine maitre. Les deux stratégies assurent la stabilité.

Conclusion

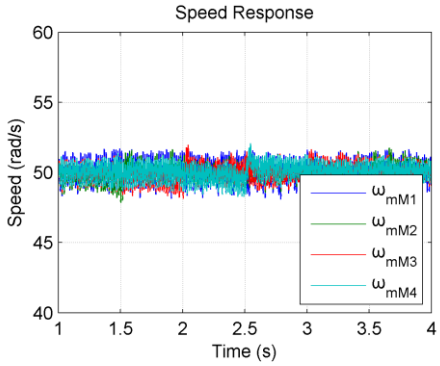

(a)

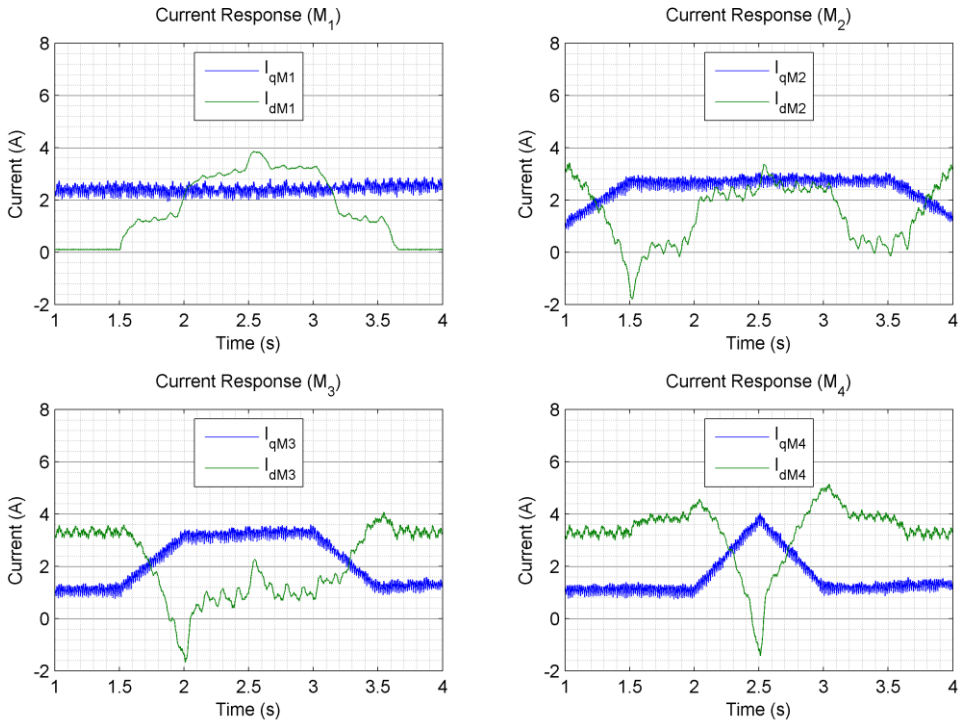

(b)

Figure 1.24 Résultats de simulation pour la stratégie sans sélection d'un maitre

Dans la thèse, nous avons conçu deux types différents de contrôleur pour le système MODMSAP et le système MOMMSAP. Ces deux solutions de commande reposent sur des principes identiques . Plutôt que de contrôler toutes les machines en même temps, il suffit de mettre l'une de ces machines en boucle fermée avec un contrôleur existant pour MSAP et laisser l'autre ou les autres en boucle ouverte. Ensuite, le courant I_d de la machine maître est utilisé pour mettre en œuvre notre stratégie de contrôle en prenant en compte la stabilité et l'efficacité énergétique. Pour la stabilité, nous nous sommes intéressé à l'existence du régime permanent c'est ce qui caractérise notre approche. Le processus d'optimisation qui minimise les pertes Joule du système détermine l'état optimal du système en donnant une valeur optimale de l'écart angulaire entre les deux machines dans le cas bi-machine. Pour le cas multi-machine l'action se fait en contrôlant le courant injecté sur l'axe d. Les simulations et les résultats expérimentaux montrent que la méthode de

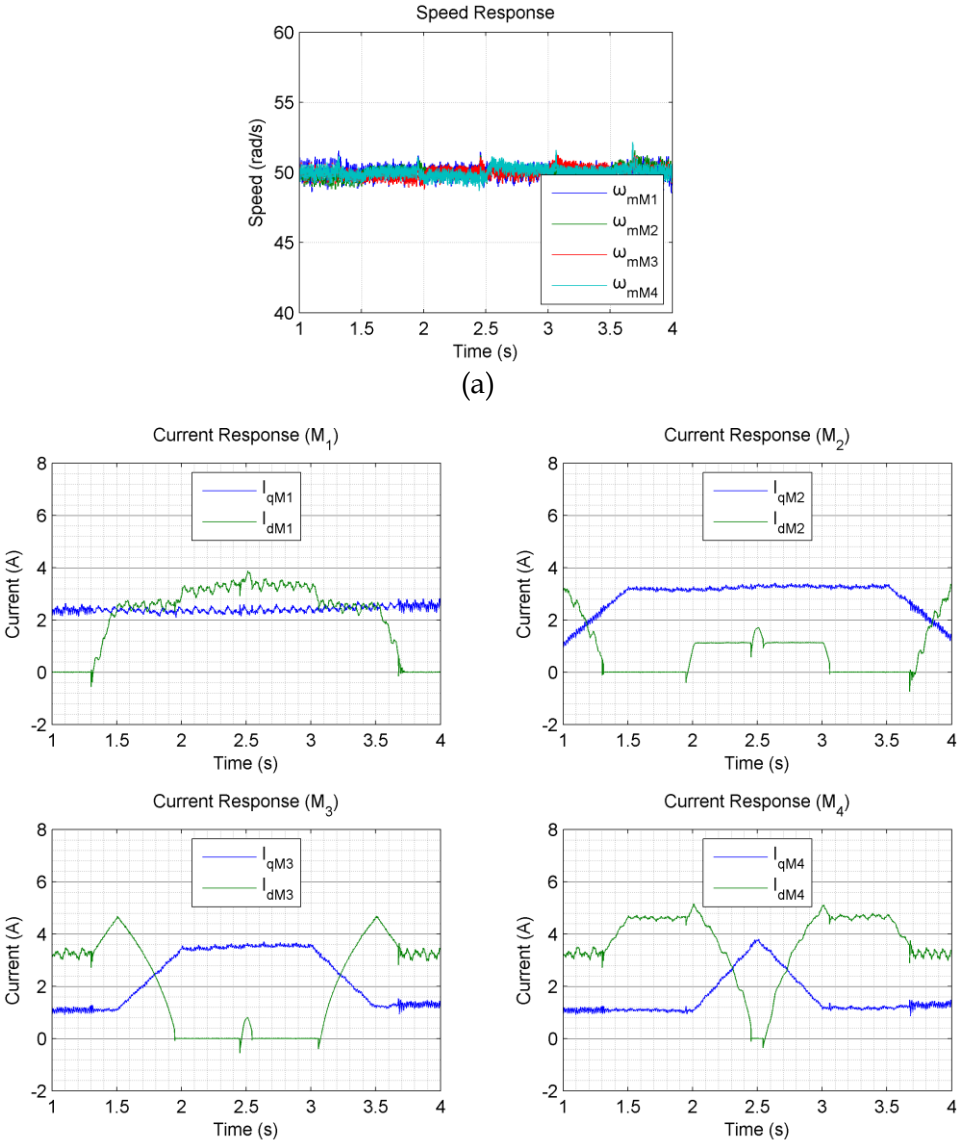

Figure 1.25 Résultats de simulation pour la stratégie avec sélection du maître

conception développée peut effectivement garantir la stabilité de plusieurs machines système.

Perspectives

D'une manière ce travail ouvre différentes perspectives comme :

La maitrise du comportement en régime transitoire.

La prise en compte d'autres pertes (pertes convertisseur, …) pour la minimisation des pertes et l'optimisation de l'efficacité énergétique.

L'extension de la commande optimale au cas multi-machine.

Le fonctionnement sans capteur mécanique

Le fonctionnement avec des machines différentes.

...

Table of contents

List of figures

List of tables

Chapter 1

Introduction

Table of content

1.1 **Research background**

During these decades, the electric motor has become a vital part of military, industry and civil applications. With the technology development, several types of motors have been invented, such as DC motor, induction motor (IM), synchronous motor, and so on. Among them, Permanent Magnet Synchronous Motor (PMSM) is a research hotspot due to the advantages of high power density, high efficiency, high reliability and simple structure, small volume and light weight. It can meet the requirements of high performance system (eg, fast dynamic response, wide speed range and high power-factor). PMSM uses a rotor structure similar to that of a DC motor. However, compared to a DC motor, PMSM overcomes its congenital defects and replaces the mechanical commutator with an electronic one. Therefore, PMSM has the advantages of a DC motor like good speed regulation performance as well as the advantages of AC motor of including simple structure, no spark, reliable operation and easy maintenance. Compared to the induction motor, there is no current in the rotor, so PMSM has a higher operating efficiency. The rotational speed is strictly equal to the electric frequency so its speed is easier to be regulated.

A PMSM must be connected to an inverter so that its position, speed and torque can be regulated. But sometimes, multiple PMSMs are used for the same purpose. For example, the bogie of a locomotive. It's a natural consideration that we can share some electronic components in the system so as to reduce the total weight and volume. The Mono-Inverter Multi-PMSM system (MIMPMSM) makes senses in these particular applications. These motors have the same speed and position in steady-state, but they must be subjected to different load torques. Unlike induction motor, which is naturally stable thanks to the slip [1][2], stability problem must be carefully considered for MIMPMSM system. Moreover, as the Maximum Torque Per Ampere (MTPA) method oriented for single PMSM cannot be adapted to a MIMPMSM system directly, efficiency optimization is also another problem. Although many researchers have given different controller solutions for the MIMPMSM system, most of them are not clear in the aspects of system stability and efficiency issues. This has become the biggest obstacle to the practical use of MIMPMSM. Therefore, the purpose of this work is to design a controller for MIMPMSM whose controllability, stability, and efficiency are fully studied and strictly proved. The proposals are then validated on a low-power experimental model (<500 w).

1.1.1 Architecture of a PMSM

A PMSM is mainly composed of two parts: stator and rotor. The stator contains a symmetrical three-phase winding and armature cores. The rotor is built up with a rotating shaft with permanent magnets installed on it. When a three-phase sinusoidal current acts on the stator coil, a magnetic flux of the same shape is generated in the gap between the stator and the rotor. The interaction between the stator flux and the rotor flux causes the

PMSM to generate electromagnetic torque.

Due to the different production processes and application requirements, PMSM has a different mechanical structure, which leads to different control principles. Depending on the back-EMF shape, we can generally classify the PMSM as being either trapezoidal or sinusoidal shaped back-EMF [3]. Figure 1.1 shows the difference.

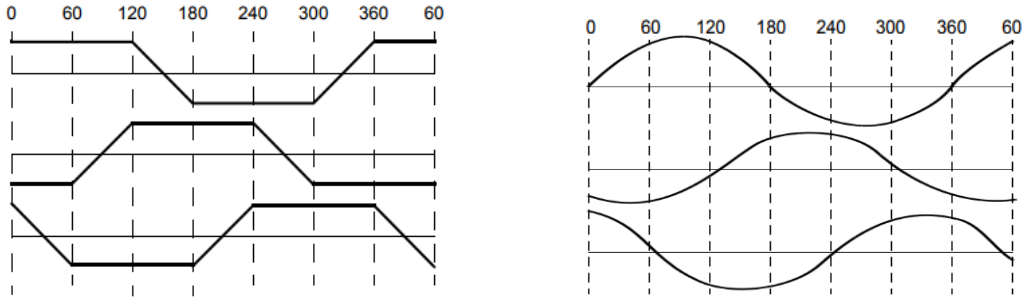

(a) (b)

Figure 1.1 Back-EMF shape of (a) BLDC motor. (b) BLAC motor

Correspondingly, the control strategy is either called Brushless DC (BLDC), whose phase current waveforms are essentially rectangular or trapezoidal, or Brushless AC (BLAC), whose phase current waveforms are essentially sinusoidal. In the case of BLDC, the phase currents only have to be commutated on and off so that it has a simple control strategy such as 6-step, hysteresis control, etc [4]. A low-cost Hall sensors are often used to sense the rotor position. On the other hand, BLAC requires a relatively high-cost resolver or encoder makes the phase current waveforms precisely controlled.

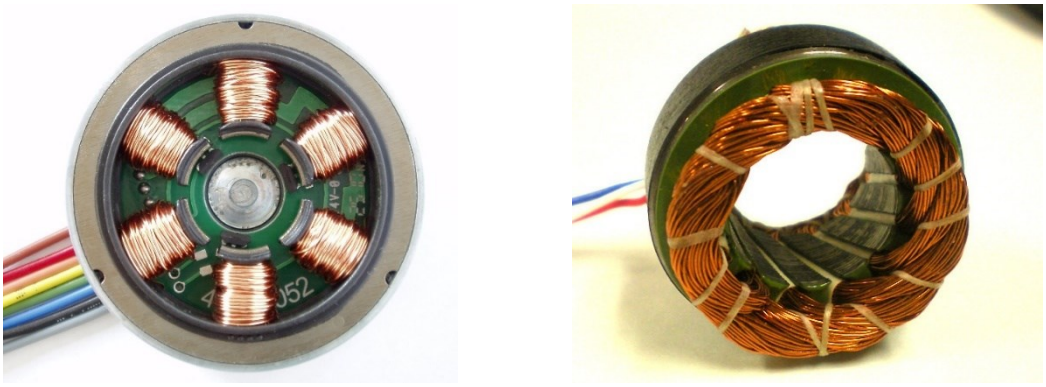

(a) (b)

Figure 1.2 Different stator coils configuration of a PMSM.

Although various rotor topologies and stator winding dispositions may exist, the major mechanical difference is the stator winding configuration [5]. BLDC motor predominantly have a concentrated nonoverlapping, fractional-slot, stator winding (Figure 1.2(a)). It has a higher torque ripple due to the difficulty in generating ideal trapezoidal phase current. So, it is mostly used in traction application, such as Electric Vehicle or UAV. While for BLAC, a distributed overlapping stator winding is generally used. It is used in high speed or position precision application, such as robotics and machine tools.

Another major difference is the Permanent Magnet (PM) mounting method on the rotor. Figure 1.3 illustrates their structure. In Figure 1.3(a), arc shaped PMs are mounted on the surface of the rotor. It is called Surface mounted PMSM, in short SPMSM. In Figure 1.3(b), PMs are buried in the cavities of the rotor core. They are called interior PMSM, in short IPMSM.

Surely, SPMSM has a limited mechanical structure strength. But from the point of view of magnetic, this structure has certain advantages. Because the air and magnet have almost the same permeability, the flux in d-axis and q-axis are equal. This means that the interaction between the rotor magnetic field and the stator magnetic field does not produce reluctance torque. On the contrary, the rotor structure of IPMSM enhances the mechanical strength, and makes the motor easier to perform field weakening control. It is more suitable for high-speed operation. However, the main drawback of the structural motor is the reluctance torque, which increases the complexity of the motor torque control as well as the installation and manufacturing process.

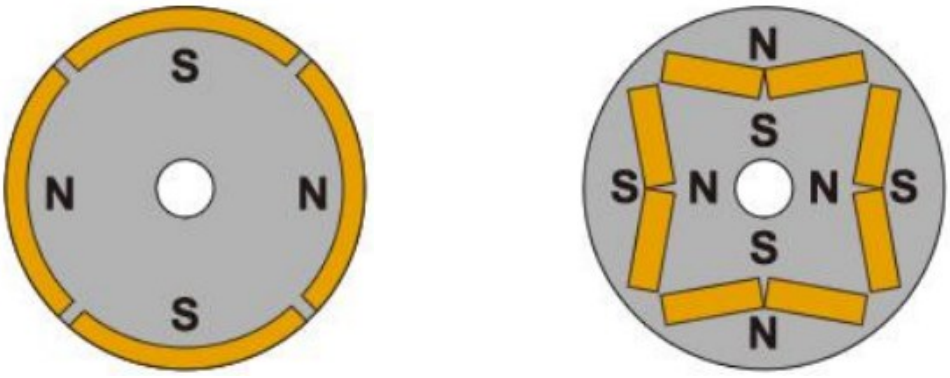

(a) (b)

Figure 1.3 Rotor structure illustration of (a) surface mounted magnet. (b) interior mounted magnet.

1.1.2 Characteristic of PMSM

- **High efficiency and power-weight ratio**

The most popular used electric machine in an electrical propulsion system are up to now IM and PMSM [5]- [7] . Compared to IM, because there is no current in the rotor [7], PMSM's rotor loss can generally be neglected. In the case of a traditional synchronous motor, PMSMs use permanent magnet rather than rotor excitation circuit to generate a constant rotor magnetic field. Therefore, the copper losses on excitation circuit no longer exists. This makes PMSM has a higher operating efficiency compared to other motors. As an example, Figure 1.4(a) and Figure 1.4(b) show the efficiency maps and speed-torque curves of the adopted IM and PMSM with rated power 40kw and 22.8kw respectively [9]. The PMSM has higher average efficiency than the IM in their respective operation speed ranges. Lastly, the PMSM has a greater ratio of operation area with efficiency over 90% than the IM.

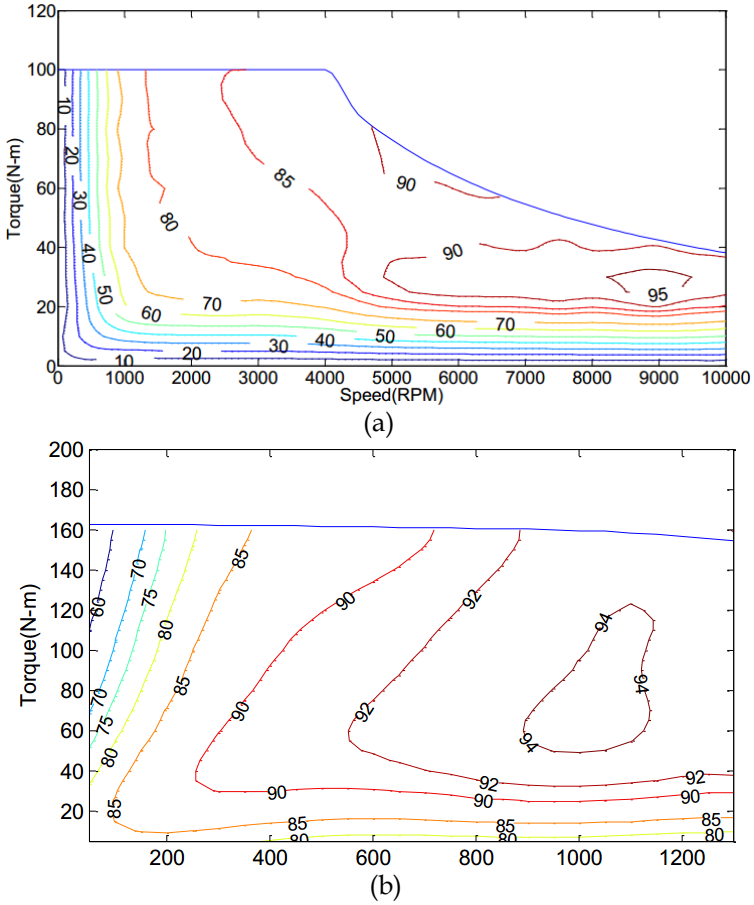

Figure 1.4 Efficiency map [9] of (a) the IM. (b) the PMSM.

Another advantage is that all heat of a PMSM is produced by the stator coil, which is much easier to perform cooling. This property is essential in high-power application.

- **High flux density and high torque-current ratio**

Recent advances in rear-earth magnets (NdFeB) gives the possibility in reaching a very high flux density. High flux density means we can achieve the same torque with less current (Ampère's Force Law), which leads to less copper losses in stator coil and higher efficiency. Meanwhile, a PMSM can produce a much higher torque than a IM can even their volume is the same. This characteristic makes many direct drive systems feasible. But drawback is also presented in high-speed situation (Faraday's law of induction). Flux weakening control must be implemented to extend its operation speed range, but its efficiency is low. Taken this into consideration, the synchronous excitation machines have reappeared in high speed-dynamic application, such as the electric vehicle (Renault ZOE).

- **Lower maintenance and high reliability**

Compared to a DC motor, PMSM overcomes its congenital defects and replaces the mechanical commutator with an electronic one. Therefore, PMSM has the advantages of a DC motor like good speed regulation performance as well as the advantages of AC motor of including simple structure, no spark, reliable operation and easy maintenance.

1.2 **Multi-PMSM System**

1.2.1 Introduction to Multi-PMSM System

Due to the lack of mechanical commutator, in order to control a PMSM, an inverter must be used to transfer a DC voltage to a sinusoidal three-phase voltage. Different structure of inverter may be used depending on application requirements, such as a 3-level 3-phase inverter [10], or a matrix inverter [11]. Here we only consider the most typical structure that a 2-level 3-phase inverter fed a PMSM (Figure 1.5).

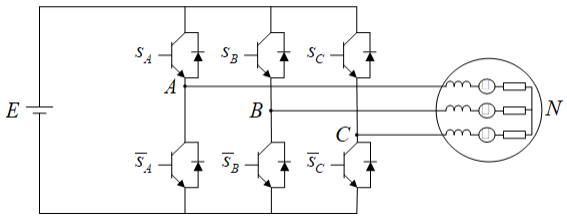

Figure 1.5 Structure of a 2-level 3-phase inverter connected to a PMSM

The state of two switches on the same leg is complementary making the phase voltage equals to V_{DC} or 0. By regulating the on-off state of three legs in the inverter, one can control the torque, speed, and position of a PMSM. In general, an inverter is required for each PMSM in the system. But sometimes, multiple PMSMs are employed in the same system. We may think that these motors can share some part of the driving structure so that the entire system weight and complexity decrease. Figure 1.6 shows the simplest architecture that all PMSMs connecting in parallel.

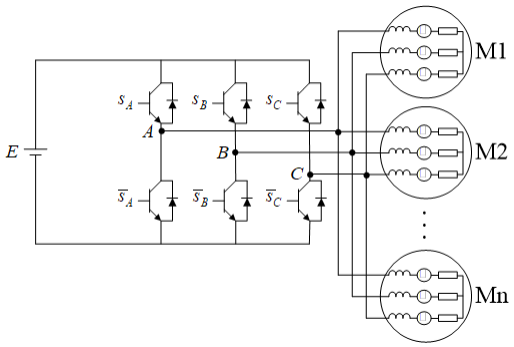

Figure 1.6 Parallel structure

In fact, the idea of shared architecture has been proposed decades ago, especially for an induction motor, and has made a lot of applications such as train traction [12], electric vehicle propulsion [1], etc. With the popularity of PMSM, the same concept, system architecture, and even control algorithms are also inherited and flourished by researchers. This main reason is that for an electrical system, the demand of reducing the number of components is conventional. Indeed, the more components used the more probability of failure. Although the current requirement may increase as the number of the motor increase, the complicity and weight of an inverter don't necessary increase with its power

capacity. Here we use SEIMENS MICROMASTER 420 inverter series as an example. Its frame size and weight are constant over a power rating from 0.12kw to 0.75kw.

Output Power	Rated input current	Rated output current	Frame size (L*W*H)	Order No.
kw	A	A	mm	
0.12	1.1	0.9	149*73*147	6SE6420-2UC11-2AA1
0.25	1.9	1.7	149*73*147	6SE6420-2UC12-5AA1
0.37	2.7	2.3	149*73*147	6SE6420-2UC13-7AA1
0.55	3.6	3.0	149*73*147	6SE6420-2UC15-5AA1
0.75	4.7	3.9	149*73*147	6SE6420-2UC17-5AA1

Thus, with such idea, we can reduce the weight and complicity of the entire system greatly. In this section, we will first give a general idea of what is a multi-PMSM system and its application. Then, some common shared architecture will be discussed including their structure, advantages and disadvantages.

1.2.2 Multi-PMSM Applications

4) Elevator doors [13]

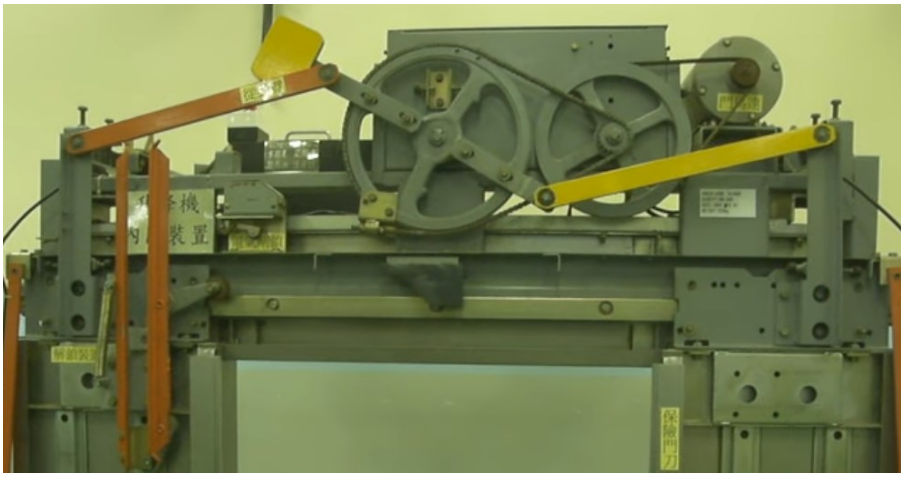

Figure 1.7 Typical driving mechanism of an elevator door opening on both sides

As shown in Figure 1.7, a conventional elevator door system has the two doors driven by a complex mechanical linkage. A motor in the right upper corner drives this mechanical system and consequently, the two doors will open and close together. This mechanical linkage system is obviously complex and easy to be failure. Instead, in the new design, each of the two doors of the elevator is actuated by a PMSM. These two motors must be fully synchronous both in normal operation and exceptional operation, for example, if one door is held, the other door must stop at the same position. Considering that a PMSM's speed is always synchronous to the voltage frequency, we may think that these motors can be put in parallel to share the inverter. On the one hand, we can eliminate the complex

mechanical linkage system. On the other hand, the complexity of the control algorithm is also reduced. Because if the two PMSMs run independently, the control algorithm must ensure their position and speed are fully synchronized. The parallel architecture does not need to consider these issues.

5) Rail transport

Because the track gauge, the worn wheel diameter and the ground clearance limit the space for a motor, in the propulsion system of a rail vehicle, a distributed traction system (Figure 1.8(a)) usually be used. Each wheel of the bogie must be equipped with a motor to meet the total traction power requirements. This makes this application ideal for a shared structure. In fact, in the case of an induction motor, the single inverter multi-motor drive system has been used widely in urban railway and subway traction system[12]. It has shown its advantages as low cost, light weight and compactness[1].

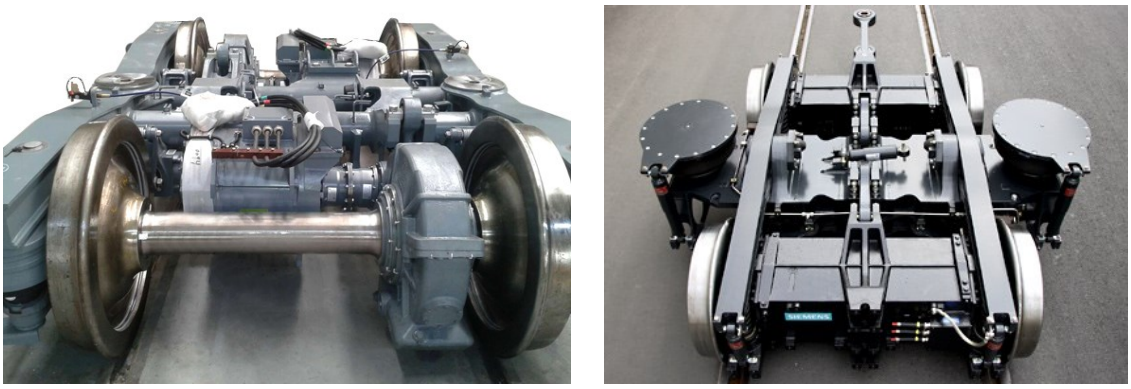

(a) (b)

Figure 1.8 Bogie structure of (a) gear drive traction. (b) gearless traction (Syntegra from Siemens)

During recent years, the idea of using PMSM as the core of a traction system has been developed for a metro or commuter train [14] and a high-speed train application [15]. In the conventional traction system, as shown in Figure 1.8 (a), a gear unit must be used to transfer the traction power from the motor to the wheel. But the characteristic of high torque-volume ration of a PMSM makes gearless traction drive system (Figure 1.8(b)) possible. Compared with the traditional transmission gear, gearless traction drive system can reduce the overall weight of the car and improve the transmission efficiency, while solve the transmission loss, noise and maintenance issues brought by transmission gear. With the successful application of induction-based shared architecture and the next generation of PMSM-based drive systems, it is foreseeable that the PMSM-based shared architecture has great potential for rail transit.

6) Aviation

Currently the flight control system still relays on mechanical power source, such as hydraulic, to drive the primary and secondary control surface, brake, landing gear, and many other essential functions, as illustrated in Figure 1.9. Under the concept of “More

Electric Aircraft"[16], the aviation domain is beginning focusing on replacing the mechanical power with electrical power. The current trend is to replace them with an electro-hydraulic actuators (EHAs) or an electromechanical actuators (EMAs)[17].

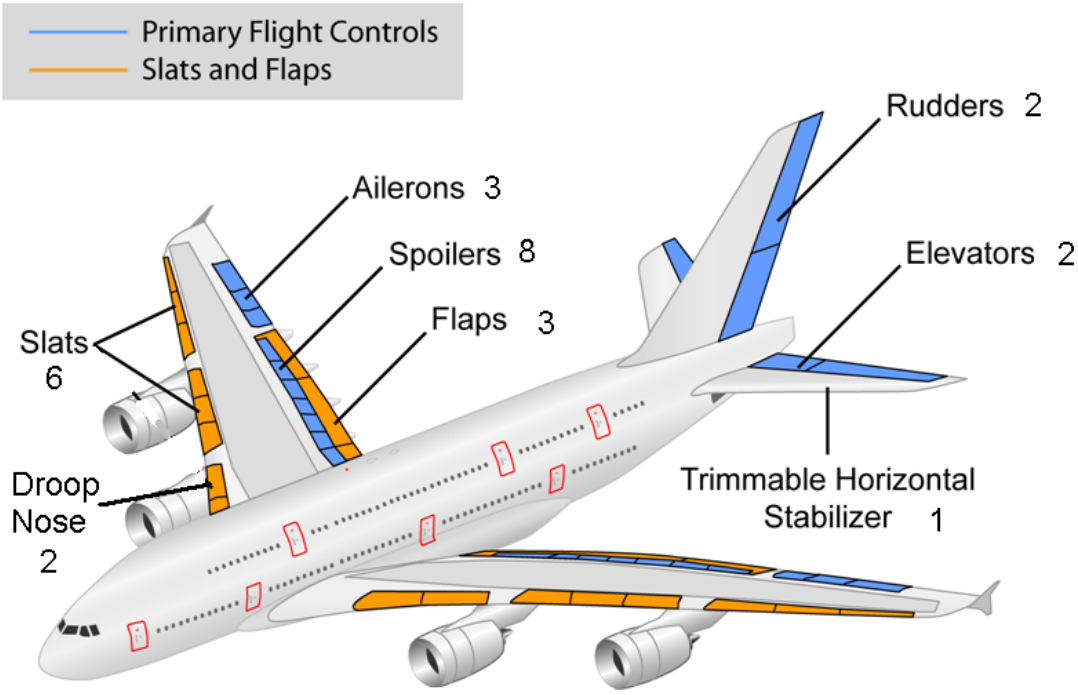

Figure 1.9 Control surface of A380.

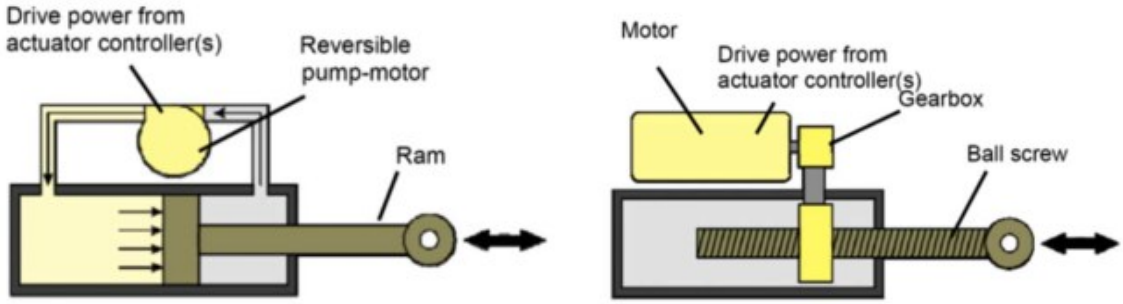

Figure 1.10 Structure diagram of (a) EHA system. (b) EMA system

Both EMA and EHA requires a motor and an inverter. But their working principle are not the same. As shown in Figure 1.10(a), the EHA system includes a reversible hydraulic pump, a hydraulic cylinder and a hydraulic tank. In contrast, the EMA does not use any hydraulic power but a gearbox and a mechanical system to convert the rotary motion into a linear motion. This allows the EMA motor to drive the control surface directly. Therefore, EMAs are more efficient than EHA and are a better choice for leak-free operation and reliability [18].

Shared architecture is very useful in the electrification of flight control system. First, aviation applications need failure-tolerance[19], especially the flight control system. For

example, the A320 has three independent hydraulic systems (green, yellow, and blue) to drive each part of the control surface of the aircraft. Each control channel (roll, pitch, yaw) can be driven by all three hydraulic systems. If an electrical actuator is used, each actuator must be equipped with multiple redundant drive systems. This will make the entire control system complex and heavy. While in the shared architecture using an inverter to drive multiple actuators, redundancy is only necessary for this inverter.

Second, some part of the control system only functions during a specified phase of flight. Such as deployment/retraction of the landing gear, leading-edge, and flaps that work only in the takeoff/landing phase. It is interesting to consider using sharing structures to operate individual systems according to the actual requirements while respecting the continuous condition of system.

Figure 1.11 Spoiler system of a commercial aircraft.

Third, multiple actuators are often assigned to drive the same object, such as an elevator, a spoiler or a flap (Figure 1.11). This evenly distributes the driving force on a long, thin control surface thereby increasing the effective aerodynamic force and reducing structural weight. These actuators are fully synchronous so the same idea of connecting PMSMs in parallel also makes sense here.

1.2.3 Different shared architecture

Depending on different requirements, shared architecture have a various structure that owns corresponding advantages and disadvantages. In this section, we will introduce and analyze some commonly seen PMSM shared architecture. Oriented from the applications introduced before, the most suitable structure will be selected as the study object of this thesis.

1.2.3.1 Sharing common legs: N motors with 2N legs

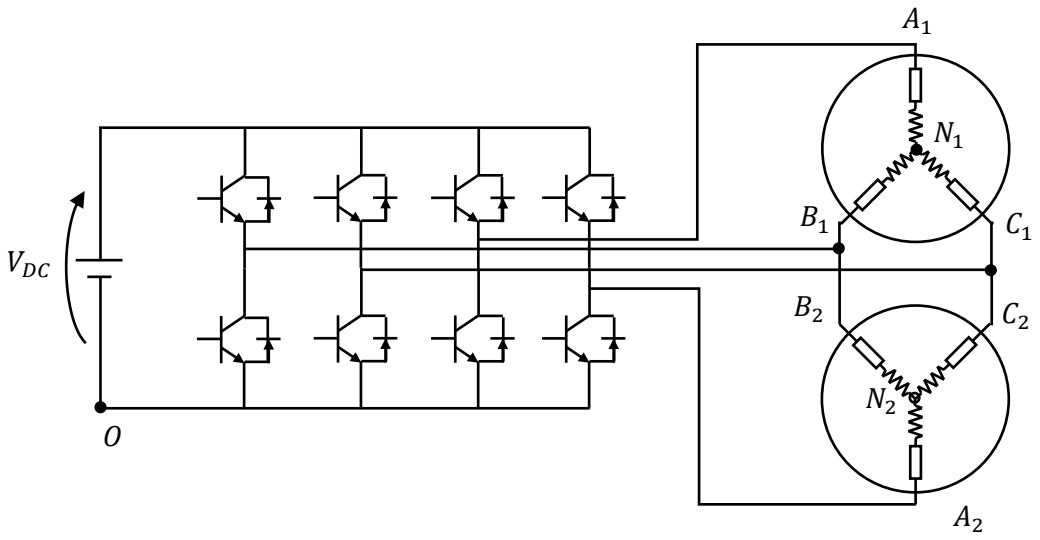

Figure 1.12 Two motors connecting to a 2-level 4-legs inverter by common legs structure

In this structure, some phases of the motors are connected together to the inverter. The rest phases connect individually to its own leg. As shown in Figure 1.12, in this case two motors must run at equal speed in Absolut value. It means that two motors can operate in the same or opposite directions. It is firstly introduced to mobile robot applications with induction motors [20].

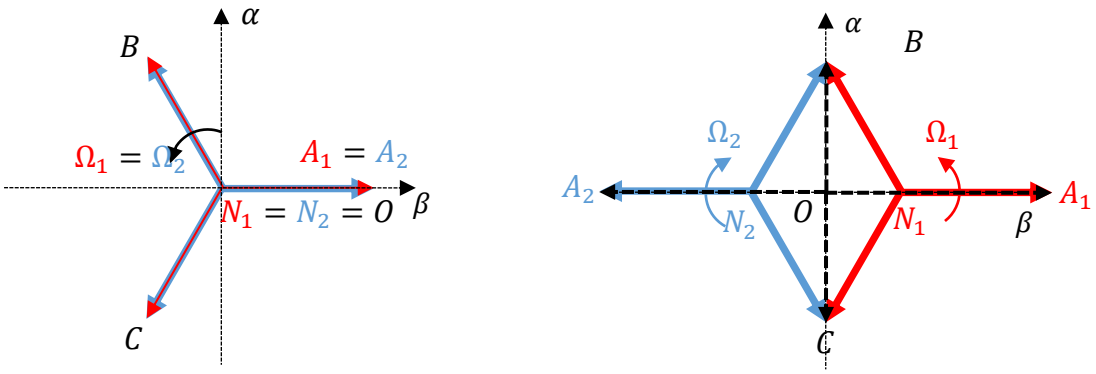

(a) (b)

Figure 1.13 Diagram of voltage vectors of (a) Same rotating direction. (b) Opposite rotating direction.

We can draw the voltage vector in the imaginary plane in order to better represent the principle. Figure 1.13 shows the voltage vectors of three phases of two motors under two cases:

(a) Rotating in the same direction. In this case $V_{B_2N_2} = V_{B_1N_1} \Longrightarrow \Omega_1 = \Omega_2$.

(b) Rotating in the opposite direction. $V_{B_2N_2} = -2V_{B_1N_1} \Longrightarrow \Omega_1 = -\Omega_2$.

1.2.3.2 Sharing common legs: N motors with 2N+1 legs

In another configuration, if only one phase of each motors is connected to the common legs, for example, a 2-level 5-phase inverter with 2 motors (Figure 1.14), all motors can run independently[21].

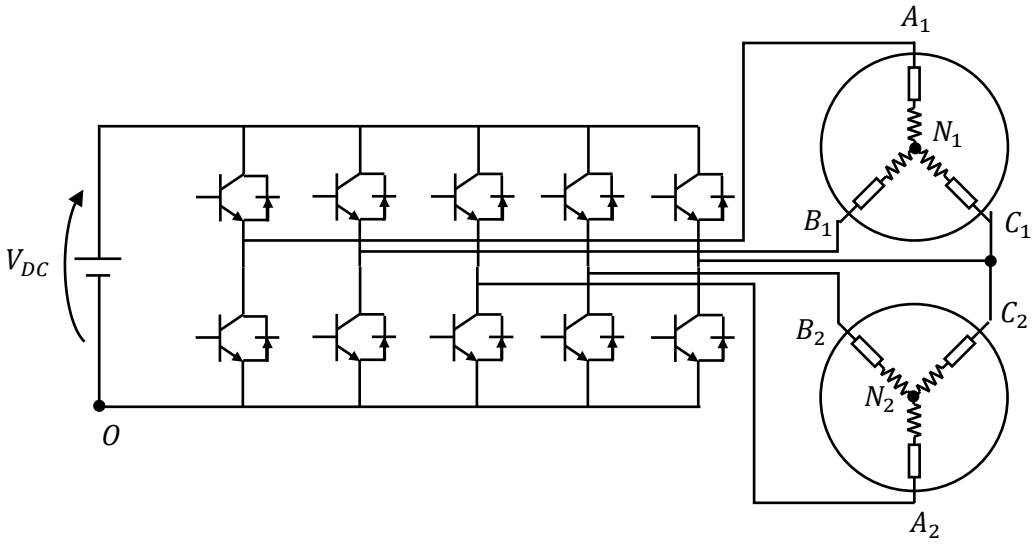

Figure 1.14 Two motors connecting to a 2-level 5-legs inverter by common legs structure

Figure 1.15 shows the corresponding voltage vector diagram.

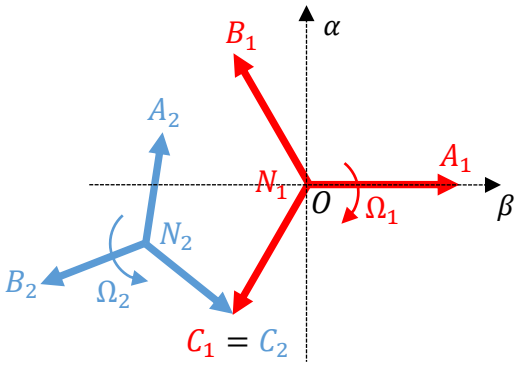

Figure 1.15 Voltage vectors diagram of 2-level 5-legs inverter driving 2 PMSMs

1.2.3.3 Sharing the midpoint structure

In this configuration, one phase of each motor will connect together to the middle point of the neutral point of the DC bus feeding the inverter. The rest two phases of each motor connect to their own legs.

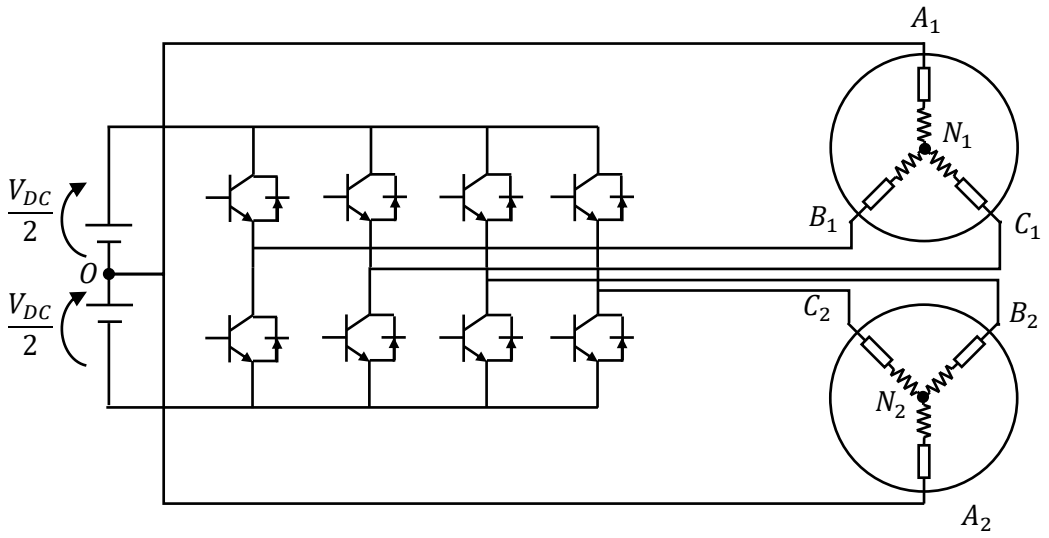

Figure 1.16 Two motors connecting to a 2-level 4-legs inverter by midpoint structure

Under this configuration, each motor can operate at its own speed [22][23]. As in the case of using common legs, the reference voltage applied to the inverter's legs will differ from the voltage calculated by the regulator. Here we give a short demonstration of this characteristic.

Because for each motor, one phase is connected to the neutral point *O*, V_{OA1} and V_{OA2} is always equal to V_O, while V_{OB1}, V_{OC1}, V_{OB2}, V_{OC2} can be regulated. Thus, **for each machine**, we can have this relationship:

$$V_{A_iN} + V_{B_iN} + V_{C_iN} = 0 \tag{1.1}$$

where i indicates the index of the motor. Then we can express the phase voltage respect to the line voltage.

$$\begin{cases} V_{A_iN} = \frac{2}{3}V_{A_iO} - \frac{V_{B_iO} + V_{C_iO}}{3} \\ V_{B_iN} = \frac{2}{3}V_{B_iO} - \frac{V_{A_iO} + V_{C_iO}}{3} \\ V_{C_iN} = \frac{2}{3}V_{C_iO} - \frac{V_{A_iO} + V_{B_iO}}{3} \end{cases} \tag{1.2}$$

Under this configuration, we can conclude that the following constraints is always valid:

$$\begin{cases} V_{A_1O} = V_{A_2O} = \cdots = V_O \\ V_{B_1O} = V_{B_2O} = \cdots = V_{BO} \\ V_{C_1O} = V_{C_2O} = \cdots = V_{CO} \end{cases} \tag{1.3}$$

Replace the corresponding elements in (1.2) with (1.3), the phase voltage of each motor

can be obtained.

$$\begin{cases} V_{A_iN} = -\frac{1}{3}\left(V_{B_iO} + V_{C_iO}\right) \\ V_{B_iN} = \frac{2}{3}V_{B_iO} - \frac{1}{3}V_{C_iO} \\ V_{C_iN} = \frac{2}{3}V_{C_iO} - \frac{1}{3}V_{B_iO} \end{cases} \tag{1.4}$$

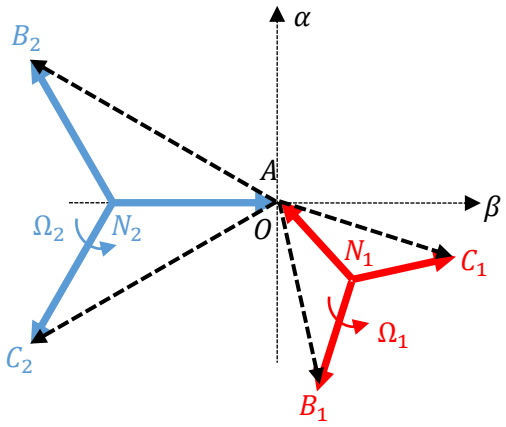

Figure 1.17 Voltage vector diagram of a 4-legs inverter driving 2 PMSMs in midpoint structure

It is easy to conclude from the voltage vector diagram (Figure 1.17) that the 2 legs corresponding to one motor must be regulated with the same amplitude but 60 degrees in phase difference (shown as the black vector). The voltage amplitude corresponding to a balanced tri-phase system is reduced by $\frac{\sqrt{3}}{3}$. Its major advantage is that the motors can operate independently with each other, while the number of electronic components can be reduced. But its disadvantage is also obvious because connecting to the exact middle point of DC bus voltage is mandatory that is usually not easy to be achieved. Otherwise, if there is voltage offset, there will be power consumption on the winding coil. Here is the prove. Assume that there is voltage offset ΔV_{DC}, as shown in Figure 1.18.

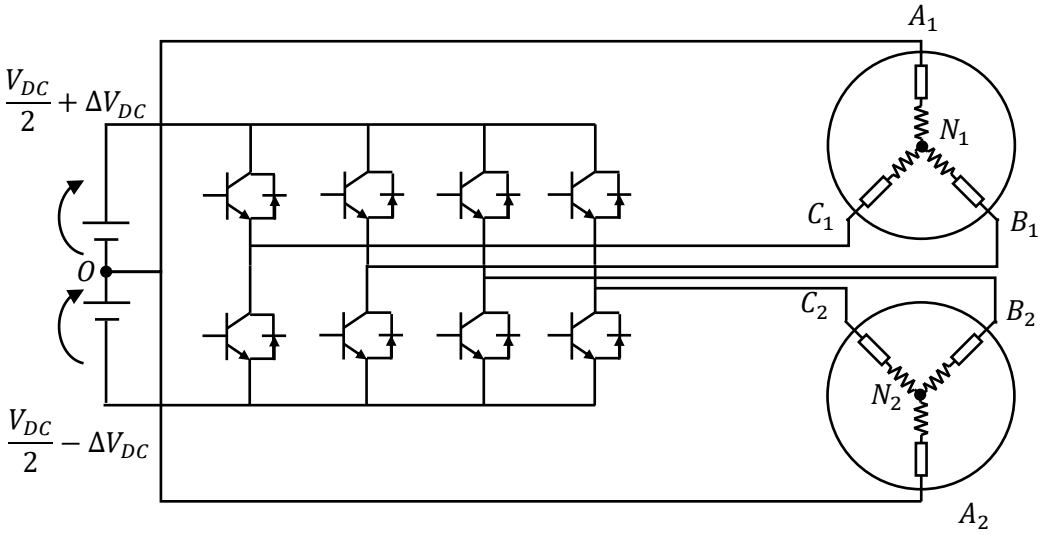

Figure 1.18 Midpoint structure with unbalanced voltage

The output voltage of each leg can be assumed as:

$$\begin{cases} V_{B_iO} = \Delta V_{DC} + \frac{V_{DC}}{2} cos\left(\theta(t) - \frac{5}{6}\pi\right) \\ V_{C_iO} = \Delta V_{DC} + \frac{V_{DC}}{2} cos\left(\theta(t) + \frac{5}{6}\pi\right) \end{cases} \tag{1.5}$$

Then insert (1.5) into (1.4), the phase voltage of each motor becomes:

$$\begin{cases} V_{A_iN} = -\frac{2}{3}\Delta V_{DC} + \frac{\sqrt{3}}{6} V_{DC}\, cos\big(\theta(t)\big) \\ V_{B_iN} = \frac{\Delta V_{DC}}{3} + \frac{\sqrt{3}}{6} V_{DC}\, cos\left(\theta(t) - \frac{2}{3}\pi\right) \\ V_{C_iN} = \frac{\Delta V_{DC}}{3} + \frac{\sqrt{3}}{6} V_{DC}\, cos\left(\theta(t) + \frac{2}{3}\pi\right) \end{cases} \tag{1.6}$$

From (1.6) we can conclude that each phase involves a constant voltage that cause continuous current on phase resistance. This current only relates to ΔV_{DC} and will cause huge power dissipation on the winding resistance.

1.2.3.4 Mixed structure

As its name presents, the mixed structure is a combination of two structures mentioned above. According to this structure, as shown in Figure 1.19, a three-legs inverter is used to drive two motors. In one hand, like the common leg structure, one phase of each motor (phase C_1 and C_2 in Figure 1.19) will be connected to the common leg of the inverter. On the other hand, like the midpoint structure, another phase of each motor (phase A_1 and A_2 in Figure 1.19)will be connected the neutral point O of the DC bus. The third phase is connected to its own legs of the inverter.

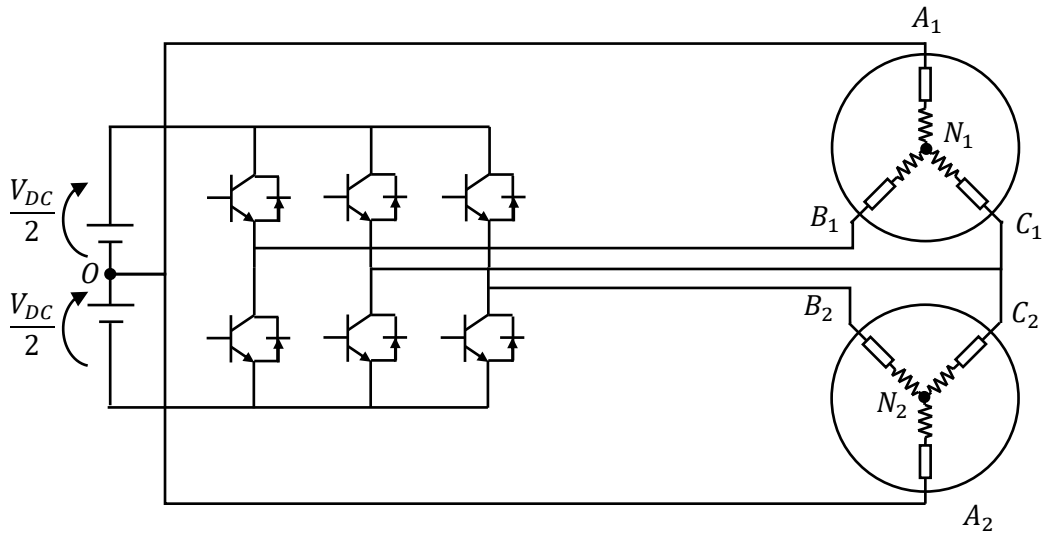

Figure 1.19 Mix structure with two motors

Under this configuration, we can conclude that the following relationship is always valid:

$$\begin{cases} V_{A_1O} = V_{A_2O} = \cdots = V_O \\ V_{C_1O} = V_{C_2O} = \cdots = V_{CO} \end{cases} \tag{1.7}$$

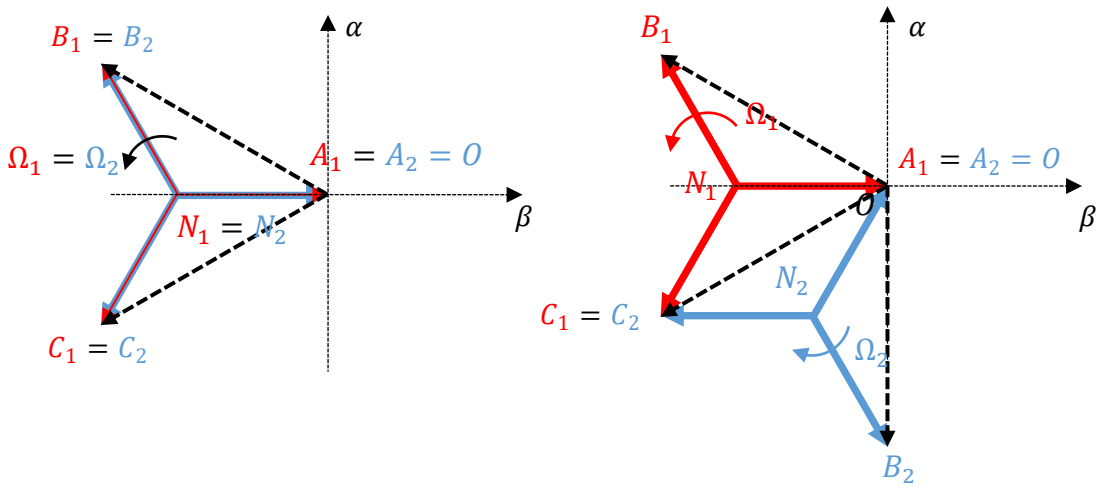

(a) (b)

Figure 1.20 Diagram of voltage vectors of (a) Same rotating direction. (b) Opposite rotating direction.

Figure 1.13 demonstrates the voltage vector diagram. Similar with the common leg structure, in such configuration there are two possibilities:

(a) Rotating in the same direction. In this case $V_{B_1O} = V_{B_2O} \Longrightarrow \Omega_1 = \Omega_2$.

(b) Rotating in the opposite direction. $V_{B_2O} = V_{B_1O} e^{j\frac{\pi}{3}} \Longrightarrow \Omega_1 = -\Omega_2$.

The corresponding reference voltage of each legs can be identified as the black vector in the diagram.

1.2.3.5 Parallel structure

This structure is the simplest in hardware configuration. In this configuration, a basic 2-level 3-legs inverter is used with each PMSM's corresponding phase connected together. No modification should be done to the motor. All motors receive exactly the same voltage both in frequency and amplitude. Figure 1.21 illustrates this configuration.

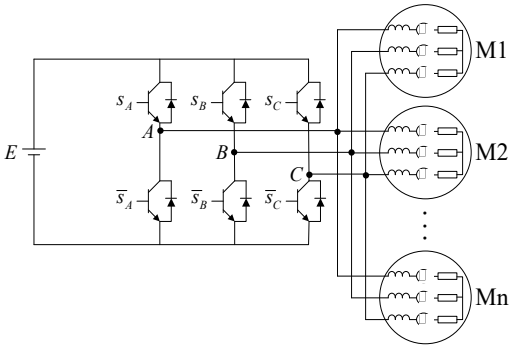

Figure 1.21 Parallel structure

But its disadvantages are also obvious. The connected motor can only operate at the same speed in steady-state. During transit situation, their speed and position may be different. Compared to the previous structure, it is impossible to control all phase voltage of these motors. Stability problem must be carefully considered when designing the controller.

1.2.3.6 Comparison of these different structures

Structure's Name	Number of legs for N motor	Degree of freedom of speed	Advantages	Disadvantages
Common legs: N motor with 2N legs	2N	$\Omega_1 = \Omega_2$ or $\Omega_1 = -\Omega_2$	Easy to implement	Over current in common legs (custom inverter needed)
Common legs: N motor with 2N+1 legs	2N+1	Independent	Independent speed operation	Over current in common legs (custom inverter needed)
Midpoint	2N	Independent	Independent speed operation	Access to neutral point is mandatory but not easy
Mixed	N+1	$\Omega_1 = \Omega_2$ or $\Omega_1 = -\Omega_2$	Less legs needed compared to the previous	Inherit from the previous
Parallel	3	$\Omega_1 = \Omega_2$	Easy to implement No hardware modification required	Not easy to control

Table 1.1Summary of different structure

In previous section, many different structures of shared architecture have been

introduced. Their characteristic and advantages/disadvantages are summarized in Table 1.1.

Each structure has its advantages and disadvantages. We must choose the most suitable one depending on the application. By comparison, we can see that the parallel architecture is best suited compared to other architectures. In our applications, all PMSM runs at the same speed. The common leg structure provides a little more degree of freedom, but these degrees of freedom are of no benefit in our cases except extra weight. Moreover, the current on the common leg is much higher than other legs which means the inverter must be customized. Using commonly used commercial inverters will lead to huge waste in capacity. The midpoint scheme allows the two motors to run independently using only a four legs inverter, but it requires that the midpoint O be strictly on the neutral voltage of the DC bus. Otherwise, it will cause the stator windings to continue to heat. In practice, it is very difficult to maintain two high-power DC voltage to be strictly consistent, and this will lead additional expenses on other hardware that not worth the candle.

Another important criterion is that the ratio between maximum voltage that a motor can receive ($V_{N_i}^{max}$) and inverter's maximum output voltage (V_O^{max}). Denote the ration as $\eta_\gamma = \frac{V_{N_i}^{max}}{V_O^{max}}$. Only the parallel structure can have $\eta_\gamma = 1$, while for other structure η_γ is always less than 1. This means that the power capacity of an inverter is reduced compared to that of classical structure.

The parallel structure uses the simplest hardware architecture and makes no need to make any changes to the existing equipment. But because of its degree of freedom relative to other architectures the lowest, its stability and performance problems are relatively more difficult to deal with. This is the main problem to be discussed in this thesis.

1.3 State-of-art control strategies for MIDPMSM system

In the parallel structure, although these machines have the same speed and position, they must be subjected to different load torques. As there is only one voltage source, the torque controller must be able to find out the best compromise respecting the torque reference and ensure the stability of all the motors. In the previous researches, people decide to start with the simplest case: 2 motors, which is called Mono-Inverter Dual-PMSM system (MIDPMSM), to explore the possibility of controlling this special system. In this section, we only give a brief introduction to these works so that we can understand how these control strategies are designed and what is the major problem of them. A more detailed introduction to these control strategies is available in Chapter 2.

The first study of the MIDPMSM system is proposed by John Chiasson in 2002 [13]. In

this paper, two motors are mechanically linked, which is not exactly the same as it is in this thesis. But he has obtained an important conclusion by studying the solution existence problem of the steady-state equations: the ability to control independent torques comes from the electrical angle displacement between two motors. This conclusion forms the feasibility and controllability criterion of this system.

In 2011, LAPLACE laboratory in Toulouse has proposed the *Master-slave* strategy[24]. It is also protected by patent [25]. It handles the MIDPMSM system by separating the two motors as master motor and slave motor. Only the master motor is closed-loop controlled, while the slave motor is left open-loop operating. The master selection is not permanent but based on the open-loop stability, which is an important stability criterion of the MIDPMSM system. Under this criterion, at each control instant the *Master-slave* strategy selects the more loaded motor as the mater so that the system stability is preserved.

As proposed in [26]-[32], the *Average* strategy is a large branch in the remaining control strategies. It is very intuitive but there is some difference in the actual implementation. [26]-[29] uses the algebra average of the current and rotor position. While in [30]-[32], which is also called $\Sigma - \Delta$ strategy, uses vector sum (Σ) and subtraction (Δ) of the d-q current in order to improve steady-state and transient performances. The average process can be also applied in the output stage, which use two independent control loops for two motors and apply the average value of their output to the inverter. These control strategies are not new because they have already been proposed for a Mono-Inverter Dual-IM system, such as [33][34]. Researchers have actually extended them to MIDPMSM system. The major problem is that these control strategies only work when the angle difference between the rotor flux is not huge. It is not a problem in IM because there is speed slip. But in the case of a PMSM, stability problem may occur as the torque does not necessarily increase when its speed decreases in a transient situation.

Direct Torque Control (DTC) is also extended to the MIDPMSM system in [35]. It divides the space vector plane is into 12 sectors of 30° each of four input information are considered, two related to the flux of each motor and two related to the torque. Based on these 16 combinations in 12 different sectors, a switching table is proposed to determine the best vector of voltage to be applied by the inverter. It is not an optimal solution for a MIDPMSM system because the look-up table is huge.

At the same time, some researchers [36]-[38] have tried to adapt *Model Predictive Control* (MPC) [39] to MIDPMSM system. It formulizes the control problem into an optimization problem that predicts the future behavior of a system and determines the optimal control output through minimizing a criterion which gives us an arbitration in selecting different control strategies. Among them, [36] has adapt the *Predictive Torque Control* (PTC) for single PMSM to MIDPMSM system by replacing the cost function with the algebra sum of the cost function of each motor. In [37], Space Vector Pulse Width Modulation (SVPWM) [40] is used to extend the possible control set in purpose of reducing the current ripple.

[38] has proved the optimal voltage vector for two motors is just the algebra average value of optimal voltage vectors of each motor. Based on this conclusion, a dead-beat controller is given. The major difference between them is the voltage vector modulation method, which in other word is the voltage vector used in optimization. The more voltage vector used, the better the cost function is minimized. Also, experiments [41][42] have shown that these control strategies have low efficiency problem. The cause lays in the cost function. An algebra sum of two cost functions oriented for single PMSM is used. But it actually over constraints the system so that the optimization process only gives out a compromised solution, which is the root cause of the low efficiency problem. In chapter 2, this problem and its solution will be discussed in detail.

1.4 **Overview of the thesis**

This thesis is organized as follows:

In Chapter I, we have introduced the application and different configuration of a MIMPMSM system. Also, a bare introduction to all proposed control-strategies is given.

Chapter II paves the way for the following chapters. In the first place, we have built the model of a MIDPMSM system step-by-step. Then all proposed control-strategies are introduced in detail. An experiment is carried to verify the feasibility and performance of them. Some numerical indicators describing different aspects of an electric system are used to precisely compare these control strategies. In final, based on the experiment data, we have figured that the over-constraint problem exists in some control strategies, which has resulted in a mismatch between the current reference and response. As a breakthrough, this conclusion leads to a new controller analysis and design method.

Chapter III mainly describes how to design an efficiency-optimal controller for MIDPMSM system. Through analyzing the solution existence problem of the steady-state model, we can obtain the structure of the controller and prove the system controllability. Then, Lagrange multiplier is used to calculate the efficiency-optimal state. The analytical solution of this optimal-state is given. Open-loop stability characteristic is used to calculated the stable region.

In Chapter IV we have tried to extend this design method to a MIMPMSM system with more than 2 motors in parallel. The simulation results show this design method is also valid in this case.

1.5 **Conclusion**

In section 1.1, we have introduced several different stator windings and rotor designs for PMSM. BLDC motors are typically used for traction applications, while BLAC motors are typically used for actuator applications due to a smoother torque output relative to

BLDC. In order to simplify the analysis, we will only consider SPMSM in this thesis. Thus, a BLAC with surface-mount permeant magnet is studied in this thesis.

In 1.2 we have introduced the multi-PMSM system including some of its typical application and some common structure sharing scheme as well as its advantages and disadvantages. In our applications, multiple actuators are often used to drive the same control object so that the position and speed of these actuators are synchronized. Considering these factors, the parallel structure is selected as the most suitable one as it uses the simplest hardware architecture and makes no need to make any changes to the existing equipment.

After that, for such a MIDPMSM system, we have summarized up all the previous studies in this area in the purpose of understanding how these control strategies are designed and what is the major problem of them. The brief analysis of these control strategies shows that the major problem is lack of strict theoretical basis, especially the controllability and stability. Moreover, as the MTPA method cannot be adapted to a MIDPMSM system directly, efficiency optimization is also another problem. The main contribution of this thesis is to propose a comprehensive yet simple efficiency-optimal controller to the MIMPMSM system. Problems of system controllability, stability limitations, and efficiency-optimization are well proved and solved under the same framework.

Chapter 2

Control strategies for Mono-Inverter Dual PMSM system - evaluation and analysis

Table of content

2.1 Introduction

In the previous chapter, a brief introduction to the MIDPMSM system is given. This introduction gives us some initial impressions and we have chosen the parallel structure as our study object. Meanwhile, we have made a brief summary of the existing control strategies and summed up their weaknesses, which leads to the research direction of this thesis. In order to pave the way for the following chapters. In this chapter, we start with modelling the MIDPMSM system in parallel structure. This section includes the definition of the d-q transform, the model of a 2-level 3-leg inverter and of a single SPMSM in d-q frame. Through merging two models of SPMSM, we can obtain the model of a MIDPMSM system. Based on this model, its controllability is proved.

After that, we will introduce the existing control strategies in detail. Then, an experiment is carried to verify the feasibility and performance of them. Some numerical indicators describing different aspects of an electric system are used to precisely compare these control strategies. In final, based on the experiment data, we have figured that the over-constraint problem exists in some control strategies, which has resulted in a mismatch between the current reference and response. As a breakthrough, this conclusion leads to a new controller analysis and design method.

2.2 Model of MIDPMSM system

As introduced in Chapter 1, a multi-PMSM system can has various of structure, such as connected in series, in parallel or share legs. In this part, the simplest structure which consists of a 2-level 3-legs inverter and two PMSMs connected parallel is studied. Its structure is shown in Figure 2.1.

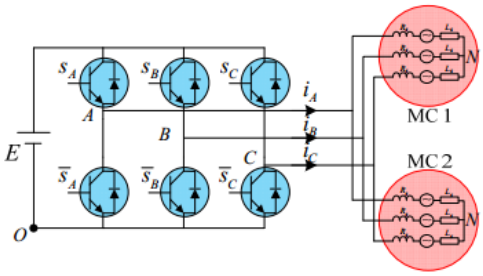

Figure 2.1 A 2-level 3-phase inverter driving 2 PSMSs in parallel

Its model, including the inverter and the two motors, is built step by step in this part.

2.2.1 Coordinate definition

A three-phase AC power supply is used to drive a PMSM. But people usually use α-β transform or d-q transform to simplify the calculation and analysis. A three-phase component can be represented by a vector in Cartesian coordinate system after such

transform. But in practice, the coefficients of these transformations are different depending on whether amplitude invariant or power invariant law is used. This difference will influence the PMSM's parameters in the model, the calculation of its torque and power, and so on. So, in this part, we use the principle of constant power, the coordinates of the transformation were defined in detail to avoid ambiguity

2.2.1.1 α-β transform

The α-β transform is a mathematical transformation that transfers tri-phase quantities into a rotating vector in Cartesian coordinate so as to simplify the analysis of three-phase circuits. For example, if the phase voltages of a tri-phase system are defined as:

$$\begin{cases} V_a = V_p \cos\theta(t) \\ V_b = V_p \cos\left(\theta(t) - \frac{2}{3}\pi\right) \\ V_c = V_p \cos\left(\theta(t) + \frac{2}{3}\pi\right) \end{cases} \tag{2.1}$$

where V_p refers to the peak value of phase voltage. Then the α-β transform is defined as:

$$\begin{bmatrix} V_\alpha \\ V_\beta \\ V_o \end{bmatrix} = \frac{2}{3}\begin{bmatrix} 1 & -\frac{1}{2} & -\frac{1}{2} \\ 0 & \frac{\sqrt{3}}{2} & \frac{\sqrt{3}}{2} \\ 1 & 1 & 1 \end{bmatrix}\begin{bmatrix} V_a \\ V_b \\ V_c \end{bmatrix} = V_p \begin{bmatrix} \cos\theta(t) \\ \sin\theta(t) \\ 0 \end{bmatrix} \tag{2.2}$$

Obviously (2.2) transfer a three-phase quantity into a rotating vector with the amplitude equals to the peak phase voltage (amplitude is not changed during transformation). V_o corresponds to the middle point voltage, it is normally negeleted because the three-phase quantity is fully balanced. While its invers-transform is:

$$\begin{bmatrix} V_a \\ V_b \\ V_c \end{bmatrix} = \begin{bmatrix} 1 & 0 \\ -\frac{1}{2} & \frac{\sqrt{3}}{2} \\ -\frac{1}{2} & \frac{\sqrt{3}}{2} \end{bmatrix}\begin{bmatrix} V_\alpha \\ V_\beta \end{bmatrix} \tag{2.3}$$

2.2.1.2 d-q Transform

d-q transform makes its coordinate rotating synchronous to a three-phase system in an effort to further simplify the analysis of three-phase circuits. Thanks to this transformation, triphase quantity can be represented by a static vector in Cartesian coordinate. Based on α-β transform, d-q transform can be simply defined as (2.4).

$$\begin{bmatrix} V_d \\ V_q \end{bmatrix} = \begin{bmatrix} \cos\theta(t) & \sin\theta(t) \\ -\sin\theta(t) & \cos\theta(t) \end{bmatrix}\begin{bmatrix} V_\alpha \\ V_\beta \end{bmatrix} \tag{2.4}$$

And consequently, the transform from a tri-phase quantity can be obtained through

replacing V_α and V_β by (2.2). The result is shown in (2.5).

$$\begin{bmatrix} V_d \\ V_q \end{bmatrix} = \frac{2}{3}\begin{bmatrix} cos\,\theta(t) & cos\left(\theta(t)-\frac{2}{3}\pi\right) & cos\left(\theta(t)+\frac{2}{3}\pi\right) \\ -sin\,\theta(t) & -sin\left(\theta(t)-\frac{2}{3}\pi\right) & -sin\left(\theta(t)+\frac{2}{3}\pi\right) \end{bmatrix}\begin{bmatrix} V_a \\ V_b \\ V_c \end{bmatrix} \tag{2.5}$$

And its inverse transform is:

$$\begin{bmatrix} V_a \\ V_b \\ V_c \end{bmatrix} = \begin{bmatrix} cos\,\theta(t) & -sin\,\theta(t) \\ cos\left(\theta(t)-\frac{2}{3}\pi\right) & -sin\left(\theta(t)-\frac{2}{3}\pi\right) \\ cos\left(\theta(t)+\frac{2}{3}\pi\right) & -sin\left(\theta(t)+\frac{2}{3}\pi\right) \end{bmatrix}\begin{bmatrix} V_d \\ V_q \end{bmatrix} \tag{2.6}$$

2.2.1.3 Power calculation issues

As above mentioned, the magnitude of the vector equals to the peak phase value during transformation, which is:

$$\left|\vec{V}_{\alpha\beta}\right| = V_p \tag{2.7}$$

$$\left|\vec{I}_{\alpha\beta}\right| = I_p \tag{2.8}$$

V_p and I_p refers to the peak value of phase voltage and current. In a balanced tri-phase system, its power can be expressed as:

$$P = \frac{3}{2}V_p I_p\, cos\,\varphi \tag{2.9}$$

where $\cos\varphi$ is the power factor. It can be noticed that when calculating the power of a tri-phase system, a coefficient $3/2$ must be added if peak phase value is used. In pursuit of better simplifying the model, it is preferred that, after α-β transform or d-q transform, the dot product of the obtained voltage and current vectors equal to the power (as shown in (2.10)).

$$P = \overrightarrow{V'_{\alpha\beta}} \cdot \overrightarrow{I'_{\alpha\beta}} = \left|\overrightarrow{V'_{\alpha\beta}}\right| \left|\overrightarrow{I'_{\alpha\beta}}\right| cos\,\varphi \tag{2.10}$$

Thus, a coefficient must be added when performing coordinate transform. Refer to (2.9) and (2.10), the coefficient (shown in (2.11)) can be easily obtained.

$$\begin{cases} \left|\overrightarrow{V'_{\alpha\beta}}\right| = \sqrt{\frac{3}{2}} V_p \\ \left|\overrightarrow{I'_{\alpha\beta}}\right| = \sqrt{\frac{3}{2}} I_p \end{cases} \tag{2.11}$$

This means that once the coefficient $\sqrt{\frac{3}{2}}$ is applied during the coordinate transform, the obtained vectors can be used directly in power calculation like they are in a DC circuit. The modified alpha-beta and d-q transform are listed below:

$$\begin{bmatrix} V_\alpha \\ V_\beta \end{bmatrix} = \sqrt{\frac{2}{3}} \begin{bmatrix} 1 & -\frac{1}{2} & -\frac{1}{2} \\ 0 & \frac{\sqrt{3}}{2} & \frac{\sqrt{3}}{2} \end{bmatrix} \begin{bmatrix} V_a \\ V_b \\ V_c \end{bmatrix} \tag{2.12}$$

$$\begin{bmatrix} V_d \\ V_q \end{bmatrix} = \sqrt{\frac{2}{3}} \begin{bmatrix} cos\,\theta(t) & cos\left(\theta(t) - \frac{2}{3}\pi\right) & cos\left(\theta(t) + \frac{2}{3}\pi\right) \\ -sin\,\theta(t) & -sin\left(\theta(t) - \frac{2}{3}\pi\right) & -sin\left(\theta(t) + \frac{2}{3}\pi\right) \end{bmatrix} \begin{bmatrix} V_a \\ V_b \\ V_c \end{bmatrix} \tag{2.13}$$

And their corresponding inverse-transform:

$$\begin{bmatrix} V_a \\ V_b \\ V_c \end{bmatrix} = \sqrt{\frac{2}{3}} \begin{bmatrix} 1 & 0 \\ -\frac{1}{2} & \frac{\sqrt{3}}{2} \\ -\frac{1}{2} & \frac{\sqrt{3}}{2} \end{bmatrix} \begin{bmatrix} V_\alpha \\ V_\beta \end{bmatrix} \tag{2.14}$$

$$\begin{bmatrix} V_a \\ V_b \\ V_c \end{bmatrix} = \sqrt{\frac{2}{3}} \begin{bmatrix} cos\,\theta(t) & -sin\,\theta(t) \\ cos\left(\theta(t) - \frac{2}{3}\pi\right) & -sin\left(\theta(t) - \frac{2}{3}\pi\right) \\ cos\left(\theta(t) + \frac{2}{3}\pi\right) & -sin\left(\theta(t) + \frac{2}{3}\pi\right) \end{bmatrix} \begin{bmatrix} V_d \\ V_q \end{bmatrix} \tag{2.15}$$

2.2.2 Model of 2-level 3-leg inverter

A 2-level 3-phase inverter is used to feed the system. Its structure is shown in Figure 2.2.

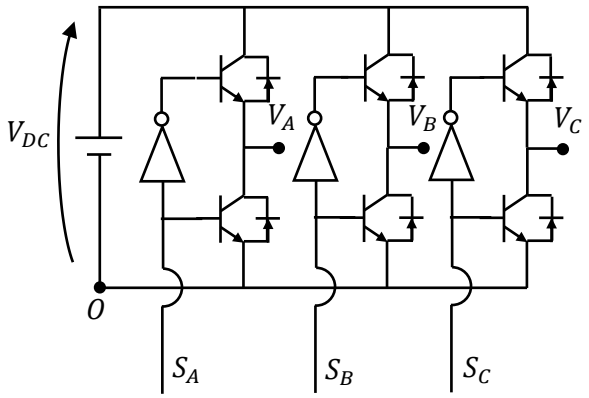

Figure 2.2 Structure diagram of a two-level three-phase inverter

An inverter is responsible for regulating a DC voltage (V_{DC}) into a three-phase AC voltage. S_A, S_B, S_C is connected to the controller's output. Each phase has two IGBTs. Their states are complementary which is ensured by an inverter placed between their input signal. With this configuration, the output voltage of each phase respect to the reference point O is shown in (2.16).

$$S_x = 0 \Leftrightarrow V_{xO} = 0 \quad S_x = 1 \Leftrightarrow V_{xO} = V_{DC} \quad x = \{A, B, C\} \tag{2.16}$$

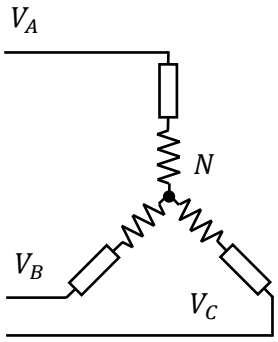

Figure 2.3 Simplified model of a PMSM

Figure 2.3 represents a simplified model of a PMSM. When it is connected to the inverter, it is possible to calculate each phase voltage respect to the inverter's input. The relationship is shown in (2.17).

$$\begin{bmatrix} V_{AN} \\ V_{BN} \\ V_{CN} \end{bmatrix} = \frac{V_{DC}}{3} \begin{bmatrix} 2 & -1 & -1 \\ -1 & 2 & -1 \\ -1 & -1 & 2 \end{bmatrix} \begin{bmatrix} S_A \\ S_B \\ S_C \end{bmatrix} \tag{2.17}$$

where V_{AN}, V_{BN}, V_{CN} represent the corresponding phase voltage.

By applying different combination of switch states, a two-levels three-legs inverter can provide $2^3 = 8$ configurations without modulation. After α - β transform, the 8 configurations can be represented by 8 voltage vectors which is stationary (Figure 2.4) respect to the stator. Two of them, V_0 and V_7, correspond to the same null vectors.

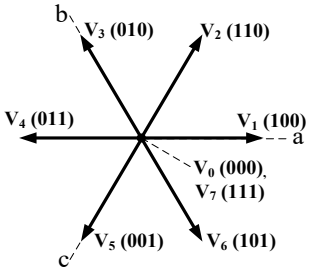

Figure 2.4 Configurations of a 2-level 3-phase inverter $V_i(S_A S_B S_C)$

2.2.3 Modelling of PMSM

In this research, a non-salient pole PMSM is considered, which means the magnetic circuit operates in linear region, the electromotive force is sinusoidal and the magnetic losses and the cogging torque are negligible. Its three-phase model is shown in (2.18).

$$\begin{bmatrix} V_a \\ V_b \\ V_c \end{bmatrix} = R_s \begin{bmatrix} I_a \\ I_b \\ I_c \end{bmatrix} + L_s \begin{bmatrix} \frac{d(I_a)}{dt} \\ \frac{d(I_b)}{dt} \\ \frac{d(I_c)}{dt} \end{bmatrix} + \begin{bmatrix} E_a \\ E_b \\ E_c \end{bmatrix} \tag{2.18}$$

where:

$V_a,\ V_b,\ V_c$: Phase voltage.

$I_a,\ I_b,\ I_c$: Phase current.

$E_a,\ E_b,\ E_c$: Electromotive force.

L_s: Stator inductance.

R_s: Stator resistance.

If d-q transform is applied on both sides of (2.18), the model of PMSM in d-q frame can be obtained:

$$\vec{V}_{dq} = R_s \vec{I}_{dq} + L_s \frac{d(\vec{I}_{dq})}{dt} + \omega_e \vec{\varphi}_{dq} \tag{2.19}$$

Here the electromotive force is expressed by the product of ω_e, the electrical speed, and $\vec{\varphi}_{dq}$, the permanent flux. Then it can be expressed in matrix form if extend the vectors in (2.19).

$$\begin{bmatrix} \frac{dI_d}{dt} \\ \frac{dI_q}{dt} \end{bmatrix} = \begin{bmatrix} -\frac{R_s}{L_s} & \omega_e \\ -\omega_e & -\frac{R_s}{L_s} \end{bmatrix} \begin{bmatrix} I_d \\ I_q \end{bmatrix} + \begin{bmatrix} \frac{1}{L_s} & 0 \\ 0 & \frac{1}{L_s} \end{bmatrix} \begin{bmatrix} V_d \\ V_q \end{bmatrix} - \begin{bmatrix} 0 \\ \frac{\varphi_p \omega_e}{L_s} \end{bmatrix} \tag{2.20}$$

Because the d-axis is aligned to the permanent flux, electromotive force only exists in q-axis. By applying the Power Invariant Law, the electrical torque (T_e) generated by PMSM can be calculated through the mechanical power (P_m):

$$T_e = \frac{P_m}{\omega_m} = \frac{\omega_e \overrightarrow{\varphi_{dq}} \cdot \overrightarrow{I_{dq}}}{\omega_m} = N_p \varphi_p I_q \tag{2.21}$$

2.3 Control strategies

2.3.1 Demonstration of feasibility

As a fundamental feasibility test, [13] has demonstrated, the ability to control independent torques comes from the electrical angle displacement between two motors' rotor. But its demonstration is not strict and complete. Here a better demonstration is given.

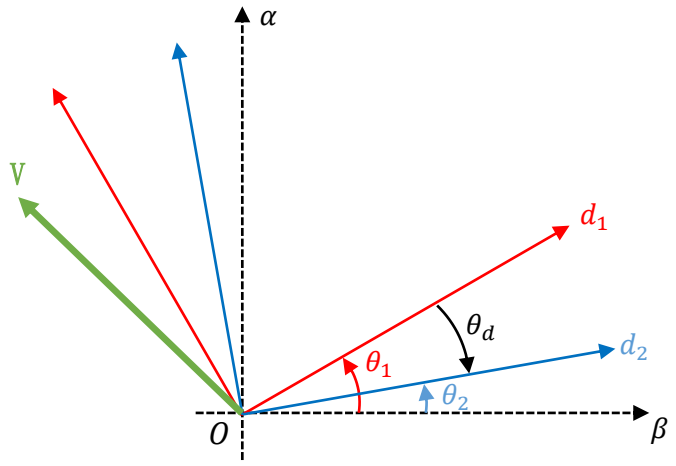

Figure 2.5 Definition of θ_d

The electrical model of a MIDPMSM system can be obtained by simply merge two single motor model together. But since d-q frame is fixed to the flux's orientation by definition, input voltage vectors $\vec{V}_{dq}$ are different in each motor's frame if their rotor position is not the same (Figure 2.5). Their voltage vector relationship can be expressed as (2.22).

$$\begin{bmatrix} V_{dM_2} \\ V_{qM_2} \end{bmatrix} = \begin{bmatrix} cos\,\theta_d & sin\,\theta_d \\ -sin\,\theta_d & cos\,\theta_d \end{bmatrix} \begin{bmatrix} V_{dM_1} \\ V_{qM_1} \end{bmatrix} \tag{2.22}$$

Here we use a set $\mathbb{M} = \{M_1, M_2, \ldots, M_N\}$ to expresses all motors involved in a MIMPMSM system. To define $\theta_d = \theta_{eM_2} - \theta_{eM_1}$, where θ_{eM_1} and θ_{eM_2} correspond to

the electrical angle of each motor. If transfer the model of MIDPMSM system into $\dot{x} = Ax + Bu$ form. As the torque control is realized by regulating the image of current in d-q frame. The feasibility of a MIDPMSM system is equivalent to the controllability of (2.23).

$$\underbrace{\begin{bmatrix} \frac{dI_{dM_1}}{dt} \\ \frac{dI_{qM_1}}{dt} \\ \frac{dI_{dM_2}}{dt} \\ \frac{dI_{qM_2}}{dt} \end{bmatrix}}_{\dot{x}} = \underbrace{\begin{bmatrix} -\frac{R_s}{L_s} & \omega_e & 0 & 0 \\ -\omega_e & -\frac{R_s}{L_s} & 0 & 0 \\ 0 & 0 & -\frac{R_s}{L_s} & \omega_e \\ 0 & 0 & -\omega_e & -\frac{R_s}{L_s} \end{bmatrix}}_{A} \underbrace{\begin{bmatrix} I_{dM_1} \\ I_{qM_1} \\ I_{dM_2} \\ I_{qM_2} \end{bmatrix}}_{x} + \frac{1}{L_s} \underbrace{\begin{bmatrix} 1 & 0 & 0 \\ 0 & 1 & L_s\varphi_f \\ cos\,\theta_d & sin\,\theta_d & 0 \\ -sin\,\theta_d & cos\,\theta_d & L_s\varphi_f \end{bmatrix}}_{B} \underbrace{\begin{bmatrix} V_{dM_1} \\ V_{qM_1} \\ \omega_e \end{bmatrix}}_{u} \tag{2.23}$$

Here the electrical speed ω_e and electrical angle difference θ_d are considered as constant variables, which is equivalent to a linearized model around this balanced point. They are treated as parameters in this demonstration. (2.23) is controllable only when R (defined in (2.24)) has full rank.

$$R = [B \quad AB \quad A^2B \quad A^3B] \tag{2.24}$$

Considering that it is difficult to evaluate the rank of R directly, (2.24) can be expressed by multiplication of two sub matrixes. It is shown in (2.25).

$$R = a \cdot b = [I \quad A \quad A^2 \quad A^3] \begin{bmatrix} B & 0 & 0 & 0 \\ 0 & B & 0 & 0 \\ 0 & 0 & B & 0 \\ 0 & 0 & 0 & B \end{bmatrix} \tag{2.25}$$

It can be proved that for two matrices a and b, the rank of their multiplied matrix is the minimal value of each matrix's rank. (2.26) shows the mathematical form.

$$Rank(ab) \leq min\big(Rank(a), Rank(b)\big) \tag{2.26}$$

The matrix *a* consists a unit matrix. Its rank is always full. Thus, it is enough to consider only the rank of B to determine the rand of R. It is obvious that, when $\cos\theta_d = \pm 1$, matrix B cannot be full rank. And consequently, the product of *a* and *b* is not full rank. This means that when θ_d is 0 or π, the current of MIDPMSM system cannot be controlled. This property conforms the conclusion of [13].

2.3.2 Average strategy

The *Average* strategy, as presented in [26]-[32], is a large branch in the control strategies for MIDPMSM system. They are first proposed for a Mono-Inverter Dual-IM system then extended to MIDPMSM system. It is the very intuitive but there is some difference in the

actual implementation. In this part, we will introduce them in detail.

2.3.2.1 Algebra average

The main problem with MIDPMSM is how to coordinate the limited output and multiple control objects. The first catalog [26]-[29] of *Average* strategy uses algebra average value of sensor information (position, current) from the two motors so that all PMSMs are taken into account by the controller.

$$\hat{\imath} = \frac{i_{M_1} + i_{M_2}}{2} \tag{2.27}$$

$$\widehat{\theta_m} = \frac{\theta_{mM_1} + \theta_{mM_2}}{2} \tag{2.28}$$

The controller configuration of this strategy is shown in Figure 2.6. A PI controller is responsible for speed tracking. It generates a torque reference to the current controller. Refer to (2.21), the torque regulating is equivalent to control a PMSM's q-axis current. The Average Technique block uses (2.27) and (2.28) to calculate the average value of rotor position ($\widehat{\theta_m}$) and phase current ($\hat{I}_a$, $\hat{I}_b$, $\hat{I}_c$). The d and q axis current ($\hat{I}_d$, $\hat{I}_q$) of this virtual motor can be consequently obtained by Park Transform defined in (2.13) using $\widehat{\theta_m}$ and $\hat{I}_a$, $\hat{I}_b$, $\hat{I}_c$. Because the speed and current controller only sees one motor, no modification should be done to them.

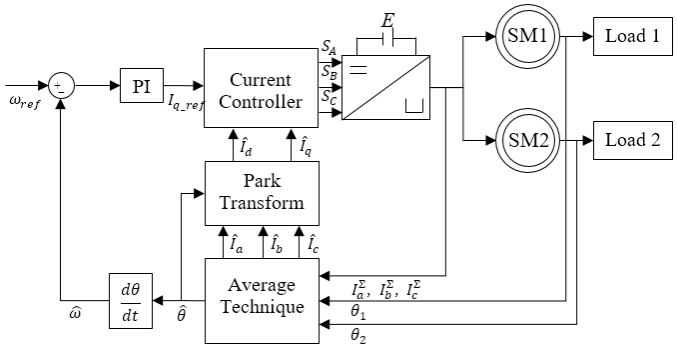

Figure 2.6 Block diagram of Average strategy with algebra average

2.3.2.2 $\Sigma - \Delta$ strategy

The second catalog [30]-[32] is also called $\Sigma - \Delta$. $\Sigma - \Delta$ controller uses vector sum (Σ) and subtraction (Δ) of the d-q current in order to improve steady-state and transient performances. Figure 2.7 shows the principle. Motor 1 and 2 are assumed to be identical and with generic unbalanced loads in the following part.

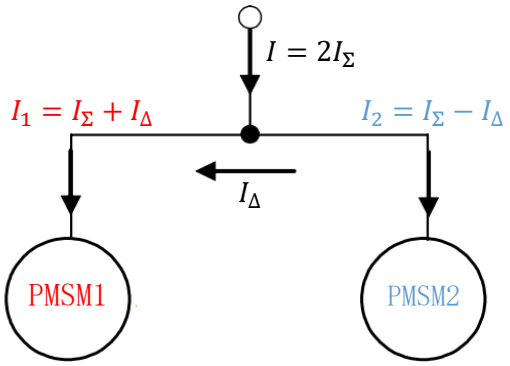

Figure 2.7 Mean and different current

where

$$I_\Sigma = \frac{i_{M_1} + i_{M_2}}{2} \tag{2.29}$$

$$I_\Delta = \frac{i_{M_1} - i_{M_2}}{2} \tag{2.30}$$

I_1 and I_2 is the current vector in a separately defined d-q frame which is represented in Figure 2.8. This frame is defined whose d-axis is along with the middle of two motor's rotor flux. θ_{eM_1} and θ_{eM_2} represents each motor's rotor electrical position. The current of each motor in this frame can be defined as:

$$I_{M_1} = \begin{bmatrix} I_{dM_1} \\ I_{qM_1} \end{bmatrix} \tag{2.31}$$

$$I_{M_2} = \begin{bmatrix} I_{dM_2} \\ I_{qM_2} \end{bmatrix} \tag{2.32}$$

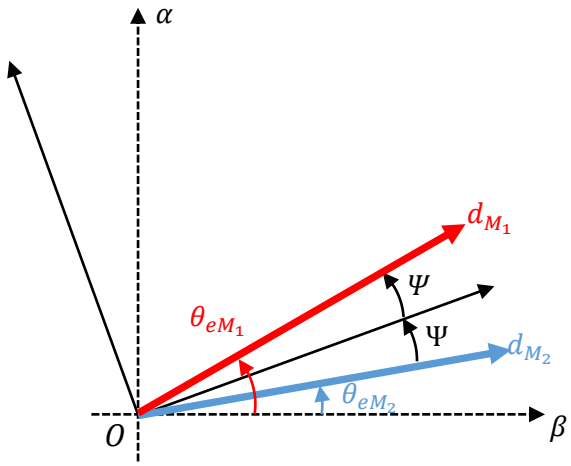

Figure 2.8 Reference systems

And consequently, the current in each motor's own d-q frame is then a rotation of Ψ and $-\Psi$ angle respectively. They can be represented through coordinate rotation of I_{M_1}

and I_{M_2}.

$$I_1' = \begin{bmatrix} cos\,\Psi & -sin\,\Psi \\ sin\,\Psi & cos\,\Psi \end{bmatrix} \begin{bmatrix} I_{dM_1} \\ I_{qM_1} \end{bmatrix} = \begin{bmatrix} cos\,\Psi\, I_{dM_1} - sin\,\Psi\, I_{qM_1} \\ sin\,\Psi\, I_{dM_1} + cos\,\Psi\, I_{qM_1} \end{bmatrix} \tag{2.33}$$

$$I_2' = \begin{bmatrix} cos\,\Psi & sin\,\Psi \\ -sin\,\Psi & cos\,\Psi \end{bmatrix} \begin{bmatrix} I_{dM_2} \\ I_{qM_2} \end{bmatrix} = \begin{bmatrix} cos\,\Psi\, I_{dM_2} + sin\,\Psi\, I_{qM_2} \\ -sin\,\Psi\, I_{dM_2} + cos\,\Psi\, I_{qM_2} \end{bmatrix} \tag{2.34}$$

Since the torque of SPMSM is only related to I_q, according to the previous definition, we can express the torque with the current term defined in the new frame.

$$T_{eM_1} = N_p \varphi_p I'_{qM_1} = N_p \varphi_p \left(I_{qM_1}\, cos\,\Psi + I_{dM_1}\, sin\,\Psi \right) \tag{2.35}$$

$$T_{eM_2} = N_p \varphi_p I'_{qM_2} = N_p \varphi_p \left(I_{qM_2}\, cos\,\Psi - I_{dM_2}\, sin\,\Psi \right) \tag{2.36}$$

Then it is adequate to define the total torque (T_Σ) and unbalanced torque (T_Δ) with reference to (2.29) and (2.30).

$$T_\Sigma = \frac{T_{eM_1} + T_{eM_2}}{2} \tag{2.37}$$

$$T_\Delta = \frac{T_{eM_1} - T_{eM_2}}{2} \tag{2.38}$$

Insert (2.35) and (2.36) into (2.37) and (2.38), after arrangements we can got:

$$T_\Sigma = N_p \varphi_p \left(cos\,\Psi\, I_{\Sigma,q} + sin\,\Psi\, I_{\Delta,d} \right) \tag{2.39}$$

$$T_\Delta = N_p \varphi_p \left(cos\,\Psi\, I_{\Delta,q} + sin\,\Psi\, I_{\Sigma,d} \right) \tag{2.40}$$

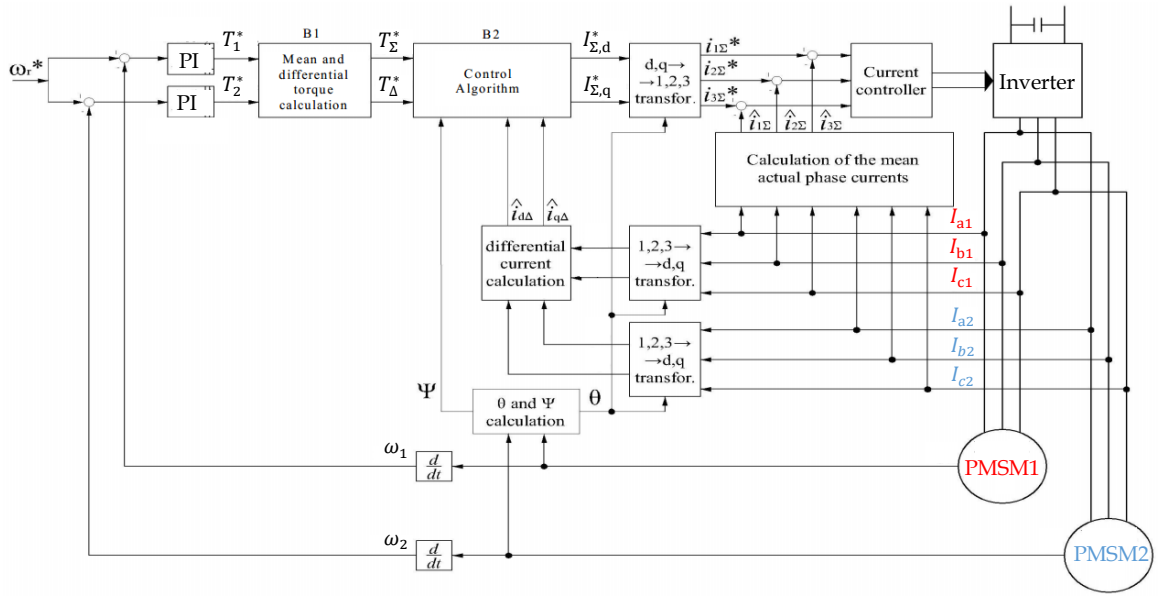

Figure 2.9 Control diagram of $\Sigma - \Delta$.

Figure 2.9 shows the control diagram of $\Sigma - \Delta$. The actual speed of each motor is separately compared with the speed reference. From the two reference torques $T_1^*$and T_2^*, the block B1 allows to evaluate the mean and differential torque reference values, which is T_Σ^* and T_Δ^*, using (2.37) and (2.38). Then, $I_{\Sigma,d}^*$ and $I_{\Sigma,q}^*$ is calculated through (2.41) and (2.42).

$$I_{\Sigma,d}^* = \frac{1}{sin\,\Psi}\left(\frac{T_\Delta^*}{N_p\varphi_p} - cos\Psi\hat{I}_{\Delta,q}\right) \tag{2.41}$$

$$I_{\Sigma,q}^* = \frac{1}{cos\,\Psi}\left(\frac{T_\Sigma^*}{N_p\varphi_p} - sin\,\Psi\,\hat{I}_{\Delta,d}\right) \tag{2.42}$$

where $\hat{I}_{\Delta,d}$ and $\hat{I}_{\Delta,q}$ are estimated using (2.33) and (2.34) based on actual sensor information. In the last step, current controller is responsible for imposing the total current of two motors. Compared to the algebra average strategy, it can provide higher transient performance by taking differential current into account.

2.3.3 Master-Slave strategy

Differ with *Average* strategy, *Master-Slave* strategy [24] handles the MIDPMSM system by separating the two motors as master motor and slave motor. At each control instant, only the master motor is under control. The slave motor is left open-loop operating. Figure 2.10 shows the controller's diagram. The controller is composed by two major section: a single PMSM current controller (red area) and master selection block (blue area). The current controller can be arbitrary since it only controls one motor.

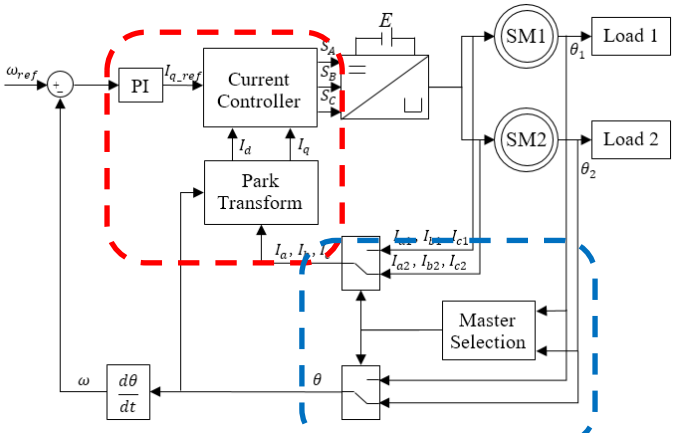

Figure 2.10 Controller's diagram of Master-Slave

2.3.3.1 Master motor selection

The master selection strategy takes the system stability into consideration. It guarantees the stability by selecting the more loaded motor as the master. This mechanism is designed based on PMSM's open-loop stability. As its name describes, PMSM is a synchronous motor target rotating speed is always equal to the frequency of the applied three-phase voltage. When this rule breaks, the motor loses stability. The open-loop

stability describes the stability criterion under this situation. Figure 2.11 represents a simple vector diagram of a PMSM.

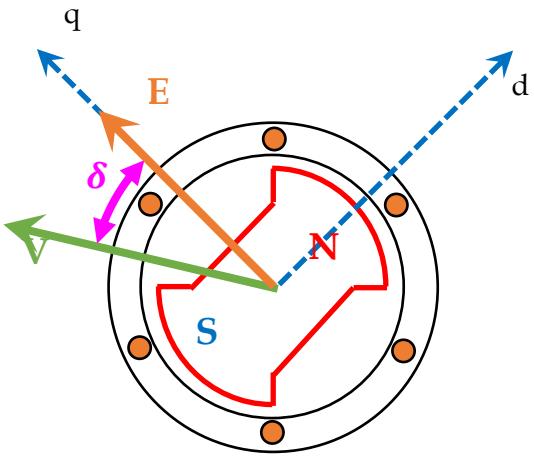

Figure 2.11 Relationship of δ angle

The d-axis is aligned with rotor's flux. V is the input voltage. E is the back-EMF. Refer to the model of PMSM (2.20), if define the angle between V and E as δ, the steady-state model of a PMSM respect to δ can be obtained. It is shown in (2.43).

$$\begin{bmatrix} -V\sin\delta \\ V\cos\delta \end{bmatrix} = \begin{bmatrix} R_s & -L_s\omega_e \\ L_s\omega_e & R_s \end{bmatrix} \begin{bmatrix} I_d \\ I_q \end{bmatrix} + \begin{bmatrix} 0 \\ \omega_e\varphi_p \end{bmatrix} \tag{2.43}$$

Treat δ as a parameter of (2.43) and I_d, I_q as unknown variable, it is possible to obtain the torque relationship respect to δ:

$$T_e = N_p\varphi_p \left(\frac{V}{\sqrt{{R_s}^2 + (L_s\omega_e)^2}} \cos\left(\delta - \tan^{-1}\frac{\omega_e L_s}{R_s}\right) - \frac{R_s\omega_e\varphi_p}{{R_s}^2 + (L_s\omega_e)^2} \right) \tag{2.44}$$

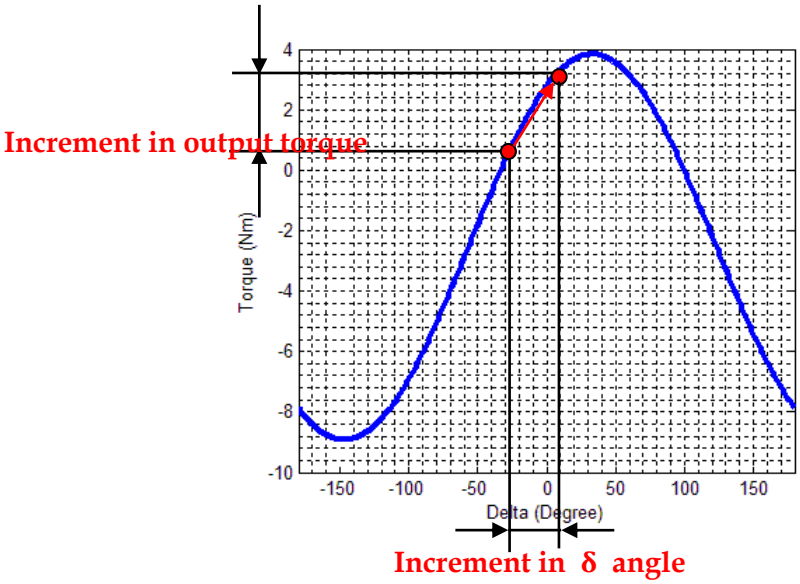

Figure 2.12 Torque curve respect to δ

Figure 2.12 shows an example curve of (2.44). From the figure, we can find that both positive slop ($\frac{dT}{d\delta} > 0$) and negative slop ($\frac{dT}{d\delta} < 0$) are presented. Image that at certain instant, if the external load is increased, the rotor's speed will decrease and consequently the δ angle increase. In the positive slop region, increment in δ angle will lead to torque increase so that the torque is compensated. Obviously, this mechanism holds true only when the applied torque doesn't exceed the maximum point. Otherwise the motor will lose synchronization.

For a MIDPMSM system, the torque-δ curve presented in Figure 2.12 is valid for all motors because they are parallel connected, their voltages are the same. For the closed-loop controlled master motor, its torque won't exceed the maximum point thanks to the speed controller. The curve in Figure 2.12 will be change respect to the torque of the master motor. We can conclude that if the more loaded motor is close-loop controlled, the system must be stable because the slave motor's torque should be within the torque range. This conclusion builds the foundation of stability.

2.3.4 Model predictive control

The third type of strategy is so called "Model Predictive Control (MPC)" [39]. It has been studied and applied in many applications with both an IM[43][44] and PMSM[54][56]. It formulizes the control problem into an optimization problem that predicts the future behavior of a system and determines the optimal control output through minimizing a criterion which gives us an arbitration in selecting different control strategies. Some researches [36]-[38] have been done to explore the possibility of using MPC to handle this

special system. In this part, the MPC strategy for single PMSM system is firstly addressed. Then in the next part, it will be extended to a MIDPMSM system. In final, these control strategies based on MPC will be introduced in detail.

2.3.4.1 MPC strategy for single PMSM system

The first thing to be defined is the prediction model. The torque control of a PMSM is realized through controlling the angle between the stator flux and the rotor flux, which is respectively controlled by I_q, component orthogonal to the rotor flux, and I_d, component parallel to the rotor flux. The speed controller will give the torque and flux reference. Thus, the MPC strategy uses the prediction model to predict the future value of torque and flux based on different input voltage. Then, the predicted future value is compared to the reference and the voltage that minimizes the distance between the future value and reference is selected and applied.

Since prediction model must be implemented in a digital controller, it's necessary to discretize the continuous state model (2.20). We usually use first-order Euler expansion to approximate the derivative operation, which is:

$$\frac{dI}{dt} = \frac{I(k+1) - I(k)}{T_s} \tag{2.45}$$

T_s is the interval of prediction. The index k represents the samples taken in T_k. Replace two derivatives in (2.20) with (2.45), the discretized state model of a single PMSM is obtained ((2.46)).

$$\begin{bmatrix} I_d(k+1) \\ I_q(k+1) \end{bmatrix} = \begin{bmatrix} 1 - T_s\frac{R_s}{L_s} & T_s\omega_e(k) \\ -T_s\omega_e & 1 - T_s\frac{R_s}{L_s} \end{bmatrix} \begin{bmatrix} I_d(k) \\ I_q(k) \end{bmatrix} + \begin{bmatrix} \frac{T_s}{L_s} & 0 \\ 0 & \frac{T_s}{L_s} \end{bmatrix} \begin{bmatrix} V_d \\ V_q \end{bmatrix} + \begin{bmatrix} 0 \\ -T_s\frac{\varphi_p\omega_e(k)}{L_s} \end{bmatrix} \tag{2.46}$$

with obvious notations,

$$I_{dq}(k+1) = A(\omega_e)I_{dq}(k) + BV_{dq}(k) + C(\omega_e) \tag{2.47}$$

Due to the limitation that the predictive model only includes the prediction of stator current but the electrical speed ω_e is not predicted, which needs modeling the mechanical part of the system. But it is adequate to keep ω_e constant during the prediction since the time constant of a mechanical system is much larger than the prediction interval, the speed changes is negligible

Second, the cost function must be defined. To have a homogeneous term, the predicted d-q frame currents $I_d(k+1)$, image of flux, and $I_q(k+1)$, image of torque, are used and compared to their reference. Then, the cost function is given by:

$$g = \left(I_d^*(k) - I_d(k+1)\right)^2 + \left(I_q^*(k) - I_q(k+1)\right)^2 \tag{2.48}$$

which should be minimized in order to find out the best voltage vector which bring the d-q frame currents to their reference. I_q^*, the torque reference, is given by speed controller. As a smooth pole motor is used, I_d^* is set to zero according to MTPA (Maximum Torque per Ampere) law.

2.3.4.2 MPC strategy for MIDPMSM system

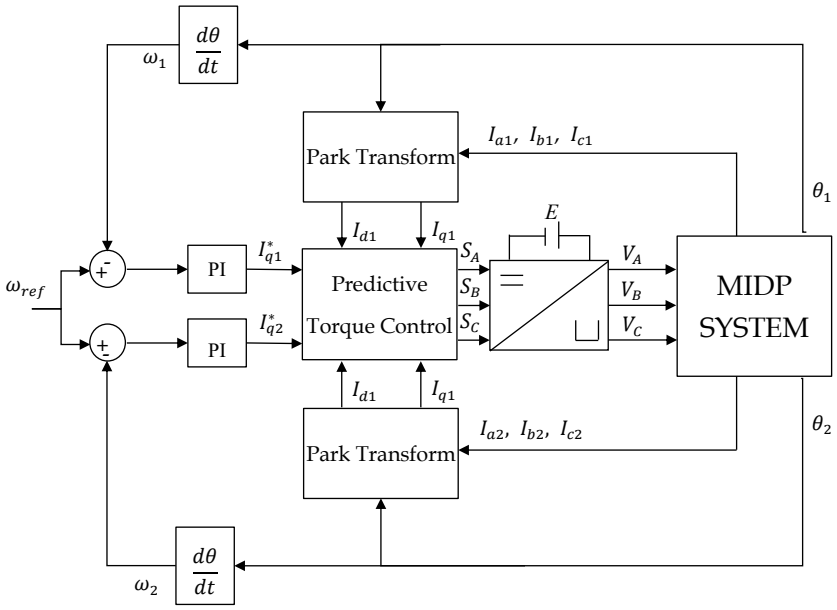

Figure 2.13 Predictive control scheme for two PMSMs connected in parallel

As shown in Figure 2.13, in this configuration, the speed control loops are independent, where two PI controllers are used to generate the torque reference for each motor. In the case of MIDPMSM system, the prediction model can be obtained by simply merge two single motor prediction model together. (3.16) shows the obtained prediction model for MIDPMSM system. Voltage vector $\vec{V}_{dq}$ is represented by its value in motor1's frame in order to simplified the equations.

$$\begin{bmatrix} I_{dM_1}(k+1) \\ I_{qM_1}(k+1) \\ I_{dM_2}(k+1) \\ I_{qM_2}(k+1) \end{bmatrix} = \begin{bmatrix} 1-T_s\frac{R_s}{L_s} & T_s\omega_e(k) & 0 & 0 \\ -T_s\omega_e(k) & 1-T_s\frac{R_s}{L_s} & 0 & 0 \\ 0 & 0 & 1-T_s\frac{R_s}{L_s} & T_s\omega_e(k) \\ 0 & 0 & -T_s\omega_e(k) & 1-T_s\frac{R_s}{L_s} \end{bmatrix} \begin{bmatrix} I_{dM_1}(k) \\ I_{qM_1}(k) \\ I_{dM_2}(k) \\ I_{qM_2}(k) \end{bmatrix} + \frac{T_s}{L_s} \begin{bmatrix} 1 & 0 \\ 0 & 1 \\ cos\,\theta_d(k) & sin\,\theta_d(k) \\ -sin\,\theta_d(k) & cos\,\theta_d(k) \end{bmatrix} \begin{bmatrix} V_{dM_1} \\ V_{qM_1} \end{bmatrix} - \begin{bmatrix} 0 \\ T_s\frac{\varphi_p\omega_e(k)}{L_s} \\ 0 \\ T_s\frac{\varphi_p\omega_e(k)}{L_s} \end{bmatrix} \quad (2.49)$$

The cost function represents the desired control strategy and the control is realized by optimizing this function at each instant of calculation. We can define two sub-criteria g_1 and g_1 for each machine:

$$g_{M_1} = \left(I_{dM_1}(k+1)\right)^2 + \left(I_{qM_1}^*(k) - I_{qM_1}(k+1)\right)^2 \quad (2.50)$$

$$g_{M_2} = \left(I_{dM_2}(k+1)\right)^2 + \left(I^*_{qM_2}(k) - I_{qM_2}(k+1)\right)^2 \quad (2.51)$$

and [36]-[38] has determined the global cost function g which has to be minimized is now the algebra sum of the two sub-criteria:

$$g = g_{M_1} + g_{M_2} \quad (2.52)$$

2.3.4.3 Predictive Torque Control

In the last part, the optimization method is responsible for obtaining the optimal voltage. MPC algorithm for MIDPMSM system has different implementation in optimization and voltage modulation method: *Predictive Torque Control (PTC)* [36], *Predictive Torque Control Split & Seek (PTCSS) [37],* and *Optimal Predictive Torque Control (OPTC)* [38].

PTC was first introduced for IM [43] and now it has been successfully applied in PMSM drives [45][46]. It belongs to the catalog "Finite Control Set-Model Predictive Control (FCS-MPC)"[46] because it uses discreate control set to minimize the cost function. In our case, the 7 basic voltage vectors of a 2 level 3-leg inverter (Figure 2.4) is used. Thus, during each calculation period, PTC predicts the currents in next-time and evaluates the resulting cost function for each of the 7 voltage vectors. After 7 iterations, the optimal voltage vector towards the criterion is kept. Figure 2.14 has illustrated the flow chart of this process.

This makes PTC is relatively fast compared to traditional cascade-PI controller [54]. Because there is no need of modulation, PTC is also very simple to implement. But its disadvantage is obvious, limited available vectors will result in high current ripple and current harmonic [45]-[47].

2.3.4.4 Predictive Torque Control Split & Seek

PTC has greater current ripple due to small amount of oltage vectors. In order to improve this performance, researchers has proposed different method [44]-[47], among them the most commonly used is using Space Vector Pulse Width Modulation (SV-PWM) [40], to extend the finite control set so as to better minimize the criterion, and consequently to improve the performance. This is the idea of the *Predictive Torque Control Split & Seek (PTCSS)* [37]. By using SV-PWM, a virtual voltage vector with arbitrary magnitude and angle can be generated from a pair of 2 real basic vectors (Figure 2.15). Based on this technology, the feasible voltage vector set can be extended from the 7 basic vectors to the entire control space of the inverter.

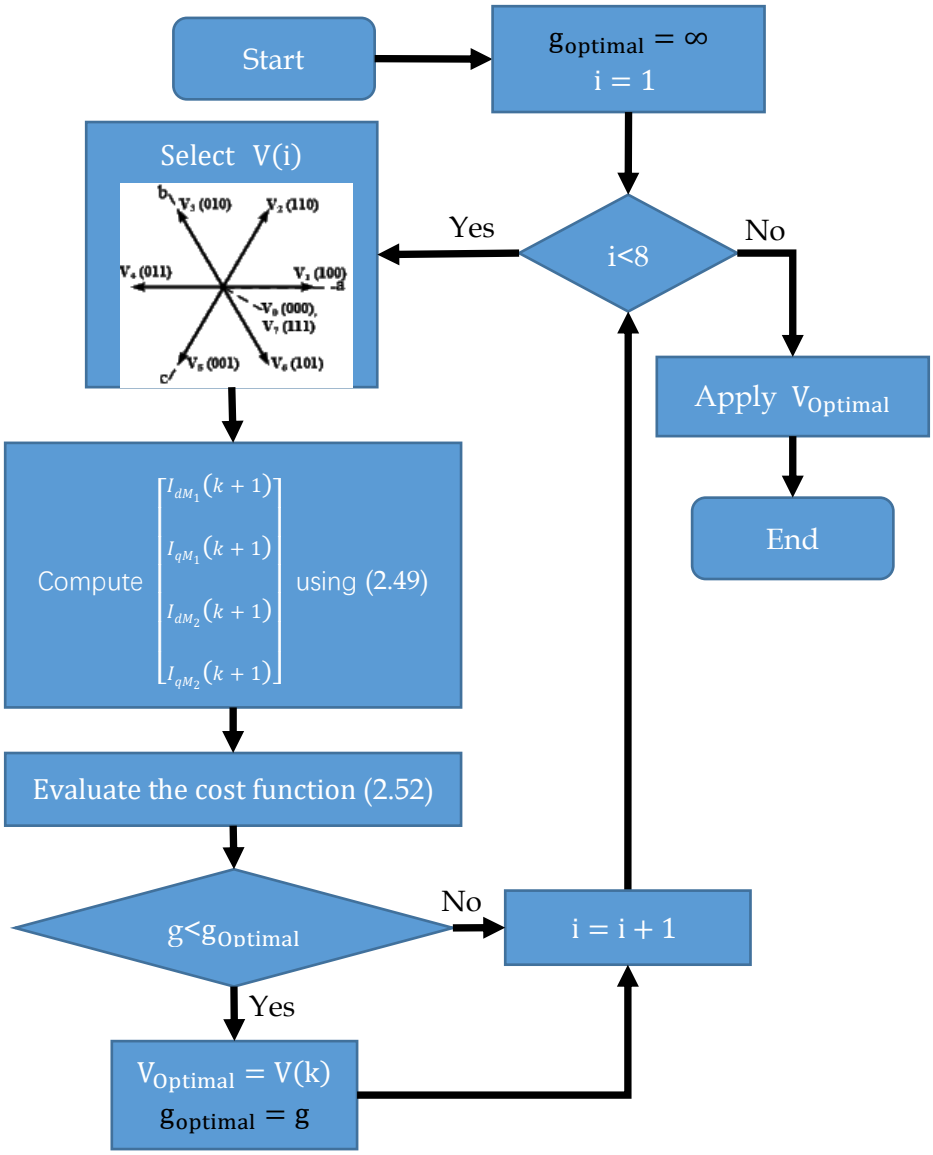

Figure 2.14 Flow chart of PTC

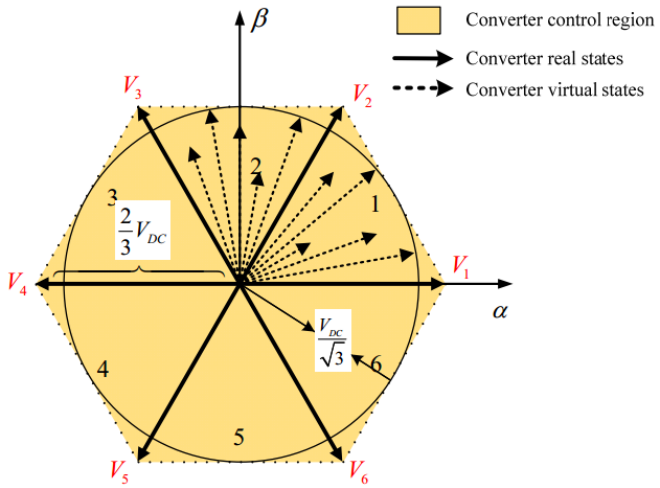

Figure 2.15 The vector space of the 2-level 3-leg inverter connected to a PMSM

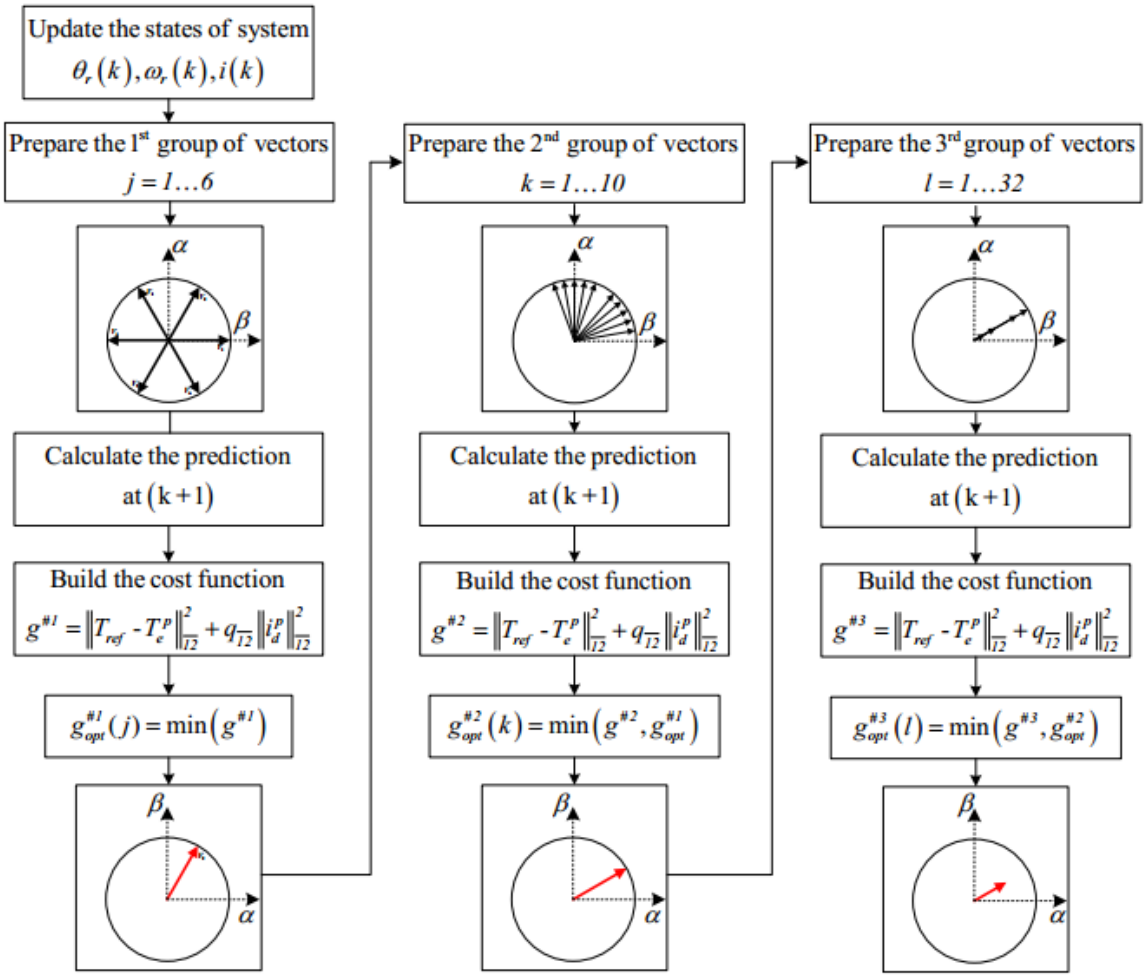

Figure 2.16 Flow chart of PTCSS

Although an infinite number of voltage vector can be used, under the framework of FCS-MPC, only finite number of vector can be evaluated. PTCSS handles this limitation by two steps. First, as shown in Figure 2.15, it discretizes the linear control space into a finite subset which is constructed based on constant angle and magnitude intervals. Here the angle and magnitude are assigned as 10° and 10V respectively. With $V_{DC} = 540V$, the total number of vectors is increased dramatically from 7 to 1152.

Second, to overcome the huge computational cost cause by dramatically increased voltage vector number, rather than evaluating all the possibilities, PTCSS use heuristic dichotomizing search so as to reduce the computational cost. It starts with evaluating the 7 basic vectors of a 2-level 3-phase inverter and determines the optimal one. In the next step, several virtual vectors defined in the two adjacent sectors of the chosen vector with an angle step of 10° will be evaluated. At this point, the angle of the optimal vector is determined. In the last step, the amplitude of the optimal vector will be determined by changing the magnitude of the candidate vector. PTCSS decreases the distance to the optimal solution and thus increase the performance concerns current & speed ripple.

2.3.4.5 Optimal Predictive Torque Control

Apart from FCS-MPC strategies, the *Optimal Predictive Torque Control (OPTC)* [38] is interested in the exact analytical solution of the optimization problem on a continuous set of voltage vectors. It uses dead-beat control [48]-[50] in order to fulfil high bandwidth requirements. In fact, the equation that predicts the currents evolution in d-q frame (2.49) can be divided into two terms: I_{RL}, the predicted free mode and I_{RF}, the predicted force mode, as follow:

$$I_{dq}(k+1) = \underbrace{A(\omega_e)I_{dq}(k) + C(\omega_e)}_{I_{RL}} + \underbrace{BV_{dq}(k)}_{I_{RF}} \tag{2.53}$$

The predicted free mode corresponds to the evolution of current that is not affected by external input. The predicted force mode indicates the additional current response caused by the voltage applied during T_s, which can be used to set the desired current.

The criterion (2.52) can be interpreted as the square Euclidian norm of the error between the predicted currents and the reference:

$$g = \left\| I_{dq}^*(k) - I_{dq}(k+1) \right\|^2 \tag{2.54}$$

Then, by replacing (2.53) in (2.54),

$$g = \left\| I_{dq}^*(k) - I_{RL} - I_{RF} \right\|^2 \tag{2.55}$$

it is clear that the criterion is minimized if and only if:

$$I_{RF} = I_{dq}^*(k) - I_{RL} \tag{2.56}$$

and with the voltage limit, it is subjected to the constraint:

$$\|I_{RF}\| \leq I_{RFmax} = \frac{V_{dc}}{\sqrt{3}} \frac{T_s}{L_s} \tag{2.57}$$

If one substitutes (2.53) into (2.56), the analytical solution of the corresponding optimal voltage vector becomes:

$$V_{dq}(k) = B^{-1}\left(I_{dq}^*(k) - A(\omega_e)I_{dq}(k) - C(\omega_e) \right) \tag{2.58}$$

$$\left\| V_{dq}(k) \right\| \leq \frac{V_{dc}}{\sqrt{3}} \tag{2.59}$$

and, *in this particular case*, it corresponds to a space state model inversion with saturation. As for the MIDPMSM system, [38] has proved that the optimal vector which minimizes the global criterion g is equivalent to the average value of the two optimal vectors minimizing respectively the two sub-criteria g_1 and g_2. Its mathematical form is shown in

(2.60) ~ (2.62).

$$V_{dqM_1}(k) = B^{-1}\left(I^*_{M_1}(k) - A(\omega_{eM_1})I_{dqM_1}(k) + C(\omega_{eM_1})\right) \tag{2.60}$$

$$V_{dqM_2}(k) = B^{-1}\left(I^*_{M_2}(k) - A(\omega_{eM_2})I_{dqM_2}(k) + C(\omega_{eM_2})\right) \tag{2.61}$$

$$V_{dq}(k) = \frac{V_{dqM_1}(k) + V_{dqM_2}(k)}{2} \tag{2.62}$$

2.4 **Experiment and Analysis**

All control strategies mentioned above have used either simulation or experiment to verify the feasibility and stability. But because of the experimental environment is different, their experimental results are not comparable. Due to the specialty of a MIDPMSM system, a minor difference in the algorithm may lead to huge differences in performance. So, it is necessary to carry out a comparative experiment to see how the difference in control strategy structure influences the final performance. Through analysis of the experimental results, we can know what the current algorithm defects, the reasons, and how to improve them. [41][42][51] have intended to propose this topic. As a summary of these researches, in this part, an experiment involving the *Average*, *Master-Slave*, *PTC, PTCSS,* and *OPTC* strategies is conducted. These strategies are put under the same experiment environment to maximum possibly remove non-algorithm factors. In the experiment two factors considered, the stability and its performance. The stability concerns not only in normal operation but also in high unbalanced torque transient situation. Then, some numerical indicators are used to precisely evaluate the performance of different aspects of a typical actuation system. In this experiment, there is an arbitrary in the current controller of *Master-Slave, PTC* for single PMSM is used in this case.

2.4.1 Experimental bench

The experiment bench is composed by four major parts:

1) Motor coupling system
2) Power supply
3) dSPACE based DS1103 R&D controller card
4) MATLAB/Simulink and Control desk software

Here we only give out a brief introduction to the mechanical and electronic devices of the experimental bench. Their detailed description and technical specification of the experiment bench can be found in [52][53]. On the contrary, the software architecture will

be discussed in detail.

2.4.1.1 Motor coupling system

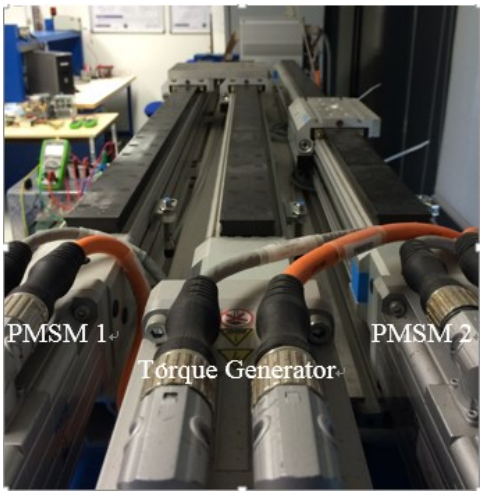

Figure 2.17 The experimental bench

Figure 2.17 shows the experiment bench. Three PMSMs were used. PMSM 1 and PMSM 2 are the experimental motors, they are identical. Each of them is equipped with a position encoder to measure rotor position and current sensors. The motor located between them is used as a controllable load torque generator. It is connected to a commercial PMSM controller and its torque can be configured by imposing a current. Each of the three PMSMs is connected to a linear ball screw actuator and drives its own axis. In this experiment, the axis of PMSM 1 was rigidly connected to the axis of the generator. Figure 2.18 presents a more understandable illustration.

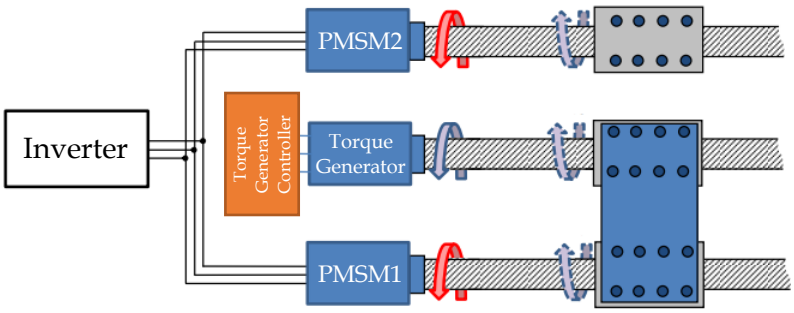

Figure 2.18 Illustration of the experimental bench

The parameters of the PMSM used in the experiment are summarized in Table 2.1.

Symbol	Description	Value
V_{dc}	Voltage of the DC bus	325V
I_n	Nominal Current	4.3A
P_n	Nominal Power	913W
R_s	Stator resistance	1.25 Ω
L_s	Cyclic inductance	1.65 mH
φ_p	Amplitude of the flux due to the magnets	0.047 Wb
N_p	Number of pairs of poles	4

Table 2.1 Parameters of PMSM

2.4.1.2 Power supply system

The typology of the power supply system is represented in Figure 2.19. It is composed of the EDF (Électricité de France) electricity network, a three-phase adjustable auto-transformer and an inverter which is composed of a rectifier, a filter and a three-leg IGBT.

The power supplied from the EDF network is 400V/50Hz three-phase. In order to adjust the DC bus voltage and to compensate the voltage variation from the network, a three-phase adjustable auto-transformer (400/450/20 AUTC from Auto'melec) is used. With this transformer, the voltage applied to the terminals of the rectifier can be adjusted. This transformer can also smooth the current return to the EDF network thanks to its inductive nature.

The adjusted three-phase voltage from the transformer is imposed to an inverter from SEMIKRON, whose technical specifications are presented in Appendix B.2 of [52]. A bridge rectifier will rectify the three-phase voltages. Two capacitors are also used to smooth the DC voltage.

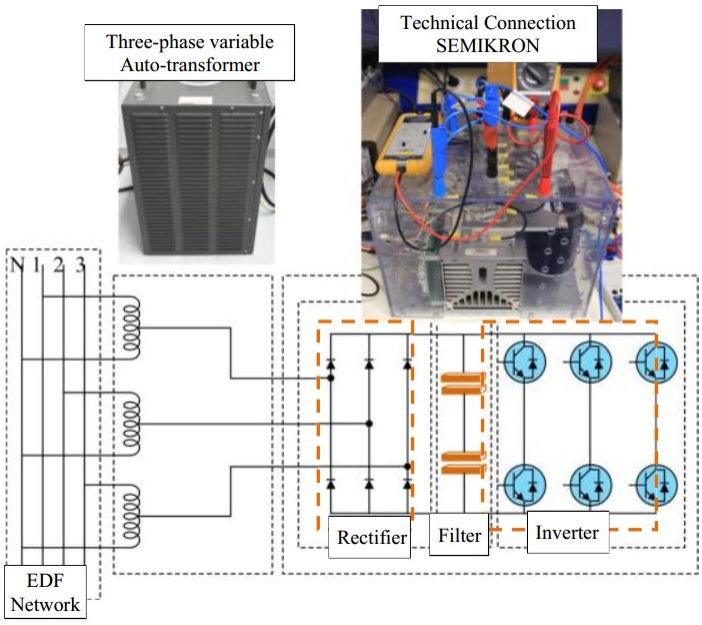

Figure 2.19 Typology of the power supply system

A 2-level three-leg inverter is used to modulate the three-phase voltage whose amplitude and frequency are controlled. These voltages will drive the two PMSMs. The PWM signals are generated under TTL technology (0-5V) by the control card and in order to control IGBTs it is necessary to use C-MOS technology (0-12V). Thus, the signals controlling the inverter are calculated and sent to each IGBT switch through an interface adapter.

2.4.2 Measurement and control implementation in dSPACE

dSPACE system is a tool oriented for fast prototyping of real-time control algorithm. It can capture the signal (analog or digital) from its I/O interface, process them, and realize the control thought its analog or digital port. dSPACE system model used in this thesis is CP1103 system with different analogue I/O and digital I/O.

The programming of dSPACE is very easy. It has provided a Real-Time Interface (RTI) library containing all the functions available in the DS1103 processor, such as analog input/output, digital input/output, encoder interface, PWM generation, and so on. Together with the Simulink, we can easily create out control algorithm by drag & drop function blocks. Then the control algorithm can be programmed to the processor by 1-click using the Simulink Real-Time Workshop.

dSPACE system is also an interface between the physical world (motors, inverter, measure sensors …) and the computer. Through Control Desk software, one can monitor any variable presented in dSPACE system by a PC.

2.4.2.1 Current measurement

Hall effect sensors type LEM LA-25-P, whose datasheet is given in the Appendix B.5.2 of [52], is used to measure the stator current I_{a1}, I_{b1}, I_{a2}, I_{b2}. The neutral points of two motors are not linked. I_{c1} and I_{c2} which circulate in the third phase are obtained by the equation in (2.63).

$$I_c = -(I_a + I_b) \tag{2.63}$$

This sensor outputs a voltage proportional to the current passing through it, whose sensitivity is 1V/A. It is connected to the analog input of dSPACE system. The connected port name is given in Table 2.2.

Input Signal	Port Name
I_{a1}	ADC17
I_{b1}	ADC18
I_{a2}	ADC19
I_{b2}	ADC20

Table 2.2 Port of current sensor

Due to the fact that the sensitivity of ADC block is 0.1/V (-10V~10V⇔-1~1), the raw output of each ADC block must multiply by 10 to obtain the correct value of current. To compensate any offset value in the sensors, a procedure for calibrating the current offset is carried out during initialization procedure.

2.4.2.2 Rotor position measurement and speed estimation

- **Rotor position measurement**

Section **4.4.1.2** of [53] has introduced in detail the hardware architecture and principle of the rotor position measurement. As illustrated in Figure 2.20, each motor is equipped with a dedicate AD2S1200 to resolve the absolute position as well as create an incremental encoder signal which gives the information to obtain the relative position of the motor. Due to the limitation of DS1103, which only allows at maximum 20 digital channel input, we cannot measure two 12bit digital signal simultaneously. A method combining the absolute position and relative position must be used.

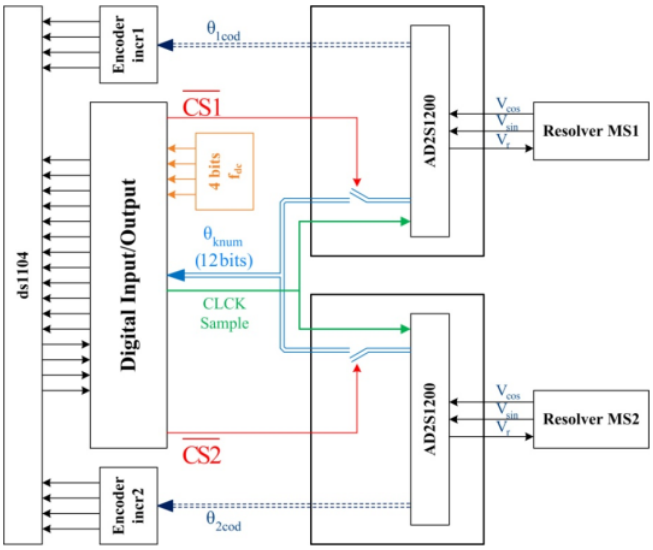

Figure 2.20 Hardware architecture of rotor position measurement

When the controller starts execution, during the initialize procedure, the absolute position of each motor will be read by setting the corresponding Chip Select (CS) port. At the same time, the relative position of each motor will be trimmed to zero. It is obvious that when the absolute position changes, the relative position also changes with the same amount. Thus, after initialization, we can calculate the absolute position of each motor by reading the relative position then adding the trim value.

- **Trigonometric function calculation of rotor position**

As trigonometric functions of rotor position (mainly $\sin\theta$ and $\cos\theta$) are widely used in coordinate transformation and control algorithm, their calculation is concentrated in the measurement part to avoid repeated calculation in control algorithm.

Since the resolution of the rotor position is 12 bits (0~4095), here we have used two

look-up tables to perform the calculation of $\sin\theta$ and $\cos\theta$. The look-up table block of Simulink is used directly. Also, some control algorithm will use the differential rotor angle, their trigonometric functions are also calculated using (2.64) and (2.65).

$$sin\,\theta_d = sin\left(\theta_{M_1} - \theta_{M_2}\right) = sin\,\theta_{M_1}\,cos\,\theta_{M_2} - cos\,\theta_{M_1}\,sin\,\theta_{M_2} \tag{2.64}$$

$$cos\,\theta_d = cos\left(\theta_{M_1} - \theta_{M_2}\right) = cos\,\theta_{M_1}\,cos\,\theta_{M_2} + sin\,\theta_{M_1}\,sin\,\theta_{M_2} \tag{2.65}$$

- **Speed estimation**

The principle of speed estimation has been well explained in [52]. It uses first-order Euler differential together with a low-pass filter to estimate the speed. We have made some improvements. As the range of the rotor position measurement is 0~4095, making differential on the boundary, e.g. 4095→0 in positive rotating or 0→4095 in negative rotating, will cause a gap in its output. Assuming the angle difference is d, a good algorithm to solve this problem is to calculate $\sin d$ then obtain the angle difference using $\sin^{-1} d$. But this method is not adequate here because the calculation frequency is very high making angle difference too small that causes a large numerical error during trigonometric function operation. On the contrary, we have used such an algorithm that at each instant, d, $d + 2\pi$, $d - 2\pi$ are calculated and their absolute value are compared. The one with minimal absolute value is chosen.

2.4.2.3 Overall architecture of the Simulink model

The controller uses a conventional two-level architecture which contains a speed controller and torque controller. The speed controller generates a torque reference for the torque controller. Different control strategies are implemented in the torque controller. In addition, a measurement block is responsible for the initialization of the sensor and data operations.

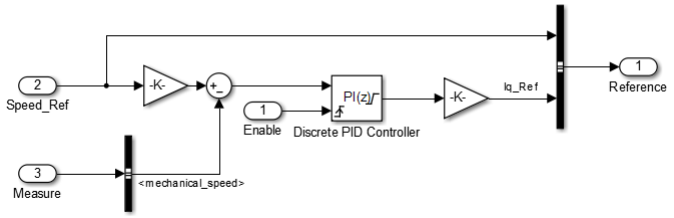

Figure 2.21 Block diagram of the speed controller

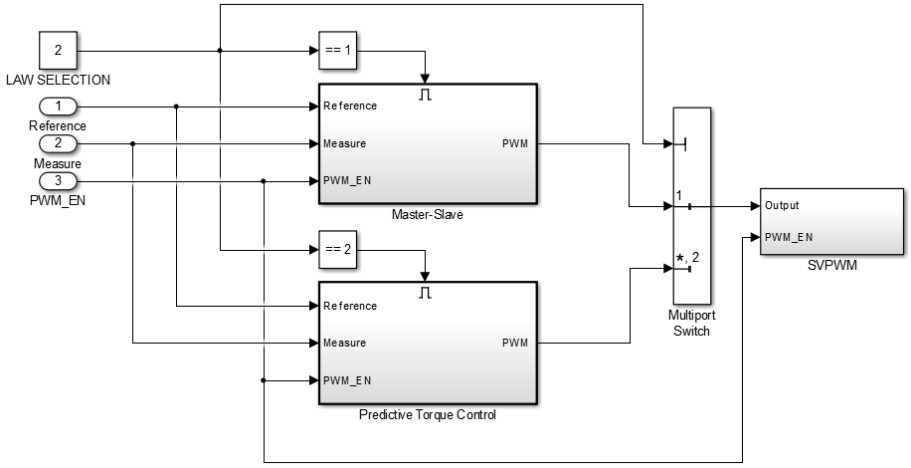

Figure 2.22 Control strategies selection of torque controller

As shown in Figure 2.21, the speed controller uses a PI controller with anti-windup. It uses the discrete PI block of Simulink directly. It runs at 1kHz and its parameters is determined by experiment. In torque controller, all control strategies are put into different sub-systems (Figure 2.22). Then, we have used a "LAW SELECTION" signal together with port-selector and Enable-port block to switch between different control strategies. In the Control Desk Software, this variable is assigned to a Listbox controls so that we can switch between different control strategies during experiment. It should be noticed that, the RTI library only allows one PWM generation block, we have to use the SVM block for all control strategies. For the PTC strategy, its output is mapped into SVM parameters.

Timing is a critical issue in implement the controller. In Simulink, the sampling time of all sub-system must be specified. "Task Transition" block must be inserted between sub-systems with different sampling time to preserve data integrity. In our model, the speed controller runs at 1KHz, the torque controller runs at 10kHz or higher. The measurement and torque controller block must be synchronized by a PWM interrupt block. It is configured to generate the interrupt signal at the middle of a modulation period because these is no state switch in any IGBT so that it is the most stable. Another reason is related to the PWM generation mechanism of dSPACE. It will be discussed in the next section.

2.4.3 Output delay consideration

2.4.3.1 Output delay validation

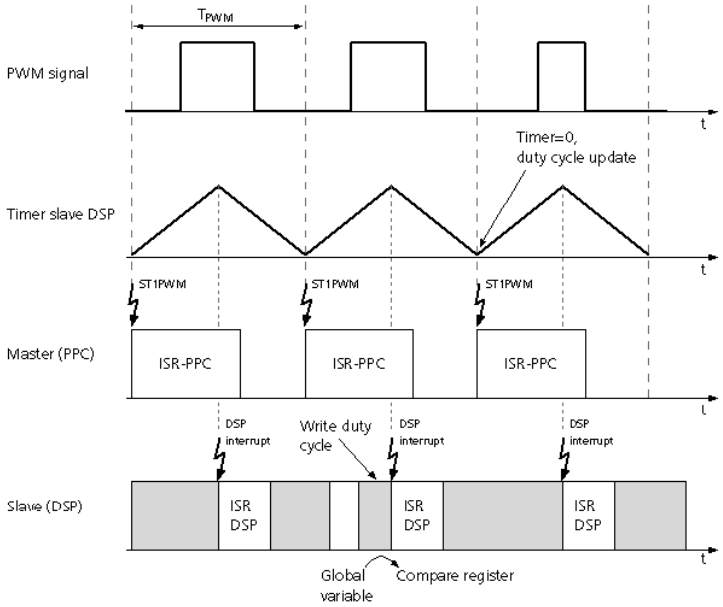

Figure 2.23 PWM update mechanism of dSPACE

A digital system can perform calculation and assigning output during one period. But this assigned output will only be executed by the start of next period [55][56]. This problem has to be considered for predictive control because it is sensitive to the prediction step. The PWM update mechanism of dSPACE is shown in Figure 2.23, which comes from the datasheet of dSPACE [54]. In dSPACE system there are two controllers: Master (PPC) and Slave (DSP). The PPC is responsible for executing the algorithm and the DSP handles complex I/Os such as ADC, Encoder and PWM modulator. In every PWM period T_{PWM}, the PPC sends PWM information to DSP and it will update the output compare register in the middle of PWM period inside an interrupt service routine (ISR). From Figure 2.23 we can conclude that if the PWM information is sent before the ISR is executed, the PWM modulator will be updated in next period. It results in the output delay depending on the timing of transmission, which is associated to algorithm execution time. It is necessary to determine the exact delay period by experiment.

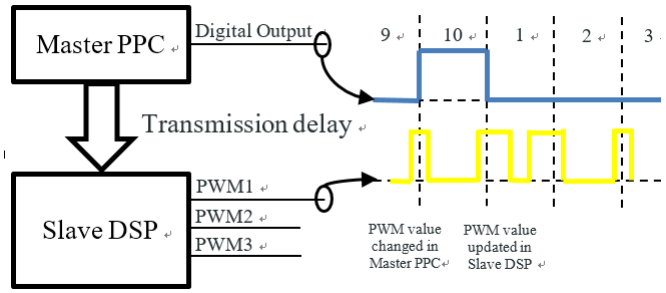

Figure 2.24 Principle of delay measurement

The test is performed in such a way that every 10 periods the PWM modulator will be assigned a different value respect to the past 9 periods. As shown in Figure 2.24, in the same period, one digital pin on the Master PPC is toggled where there is no transmission delay. Then the two outputs are captured by an oscilloscope (shown in Figure 2.25).

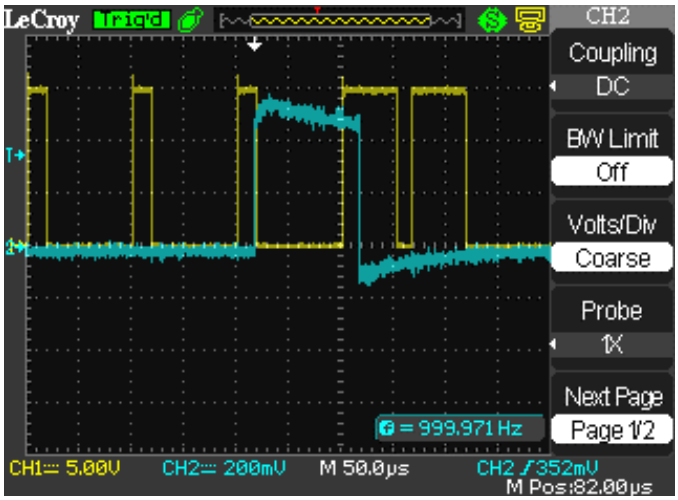

Figure 2.25 PWM output captured by oscilloscope

Thus, in order to cancel the uncertainty in PWM generation delay, we have to make the control strategies to be executed in the middle of a PWM period so that the result will be definitively sent to the Slave DSP before the next middle of period.

2.4.3.2 Modification of predictive control strategies

Because there is one-step delay in PWM generation, as shown in Figure 2.26, this means that the input is sampled at t_k (k_{th} time instant), and the output is updated at t_{k+1}. So, during the period t_k, the predictive model must be able to estimate the system response at t_{k+2} to determine the output at t_{k+1}.

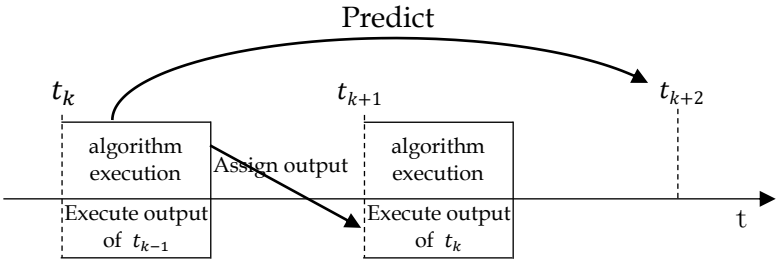

Figure 2.26 Timing diagram of MPC with 1-step delay

For FCS-MPC, as presented in [54], an iterative two-step predictive model must be used. It is indicated as below:

$$\hat{I}_{dq}(k+1) = AI_{dq}(k) + BV_{dq}(k) - C \tag{2.66}$$

$$\hat{I}_{dq}(k+2) = A\hat{I}_{dq}(k+1) + BV_{dq}(k+1) - C \tag{2.67}$$

In the first step, $\hat{I}_{dq}(k+1)$ is predicted with the voltage vector $V_{dq}(k)$ obtained

in t_{k-1}. In the second step, PTC and PTCSS will evaluate the voltage vector $V_{dq}(k+1)$ as described previously, while in the case of OPTC, [56] gives out the analytic solution directly:

$$V_{dq}(k+1) = B^{-1}\left(I_{dq}^{*} - A\left(AI_{dq}(k) + BV_{dq}(k) - C\right) + C\right) \tag{2.68}$$

2.4.4 Experiment result

The purpose of this experiment is to test the stability and its performance. The operation speed is determined by multiple factors. First, the nominal speed ($V_{nominal}$) of the experimental motor is 6250 RPM (654 rad/s). But our experimental bench cannot operate at this speed due to the mechainical limitation of the track. Its maxmimal speed is around 1m/s, or 300 rad/s equalent to the speed of the motor. During the experiment, we plan to have a 2 second sampling intervcal to calculate the performance indicator. In this period, the motor must be in fully steady speed operation. Thus, we also add a 0.5s slop speed profile both in acceleration and deceleration phase. Taking these factors into account, the experiment speed is determined as 40 rad/s. This speed is much lower than the nominal speed, it won't influerence the result because we are intreseted in the performance difference between these control strategies rather than their absolut performance.

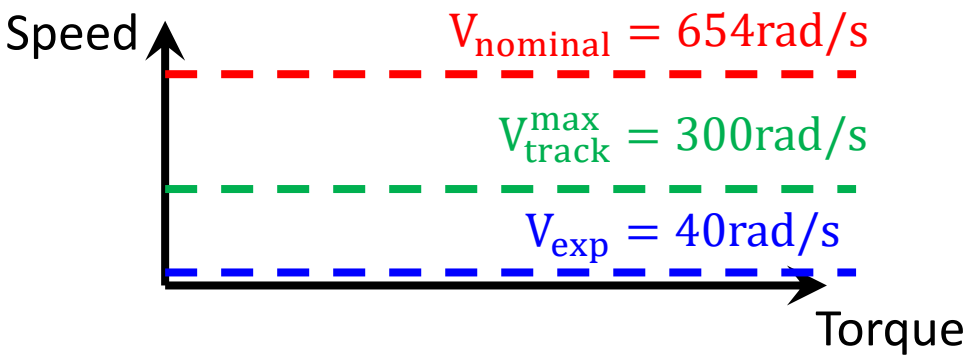

Figure 2.27 Different speed profile

The stability concerns not only in normal operation but also in high unbalanced torque transient situation. So, during the experiment, the two motors were first put in steady state. Then, an external load torque was applied to motor 1 so as to test the system transient as well as robustness under unbalanced load torque situation. Its shape is shown in Figure 2.28.

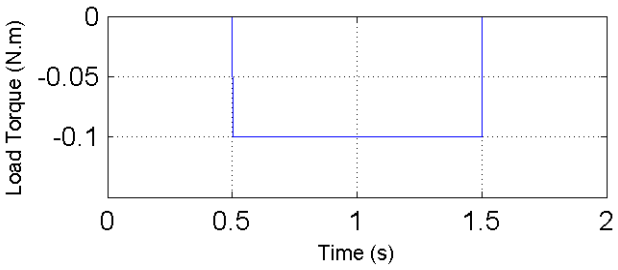

Figure 2.28 Load torque applied to motor 1

For the performance, some numerical indicators are used to precisely evaluate the performance of different aspects of a typical actuation system. They will be introduced in the next section. Figure 2.29-Figure 2.33 show the speed response, current response, and FFT result of one phase current respectively. The FFT result is used to calculate the THD of each control strategy. The current response clearly shows PTCSS and OPTC have less current ripple respect to PTC. By comparing Figure 2.32 and Figure 2.33, we can find that the total current from the inverter is less than the sum of the peak value of each machine. And all control strategies can properly operate under unbalanced load torque situation. Their performance indicator results are summarized in Table 2.3.

2.4.5 Performance analysis

2.4.5.1 Introduction to performance indicators

Four performance indicators which evaluate different aspect of the candidate control strategies are employed in making the comparison.

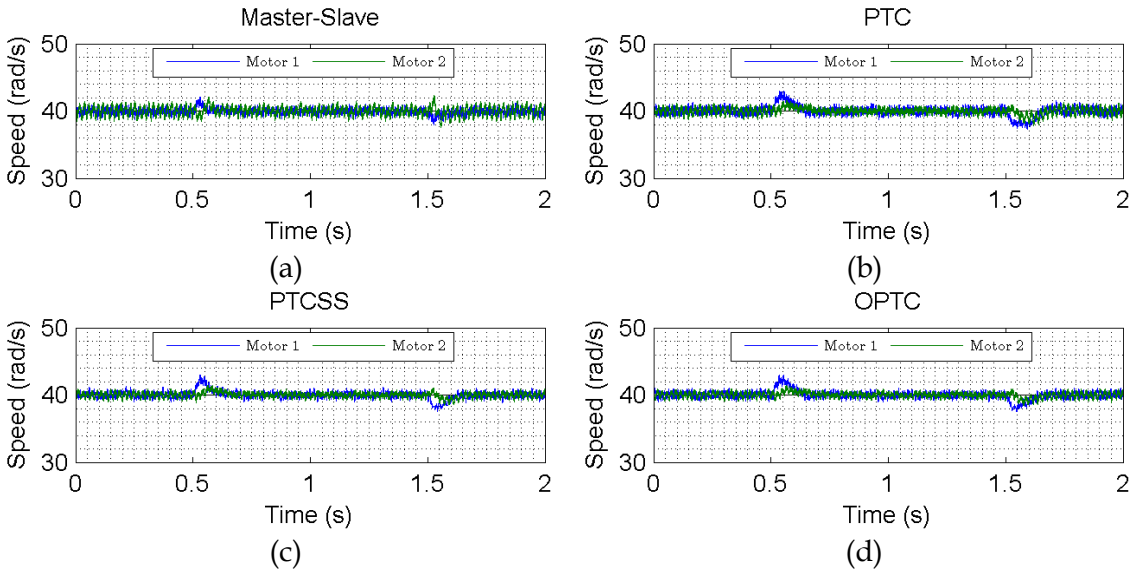

Figure 2.29 Speed response of the experiment result

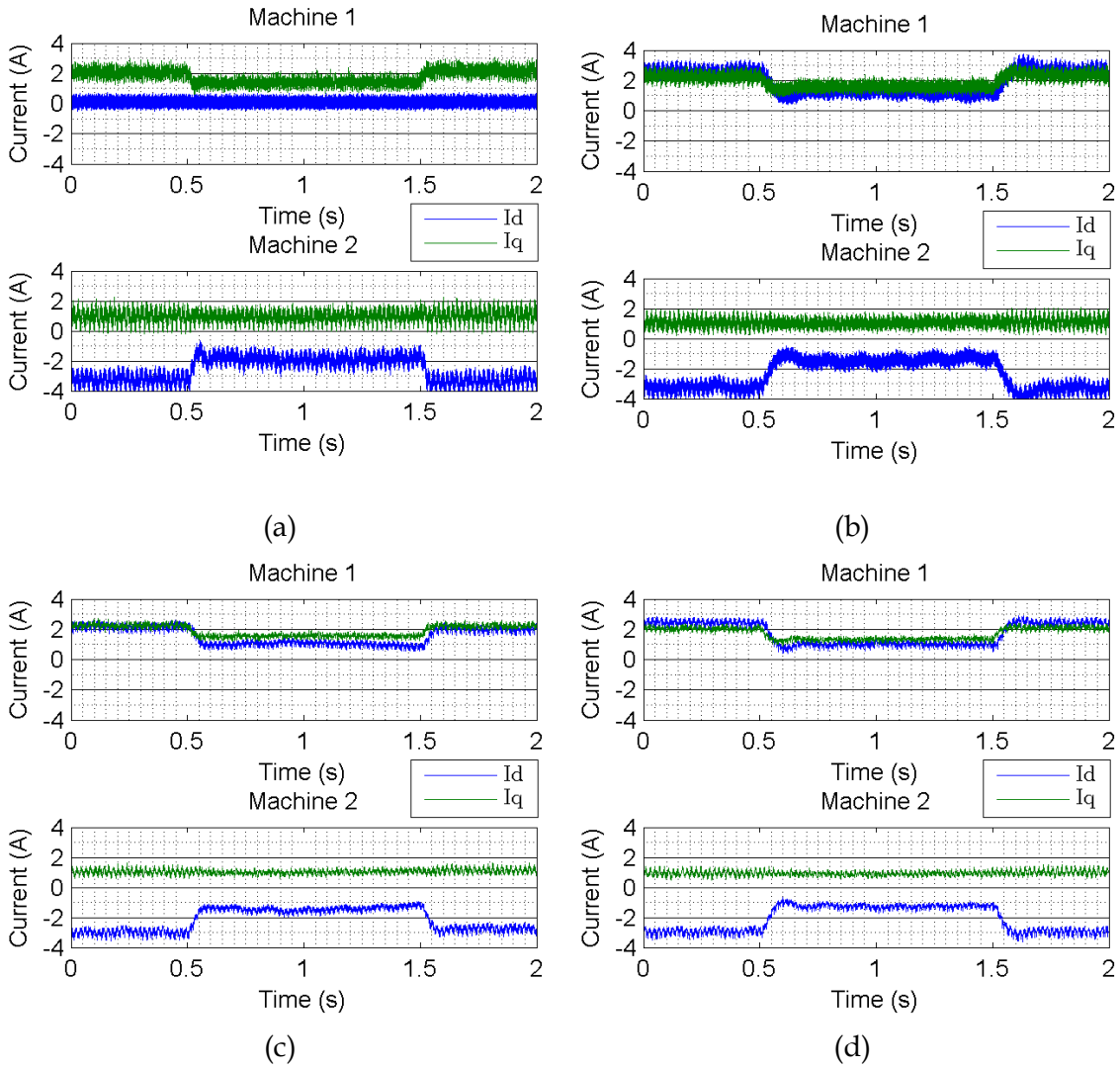

Figure 2.30 Current response of the experiment result

1) Integration Squared Error (ISE) of Speed

Integrated Squared Error (ISE) can be used to estimate the total error between two variables during a time period, such as [57][58]. Hence ISE between the speed reference and actual system response is evaluated in order to indicate the control precision of each control strategy.

$$ISE_{speed} = \int_0^t \left(\omega^*_{mM_1}(t) - \omega_{mM_1}(t)\right)^2 + \left(\omega^*_{mM_2}(t) - \omega_{mM_2}(t)\right)^2 dt \tag{2.69}$$

where ω^*_m and ω_m are the reference speed and actual mechanical speed of each machine. Since the measurement data are discrete, discrete integration is carried out as shown in (2.70).

$$ISE_{speed} = \sum_{k=1}^{N} \left[\left(\omega^*_{mM_1}(k) - \omega_{mM_1}(k)\right)^2 + \left(\omega^*_{mM_2}(k) - \omega_{mM_2}(k)\right)^2\right] \cdot T_s \tag{2.70}$$

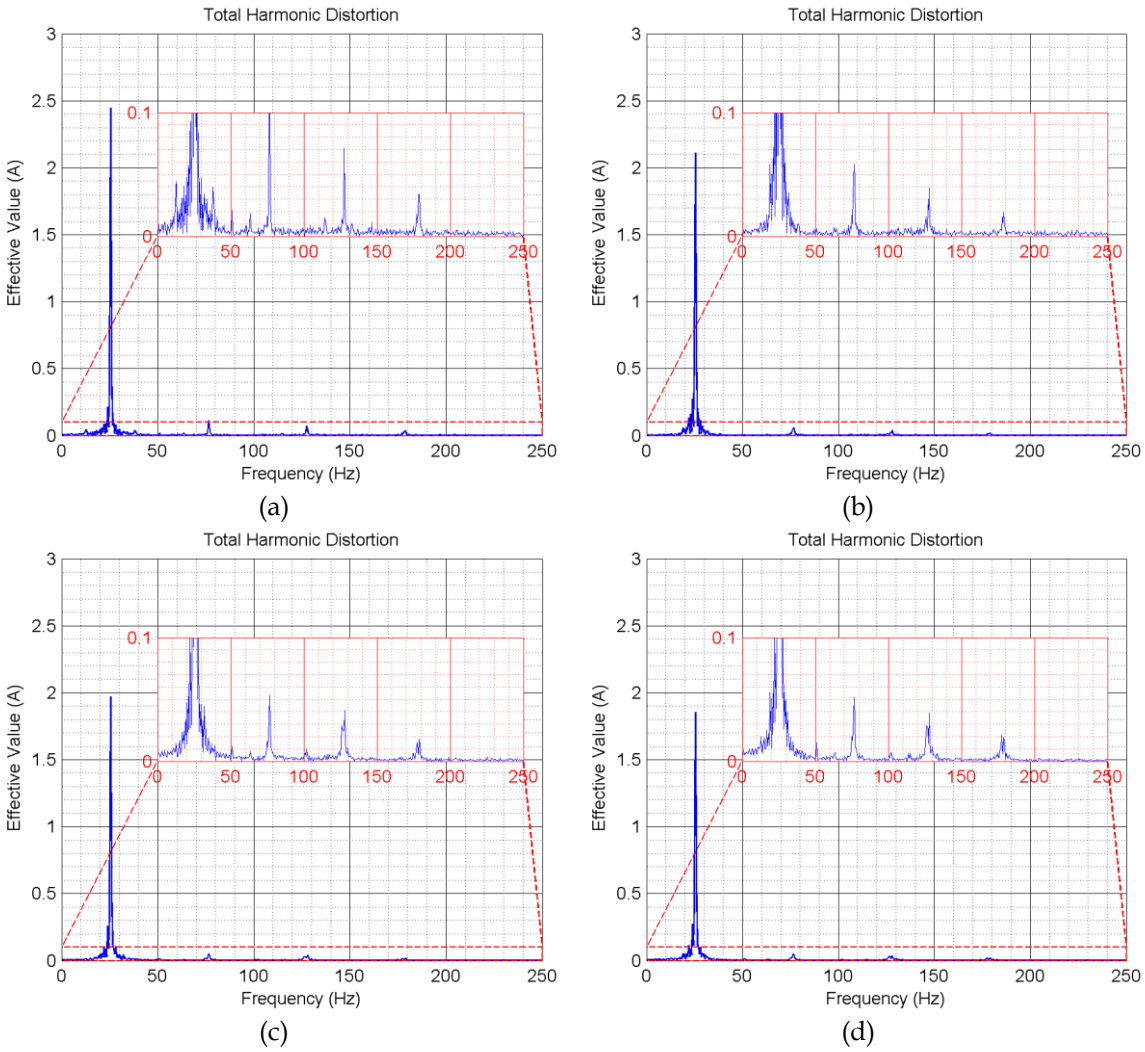

Figure 2.31 Total harmonic distortion result

where T_s represents the sampling period. In the case of Master-Slave, PTCSS and OPTC, it is equal to the switching interval, which is 100us (10kHz), and for PTC, it is equal to the calculation period (100us). The total number of samples N is consequently 20,000 and 30,000 for the two types of frequency.

2) Motor Efficiency

In a PMSM various of losses presents, including the copper loss, iron loss and stray losses [59]. The copper loss (P_{cu}) is generated by the stator winding resistance. So, P_{cu} can be generally defined as:

$$P_{cu} = R_s\left({I_{dM_1}}^2 + {I_{dM_2}}^2 + {I_{qM_1}}^2 + {I_{qM_2}}^2\right) \tag{2.71}$$

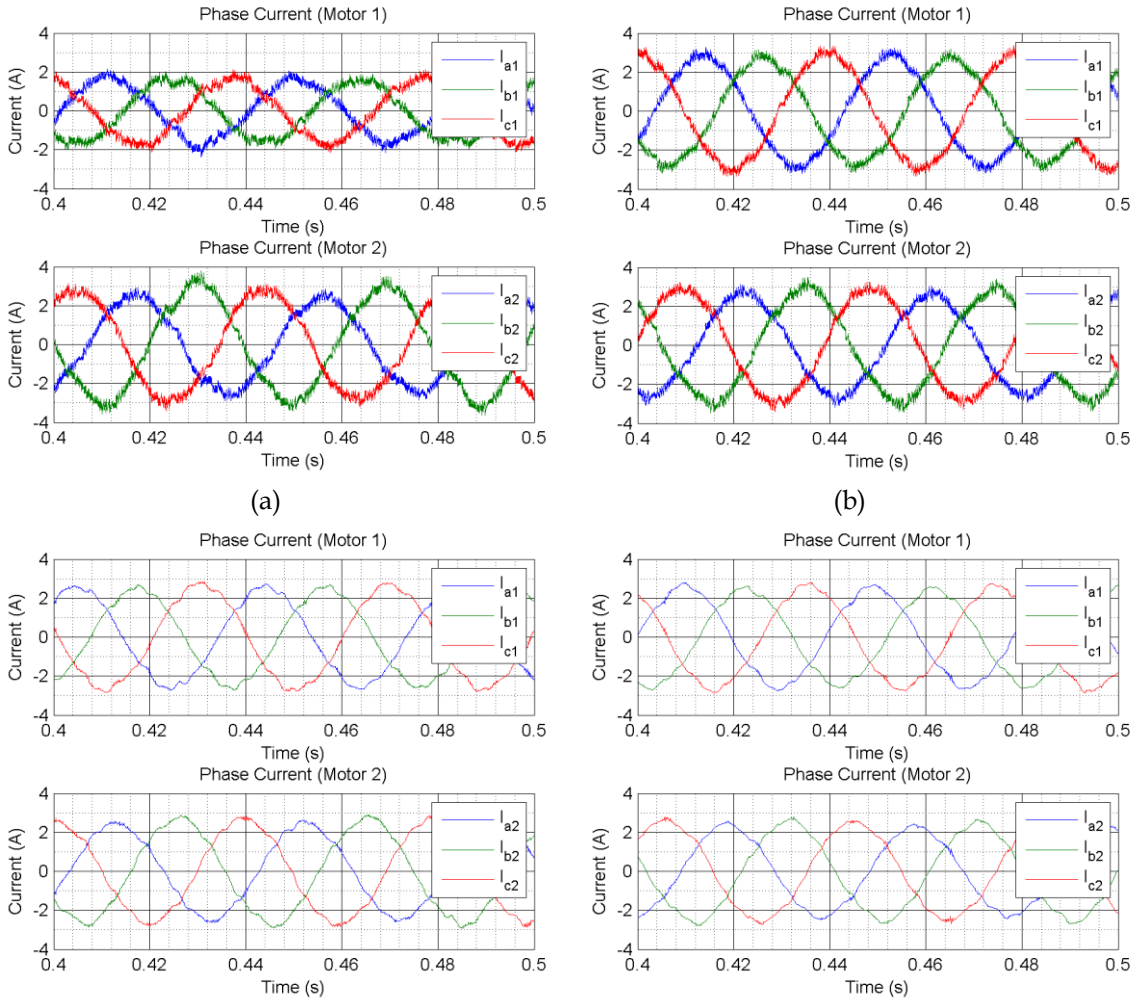

Figure 2.32 Phase Current of each motor

The iron loss (P_{fe}) is caused by the non-linearity of the magnate including hysteresis loss, eddy current loss, and the excessive loss if the magnetic steel is excited by sinusoidal magnetic field. In an electric machine, this loss is linked to the flux-linkage (φ_p) and electrical speed (ω_e) instead, which can be easily derived either from simulation or experimental data [60]. Therefore, the total iron losses can be modelled by the function of speed and flux-linkage [61][62].

$$P_{fe} = k_e(\omega_e\varphi_p)^{3/2} + (k_h\omega_e + k_c{\omega_e}^2){\varphi_p}^2 \tag{2.72}$$

where k_e, k_h and k_c are the coefficient of the hysteresis loss, eddy current loss and excessive loss in function of the φ_p and ω_e.

The stray loss term consists of the losses arising from non-uniform current and magnetic flux distortion [63], and is ignored here. Because in the experiment the speed and flux are the same for each control strategy, the iron loss keeps the same. In order to evaluate the influence of different control strategy, only the copper loss is considered in this indicator. Then motor efficiency is defined as the ratio between mechanical energy

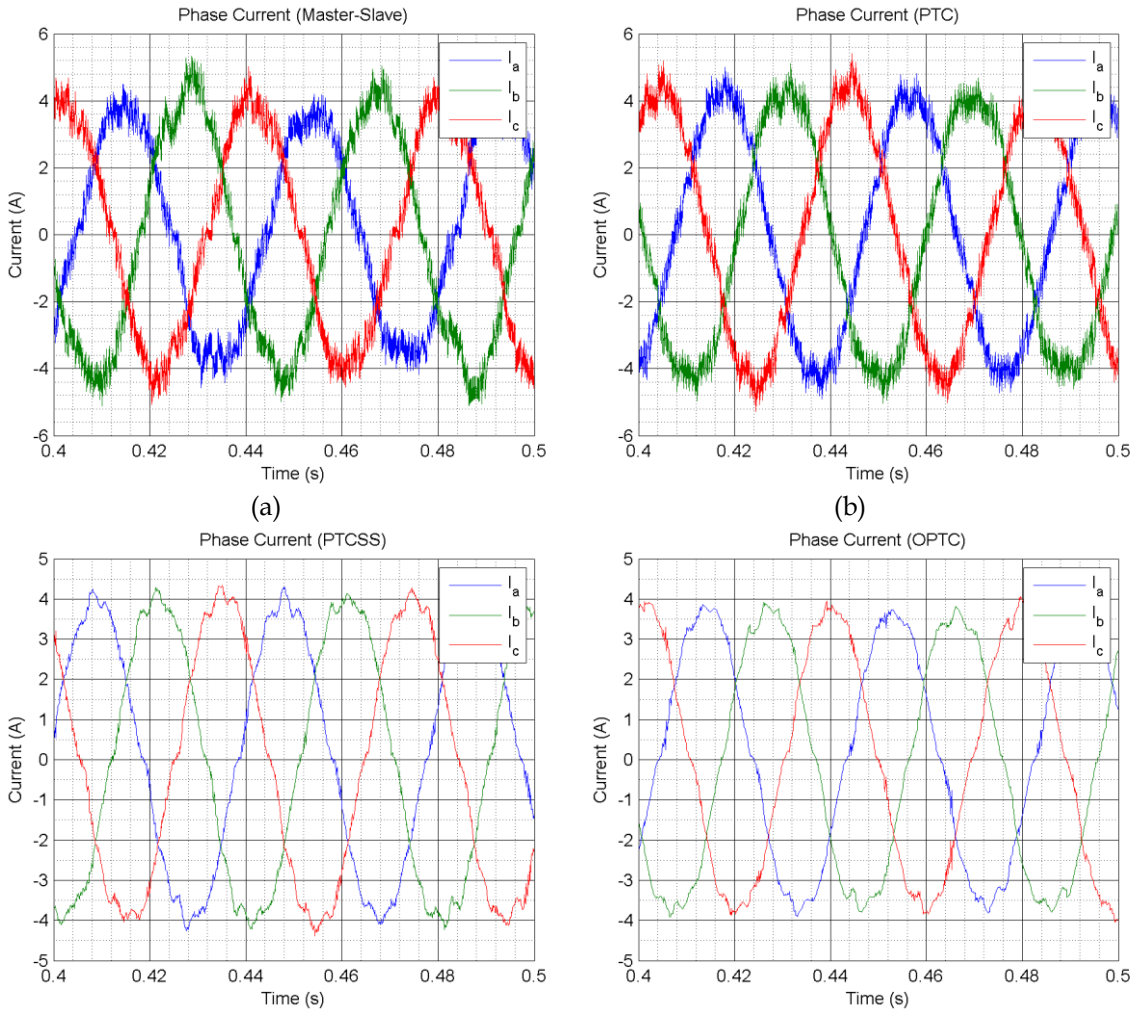

Figure 2.33 Phase Current of the inverter

and electrical energy. The mechanical energy (E_m) can be calculated as the sum of the products between the speed and torque of each motor.

$$E_m = \sum_{k=1}^{N} N_p \varphi_p \left[I_{qM_1}(k)\omega_{mM_1}(k) + I_{qM_2}(k)\omega_{mM_2}(k) \right] \cdot T_s \tag{2.73}$$

Energy loss due to copper loss (E_{cu}) is estimated using (2.74).

$$E_{cu} = \sum_{k=1}^{N} \left[I_{dM_1}(k)^2 + I_{dM_2}(k)^2 + I_{qM_1}(k)^2 + I_{qM_2}(k)^2 \right] R_s \cdot T_s \tag{2.74}$$

Meanwhile the electrical energy is estimated using the sum of E_{cu} and E_m. Thus, the motor efficiency η_{motor} can be calculated by (2.75).

$$\eta_{motor} = \frac{E_m}{E_m + E_{cu}} \times 100\% \tag{2.75}$$

3) Inverter Losses

Inverter loss is mainly consisted of three parts: conduction losses (P_{con}), switching losses (P_{sw}), and blocking (leakage) losses (P_b) [64].

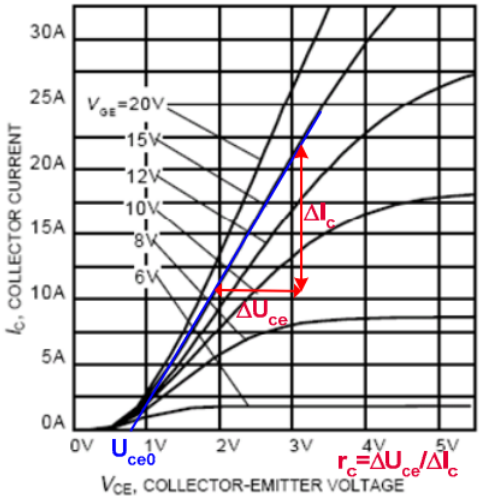

Figure 2.34 Typical output characteristics of an IGBT

Conduction losses of the IGBT were related to conduction voltage drop, current, duty cycle, and junction temperature [65]. It is often modelled with a collector-emitter voltage (U_{ce}) and a collector-emitter on-state resistance (R_c).

$$P_{con}(t) = U_{ce}(t)I_c(t) + R_c I_c(t)^2 \tag{2.76}$$

In this way, the non-linear characteristic of the current-voltage dependency is modeled in a simple way. These two parameters can be found out in the datasheet of an IGBT with the method presented in Figure 2.34. But it is obvious that U_{ce} and R_c are not permanent parameters which makes difficulties in actual calculation.

Switching losses were composed by the opening losses and turn-off losses. Figure 2.35 shows an example of transistor switching action waveform in one switching cycle [66]. The switching losses can be approximately expressed as:

$$P_{sw} = \frac{1}{T}\sum_{j=1}^{N}\frac{1}{6}v_j i_j\left(T_{on} + T_{off}\right) \tag{2.77}$$

where T is the fundamental frequency of the PWM period, T_{on} is the turn-on time and T_{off} is the turn-off time. N is the total number of the switching cycles in one period T, j is the j-th switching, and v_j, i_j are the instantaneous values of voltage and current at j-th switching. From (2.77), it is easy to conclude that switching loss can be reduced by reducing the switching frequency or by reducing the instantaneous value of current or voltage during switching interval.

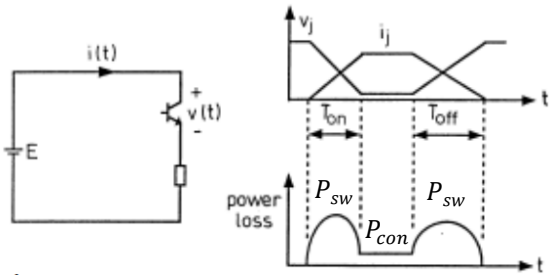

Figure 2.35 Transistor switching action waveform in one switching cycle

There are still various of losses in an inverter such as blocking (leakage) losses, diode conduction losses, and so on. Considering that we are focusing on comparing the inverter losses respect to different control strategies rather than the actual losses caused, which is out of the scope of this thesis. Here we will focus on the switching losses only. Because first, it is complex to calculate the conduction losses, the temperature or working condition will influence the parameters. Due to the fact that our experiment environment, including the load torque applied, the maximum speed, is fixed. The difference between different control strategies is assumed to be not significant. Second, with the switching frequency increases, the state change of IGBTs used in an inverter contributes a significant amount to the total system losses [64][66]. Recalling that PTC and PTCSS are variable frequency and OPTC is fixed frequency, therefore it worth studying the actual difference of switching loss between them. Since the switching losses only happens when IGBT changes state, we propose an easy but representative indicator that directly counting their switching times to approximately evaluate the switching losses.

4) Total Harmonic Distortion (THD)

The Total Harmonic Distortion (THD) is defined as the ratio between the power of all harmonic components and the fundamental frequency. This indicator characterizes the power quality of electric power systems. In our indicator until the 3rd harmonic is considered. It is calculated as:

$$THD = \frac{I_2 + I_3 + I_4}{I_{fundamental}} \times 100\% \tag{2.78}$$

2.4.5.2 Indicator results and analysis

All performance indicators are calculated only in the time region shown in Figure 2.29 and Figure 2.31. They have taken the average value of five independent experiments to compensate the random influence.

From the perspective of power quality, the experiment result proves the expectations. From Figure 2.32 we can easily identify the difference. Master-Slave and PTC, which use only 7 voltage vectors, have a more significant current ripple than PTCSS and OPTC which uses SVPWM instead. During operation, the optimization process must generate a sequential of different voltage vector to approach the optimal one. This will lead to high

THD. Therefore, SVM is preferred concerning current ripple.

THD should not been influenced by the current ripple, because the frequency of the ripple is much higher than the fundamental frequency. On the other hand, Master-Slave and PTC have the almost the same level of current ripple, but Master-Slave has higher THD than PTC while PTC, PTCSS, OPTC have almost the same. This means that THD is control strategy influenced indicator. we can identify from Figure 2.32 there is more current distortion in Master-Slave than other control strategies.

From the perspective of inverter losses, Master-Slave and Predictive Torque Control have used only half switching times of other control strategies. Of course, this has a penalty on the control quality, the speed ripple of Master-Slave and PTC is higher than PTCSS and OPTC.

From the perspective of control quality, especially in unbalanced torque situation, Master-Slave is much better than other three control strategies. In Figure 2.29, when the external load torque is applied in 0.5s, Master-Slave can compensate it much faster than other three strategies, which leads to smaller variation in speed response. Relatively speaking, the other three strategies use independent speed controller that causes the slow response.

However, from the perspective of η_{motor}, the result is not satisfactory. The efficiency of control strategies using unique cost function for two motors is much lower than *Master-Slave* even the cost function (2.52) has taken efficiency into account. Considering that PTC and Master-Slave have higher current ripple, a higher current ripple will definitively cause higher joule loss. But it only happens under the same control strategy. In this experiment, PTC, PTCSS, and OPTC have obvious higher I_d current than Master-Slave that leads to higher joule loss even they have less current ripple.

As the efficiency of PTC, PTCSS, OPTC is relatively close, its cause may relate to the control strategy. In fact, the cost function (2.52) has over constrained the system. If look back to the predict model (2.49) and the cost function, the optimization process tends to find the best voltage vector that makes the prediction equal to the reference and response, which is:

$$\begin{bmatrix} I_{dM_1}(k+1) \\ I_{qM_1}(k+1) \\ I_{dM_2}(k+1) \\ I_{qM_2}(k+1) \end{bmatrix} = \begin{bmatrix} 0 \\ I^*_{qM_1} \\ 0 \\ I^*_{qM_2} \end{bmatrix} \tag{2.79}$$

Obviously, it is not feasible because there are 4 equations in (2.49), but only 2 unknown variables (V_{dM_1},V_{qM_2}) left. Thus, the optimization process can only give out a compromise voltage vector. With this functioning stability is not guaranteed and so that the solution is

not optimal. Refer to Table 2.3, the indicators of *Master-Slave* among each time of experiment are relatively close. But in the case of PTC, PTCSS, and OPTC, high variation can be identified. This means that the operation state of those control strategies is undetermined which can be influenced by external facts such as rotor starting position.

2.5 **Conclusion**

In this chapter, the existing control strategies for MIDPMSM system as well as their performance are illustrated in detail. Four different control strategies based on model predictive control, including different cost functions, optimization and modulation methods, have been tested. In Figure 2.36 we have gathered all performance indicators for each control strategy using a radar chart for the sake of simplicity. It shows that each strategy has its own advantages in different respects.

	No.	THD (%)	ISE (rad2/s)	Switching Loss (count)	η_{motor}
Master-Slave	1	5.05%	1.17	42126	58.53%
	2	4.83%	1.14	42232	58.79%
	3	4.87%	1.19	42154	58.29%
	4	5.52%	1.22	42078	58.31%
	5	5.83%	1.28	42072	57.88%
	Avg.	5.22%	1.20	42132	58.36%
Predictive Torque Control	1	3.71%	1.38	41464	53.40%
	2	3.44%	1.19	41396	54.49%
	3	3.14%	1.23	41456	53.92%
	4	4.03%	1.57	40940	50.84%
	5	3.55%	1.30	41314	52.81%
	Avg.	3.57%	1.33	41314	53.09%
Predictive Torque Control Split & Seek	1	3.68%	0.92	80000	53.37%
	2	3.74%	1.03	80000	52.20%
	3	3.68%	0.96	80000	55.41%
	4	3.49%	0.95	80000	54.13%
	5	3.43%	1.08	80000	53.29%
	Avg.	3.60%	0.99	80000	53.68%
Optimal Predictive Torque Control	1	3.08%	1.04	80000	56.14%
	2	3.71%	1.71	80000	47.16%
	3	4.08%	0.98	80000	57.78%
	4	3.64%	1.40	80000	50.66%
	5	3.72%	1.15	80000	53.88%
	Avg.	3.65%	1.26	80000	53.12%

Table 2.3 Experiment result

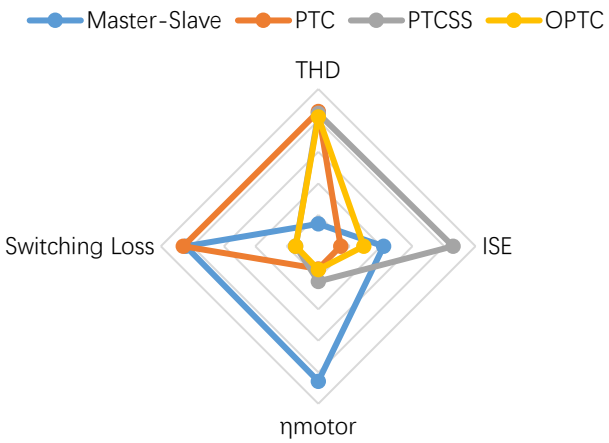

Figure 2.36 Performance comparison of all control law (the best is at the border)

As a summary, the modulation method has the greatest impact on current ripple. Increasing the number of voltage vector can greatly improve this performance. But small number of voltage vector can reduce the switching losses of inverter. In practice, these two aspects need to be coordinated. Master-Slave has the best control quality because it can better compensate the external load torque variation. This means that handling torque variation in speed control loop maybe not a good idea.

The most important is that experimental results have shown that the efficiency of a unique cost function is lower than that of a master-slave. The analysis has shown that it is due to the over-constrained situation. Oriented from a MIDPMSM, this is an important discovery for designing the controller and for efficiency optimization. A detailed expansion will be given in the next chapter.

Chapter 3

Controller design and efficiency optimization

Table of content

3.1 Introduction

The experiment test in the last chapter has demonstrated the effectiveness of existing control strategies including Average Techniques, DTC, MPC, and Master-Slave. Meanwhile, it also shows that the efficiency of a MIDPMSM system without optimization can be very low (about 60%). For a single-motor system, the efficiency is usually at least 90% by applying MTPA (Maximum Torque Per Ampere) strategy. The efficiency problem must be solved before it is put into real applications.

MTPA law is the major optimization objective for a PMSM. This is because the stator resistance causes the majority of the energy loss. Due to the fact that torque is determined by the application, minimizing the stator current while keeping the torque is the key to the optimization. For a non-salient pole motor, its MTPA law is as simple as setting $I_d^* = 0$ in the current controller [67][68], which consequently set the stator flux perpendicular to the rotor's flux. But this strategy cannot be applied to a MIDPMSM directly. As proven in 2.3.1, angle displacement between two motors' rotor must be preserved for independent torque controllability. Therefore, it is impossible to set the stator flux perpendicular to both motors' rotor flux at the same time.

But on the other hand, the MTPA method for a salient pole PMSM [69][70] gives us an inspiration. It is more complex because it uses the steady-state model to online calculate the MTPA operation point based on current operation state. In other words, the I_d^* is not always equal to zero but a value determined by speed and torque. This method can also be used in the case of a MIDPMSM system. Many researches, such as [32][72][73][74], have adapted this efficiency optimizing method for MIDPMSM system. These controllers will be introduced and analyzed in detail in this chapter.

Based on these researches, in this chapter, a comprehensive yet simple efficiency-optimal controller solution to the MIDPMSM system is given. All aspects of the controller, such as system controllability, determinacy, stability, and limitation determination, are studied and proved. Considering that open-loop optimization is utilized, a parameter-sensitivity study is also given. During the experimental part, its feasibility and stability are verified; its efficiency is better than existing control strategies.

3.2 Introduction and analysis of existing controller

3.2.1 $\Sigma - \Delta$ strategy

The principle of $\Sigma - \Delta$ strategy has been introduced in section 2.3.2.2. It uses the total current from the inverter, which is defined as:

$$I_{\Sigma} = \frac{I_{M_1} + I_{M_2}}{2} \tag{3.1}$$

Thus, under the definition of MTPA, the maximum efficiency point is defined when $|T_{\Sigma}|/|I_{\Sigma}|$ gets the maximum value, where $|I_{\Sigma}|$ is defined as (3.2).

$$|I_{\Sigma}| = \sqrt{{I_{\Sigma,d}}^2 + {I_{\Sigma,q}}^2} \tag{3.2}$$

But there is an error. (3.2) has defined the total current as the magnitude of the vector summed current, which is:

$$|I_{\Sigma}| = |I_1 + I_2| \tag{3.3}$$

It is in fact the total current of the equivalent motor [71]. Due to the efficiency is mainly related to the power losses on the resistance of stator windings, the total current must be the algebra sum of each motor's current. That is:

$$I_{Total} = |I_1| + |I_2| \tag{3.4}$$

Obviously, $|I_{\Sigma}|' \geq |I_{\Sigma}|$ because for two vectors, the magnitude of their vector sum is less or equal to their algebra sum. In Figure 2.32 and Figure 2.33, we have already shown that the peak value of the total current from the inverter is less than that of each machine. As introduced before, the stator resistance causes most of the energy loss. Minimizing the total current of the two-parallel connected motor doesn't consequently minimize the total stator current. We can conclude that the efficiency optimization proposed in [32] couldn't be valid.

3.2.2 Stator current minimization

Proposed in [72][73], the author has used a more explicit optimization method. Differ from [32], the optimization objective becomes minimizing the copper loss from the motor:

$$P_{copper} = R_s\left({I_{dM_1}}^2 + {I_{qM_1}}^2 + {I_{dM_2}}^2 + {I_{qM_2}}^2\right) \tag{3.5}$$

Considering that the output torques depend on the loads, I_{qM_1} and I_{qM_2} are determined according to the output torque. They are not arbitrary. Thus, the cost function must be modified as:

$$g = {I_{dM_1}}^2 + {I_{dM_2}}^2 \tag{3.6}$$

The steady-state model of a MIDPMSM system is used to calculate the optimal efficiency state. Its optimization procedure is introduced below. (3.7) shows the steady-state model of a PMSM.

$$\begin{bmatrix} V_d \\ V_q \end{bmatrix} = \begin{bmatrix} R_s & -L_s\omega_e \\ L_s\omega_e & R_s \end{bmatrix} \begin{bmatrix} I_d \\ I_q \end{bmatrix} + \begin{bmatrix} 0 \\ \omega_e\varphi_p \end{bmatrix} \tag{3.7}$$

Because two motors are connected in parallel, their stator voltage is the same. (3.8) can

be applied.

$$V_{dM_1}{}^2 + V_{qM_1}{}^2 = V_{dM_2}{}^2 + V_{qM_2}{}^2 \tag{3.8}$$

By substituting the voltage elements in (3.8) with (3.7). An equation representing the operation point of a MIDPMSM system can be obtained.

$$\left(I_{dM_1} + \frac{\beta}{2\alpha}\right)^2 - \left(I_{dM_2} + \frac{\beta}{2\alpha}\right)^2 = \frac{\gamma_2 - \gamma_1}{\alpha} \tag{3.9}$$

where

$$\begin{aligned} \alpha &= R_s{}^2 + (\omega_e L_s)^2 \\ \beta &= 2L_s\omega_e{}^2\varphi_p \\ \gamma_1 &= \left(R_s{}^2 + (\omega_e L_s)^2\right)I_{q1}{}^2 + 2R_s\omega_e\varphi_p I_{q1} + \omega_e{}^2\varphi_p{}^2 \\ \gamma_2 &= \left(R_s{}^2 + (\omega_e L_s)^2\right)I_{q2}{}^2 + 2R_s\omega_e\varphi_p I_{q2} + \omega_e{}^2\varphi_p{}^2 \end{aligned} \tag{3.10}$$

Each $\left(\mathrm{I_{dM_1}}\middle|\mathrm{I_{dM_2}}\right)$ pair defined in (3.9) is an operation point of a MIDPMSM system. Then Lagrange multiplier can be used to calculate the extreme value of (3.6). The Lagrange can be defined as:

$$L\left(I_{dM_1}, I_{dM_2}, \lambda\right) = g\left(I_{dM_1}, I_{dM_2}\right) + \lambda\left(\left(I_{dM_1} + \frac{\beta}{2\alpha}\right)^2 - \left(I_{dM_2} + \frac{\beta}{2\alpha}\right)^2 - \frac{\gamma_2 - \gamma_1}{\alpha}\right) \tag{3.11}$$

where λ is the Lagrange multiplier. Then the solution of the partial derivative of (3.11) represents the extreme value of (3.6), which are the candidates of optimal efficiency point. (3.12) to (3.14) shows the results after the partial derivative.

$$\frac{\partial L\left(I_{dM_1}, I_{dM_2}, \lambda\right)}{\partial I_{d1}} = 2I_{dM_1} + 2\lambda\left(I_{dM_1} + \frac{\beta}{2\alpha}\right) \tag{3.12}$$

$$\frac{\partial L\left(I_{dM_1}, I_{dM_2}, \lambda\right)}{\partial I_{d2}} = 2I_{dM_2} - 2\lambda\left(I_{dM_2} + \frac{\beta}{2\alpha}\right) \tag{3.13}$$

$$\frac{\partial L\left(I_{dM_1}, I_{dM_2}, \lambda\right)}{\partial \lambda} = \left(I_{dM_1} + \frac{\beta}{2\alpha}\right)^2 - \left(I_{dM_2} + \frac{\beta}{2\alpha}\right)^2 - \frac{\gamma_2 - \gamma_1}{\alpha} \tag{3.14}$$

Through merging (3.12) and (3.13) together, it is possible to obtain

$$I_{d2} = -\frac{I_{dM_1}\beta}{4\alpha I_{dM_1} + \beta} \tag{3.15}$$

(3.15) represent the MTPA curve of the MIDPMSM system.

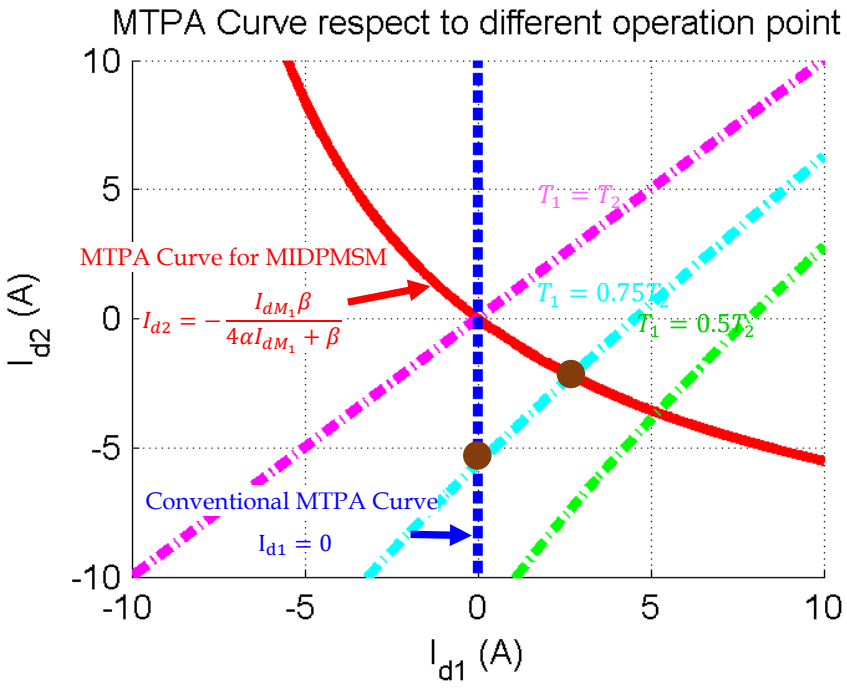

Figure 3.1 MTPA curve and different operation curve

We can draw the MTPA trajectory, as depicted in (3.15) and different operation curve according to the load torque of the motor 1, as defined by (3.9), in Figure 3.1 for better understanding. These two motors are operating in rated speed and torque. The MTPA trajectory drawn with solid line is independent to the torque and unique for the certain speed. In contrast, the operation curves are output torque dependent of the two motors. Their intersection is the MTPA operation point of certain speed and torque condition, which can be calculated by replacing I_{dM_2} in (3.14) by (3.15).

The blue dashed line represents the conventional MTPA method. The operating point is decided on the $I_{dM_1} = 0$ line to minimize the current of the M_1. Obviously, this method is valid only when two motors has the same torque.

3.3 **Controller design**

In 3.2 we have barely introduced two efficiency-optimal control strategies. They have the same optimization procedure: Define an efficiency cost function and use the steady state model to calculate the optimal state. Then this optimal state is imposed by the controller. But these studies are not complete. First, because the open-loop optimization is used, it must be proved that the controller can always impose the specified state. Second, neither of them have proved their stability or given out a stable criterion. These two problems make the control strategies not clear in the aspects of system stability and efficiency issues. This has become the biggest obstacle to the practical use of MIMPMSM. Thus, in this part, based on the optimization idea proposed in previous researches, a controller is designed in an explicit way. Including its structure, stability criteria are developed. Moreover, because the open-loop optimization heavily relays on precision of

model parameters. A study on motor parameter sensitivity is provided.

3.3.1 Controller Structure design

MIDPMSM is a Multi-Input Multi-Output (MIMO) system. A controller can be seen as a constraint applied to the system output. It must be designed properly. With limited input, if the system is over-constrained, there will be a conflict between different control requirement. Just like increasing the current of a bulb to make it brighter while decreasing the current to make it cooler. These two constraints (brightness and temperature) cannot be applied at the same time if there is only one input (the current). On the contrary, in the under-constrained situation, some the system output becomes uncontrollable. Both of two situations make the system undetermined and difficult to analyses because its behavior is unpredictable. So, the system determinacy must first be considered because it affects the structure of the controller.

In mathematics, the system determinacy is equivalent to the solution existence problem of its steady-state. If the solution number is finite, the system is determined. Otherwise, if the solution number is zero or infinite, the system is either over-constrained or under-constrained. This conclusion can be adapted to MIDPMSM directly. The steady-state model of the MIDPMSM system can be got through setting the derivatives in (2.23)to zero. The result is shown in (3.16).

$$\begin{bmatrix} 1 & 0 \\ 0 & 1 \\ cos\,\theta_d & sin\,\theta_d \\ -sin\,\theta_d & cos\,\theta_d \end{bmatrix} \begin{bmatrix} V_{dM_1} \\ V_{qM_1} \end{bmatrix} = \begin{bmatrix} R_s & -L_s\omega_e & 0 & 0 \\ L_s\omega_e & R_s & 0 & 0 \\ 0 & 0 & R_s & -L_s\omega_e \\ 0 & 0 & L_s\omega_e & R_s \end{bmatrix} \begin{bmatrix} I_{dM_1} \\ I_{qM_1} \\ I_{dM_2} \\ I_{qM_2} \end{bmatrix} + \begin{bmatrix} 0 \\ \omega_e\varphi_p \\ 0 \\ \omega_e\varphi_p \end{bmatrix} \tag{3.16}$$

From (3.16) we can find that the MIDPMSM system has two input variables (V_{dM_1}, V_{qM_1}) and six state variables (I_{qM_1}, I_{qM_2}, I_{dM_1}, I_{dM_2}, θ_d, ω_e). Amongst them the torque and speed (I_{qM_1}, I_{qM_2}, ω_e) are defined by external requirements. They must be treated as known variables in (3.16). Then in (3.16) there are 5 unknown variables left but only 4 equations available. Now the controller design problem becomes solution existence problem of (3.16). If a controller is designed to regulate only the speed and torque, obviously, unknown variable is one more than equation. The system is under-constrained (solution number is infinity). On the contrary, if a controller tries to bring more than 4 variables to their reference, for example, both motor's I_d equal to zero, the system becomes over-constrained (no solution exists). In the previous chapter's experiment test, in the case of MPC based control strategies, current offset between reference and response exists. This is because that linear quadratic optimization method is used, a solution with minimal distance to the control objective is obtained. While from the point of view of control quality, none of the control objective is achieved since static error always exists.

In order to make the MIDPMSM system properly operate, in the first place, the controller must and only can apply an additional constrain amongst I_{dM_1}, I_{dM_2} or θ_d so

that the MIDPMSM system is adequate constrained (solution number is finite). Then, the controller set a reference value obtained by efficiency optimal procedure to this additional constrained variable. As the system is determined, one of the possible states should correspond to maximum efficiency state. *Stator Current Minimization* has chosen I_{dM_1} as the constrained variable. But the analysis here provides a systematic explanation to the control scheme design. Here θ_d is selected as the controlled variable. (3.16) can be rewritten in the non-homogeneous linear equation form (shown in (3.17)).

$$\begin{bmatrix} -R_s & 0 & 1 & 0 \\ -\omega_e L_s & 0 & 0 & 1 \\ 0 & -R_s & cos\,\theta_d & sin\,\theta_d \\ 0 & -\omega_e L_s & -sin\,\theta_d & cos\,\theta_d \end{bmatrix} \begin{bmatrix} I_{dM_1} \\ I_{dM_2} \\ V_{dM_1} \\ V_{qM_1} \end{bmatrix} = \begin{bmatrix} -\omega_e L_s I_{qM_1} \\ R_s I_{qM_1} + \omega_e \varphi_p \\ -\omega_e L_s I_{qM_2} \\ R_s I_{qM_2} + \omega_e \varphi_p \end{bmatrix} \tag{3.17}$$

Its corresponding solution is:

$$\begin{cases} I_{dM_1} = \dfrac{Ay - B}{Z^2 x} - \dfrac{C}{Z^2} \\ I_{dM_2} = \dfrac{A - By}{Z^2 x} - \dfrac{C}{Z^2} \\ V_{dM_1} = y\left(R_s I_{dM_2} - \omega_e L_s I_{qM_2}\right) - x\left(R_s I_{qM_2} + \omega_e L_s I_{dM_2} + \omega_e \varphi_p\right) \\ V_{qM_1} = x\left(R_s I_{dM_2} - \omega_e L_s I_{qM_2}\right) + y\left(R_s I_{qM_2} + \omega_e L_s I_{dM_2} + \omega_e \varphi_p\right) \end{cases} \tag{3.18}$$

Where

$$\begin{aligned} Z &= \sqrt{{R_s}^2 + (\omega_e L_s)^2} \\ A &= Z^2 I_{qM_1} + R_s \omega_e \varphi_p \\ B &= Z^2 I_{qM_2} + R_s \omega_e \varphi_p \\ C &= L_s {\omega_e}^2 \varphi_p \\ x &= sin\,\theta_d \\ y &= cos\,\theta_d \end{aligned} \tag{3.19}$$

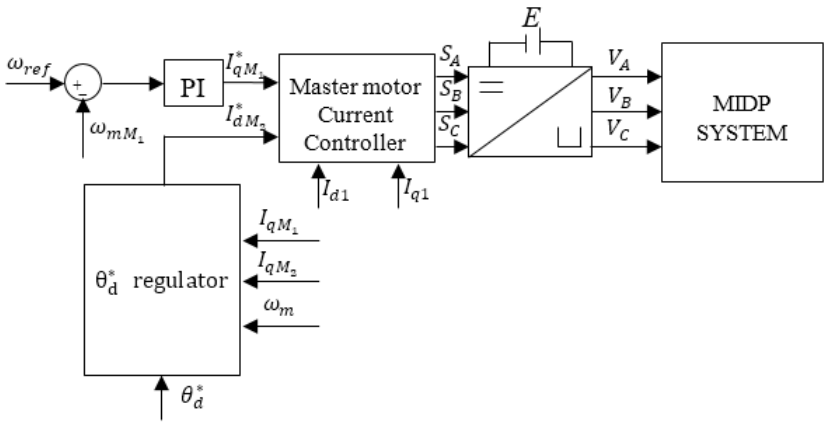

Figure 3.2 Block diagram of proposed controller

Figure 3.2 shows the proposed controller block diagram. The controller consists of two blocks: master motor controller and θ_d regulator. The master controller only controls

M_1. M_2 is left open loop. In the master controller, a regular vector current controller is used. Space Vector Modulation (SVM) generates the desired voltage vector. The I_{qM_1} reference is given by a PI speed controller. The I_{dM_1} reference is given by the θ_d regulator. The principle of the controller is to:

4) Calculate the optimal steady-state through θ_d.

5) Obtain the system state by (3.19).

6) Set I_{d1}^* to the same value as that in the optimal state.

Steps 2 and 3 are processed by the θ_d regulator. This method uses θ_d to calculate the optimal system state because taking θ_d as a known variable makes the state solution of (3.17) linear and unique. This property simplifies the analysis and results greatly. Moreover, the state is set by I_{dM_1} which is easier to implement.

3.3.2 θ_d regulator

Although determined system leads to finite number of possible state, however, it must be proved beforehand that the I_{d1} set can drive the system only to the given state (that the response is unique). This precondition is linked to the solution condition of a MIDPMSM system for a given I_{dM_1} and its stability. The proof assumes that for both two motors:

- The rotational speed (ω_m) is positive.
- Operate as motor, which means the term A and B in (3.19) are definitively positive.

3.3.2.1 Solution condition of θ_d

The prove starts with the situation of θ_d with respect to I_{dM_1}, which is:

$$I_{dM_1} = \frac{A\cos\theta_d - B}{Z^2 \sin\theta_d} - \frac{C}{Z^2} \tag{3.20}$$

Defining the value range of θ_d as $\left(-\frac{\pi}{2}, \frac{\pi}{2}\right)$, $\cos\theta_d$ and $\sin\theta_d$ in (3.20) can be replace by:

$$\begin{cases} \cos\theta_d = \sqrt{1-k^2} \\ \sin\theta_d = k \end{cases} \tag{3.21}$$

Then (3.20) can be transferred into a quadratic equation respect to k. After arrangement, the equation becomes:

$$\left(\left(I_{dM_1}Z^2 + C\right)^2 + A^2\right)k^2 + 2\left(I_{dM_1}Z^2B + BC\right)k + B^2 - A^2 = 0 \tag{3.22}$$

Then the corresponding solution of k is shown below.

$$\begin{cases} k_1 = \dfrac{-\left(I_{dM_1}Z^2 + C\right)B + A\sqrt{A^2 - B^2 + \left(I_{dM_1}Z^2 + C\right)^2}}{\left(I_{dM_1}Z^2 + C\right)^2 + A^2} \\ k_2 = \dfrac{-\left(I_{dM_1}Z^2 + C\right)B - A\sqrt{A^2 - B^2 + \left(I_{dM_1}Z^2 + C\right)^2}}{\left(I_{dM_1}Z^2 + C\right)^2 + A^2} \end{cases} \tag{3.23}$$

k_1 and k_2 represent two possible solutions of $\sin\theta_d$ and consequently θ_d corresponding to a defined I_{dM_1}. This means that if I_{dM_1} is set, there are at most two possible states. Obviously, the steady-state exists when and only when these are real solutions, which the discriminant under the square root should be greater or equal to zero. It can be expressed by the inequality in (3.24).

$$Z^4 {I_{dM_1}}^2 + 2CZ^2 I_{dM_1} + C^2 + A^2 - B^2 \geq 0 \tag{3.24}$$

(3.24) can be seen as a quadratic function with respect to I_{dM_1}. Since Z^2 is always positive, this quadratic function has an open up-shaped curve.

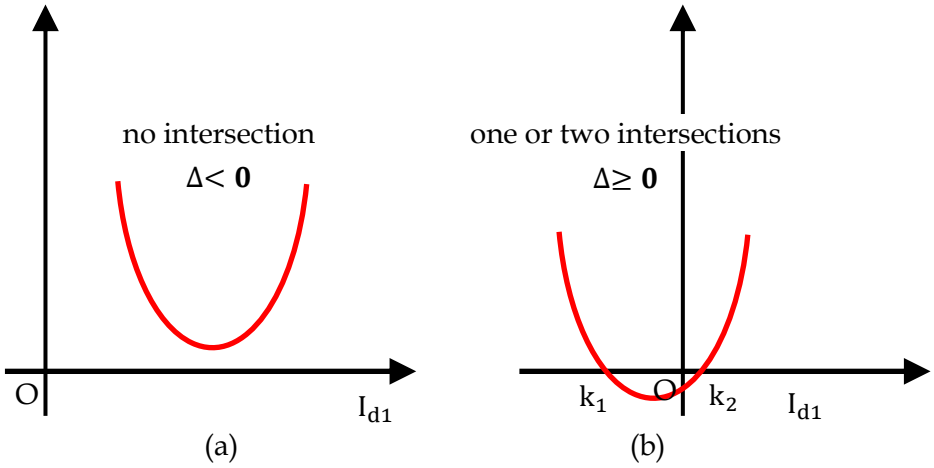

Figure 3.3 Two possible function image of (3.34)

Then, in order to solve (3.24), it is necessary to discuss the discriminating relationship which is:

$$\Delta = 4Z^2(B^2 - A^2) \tag{3.25}$$

Depending on the value of (3.25), there are two possible situations that has to be discussed separately. They are illustrated in Figure 3.3 (a) and (b) respectively.

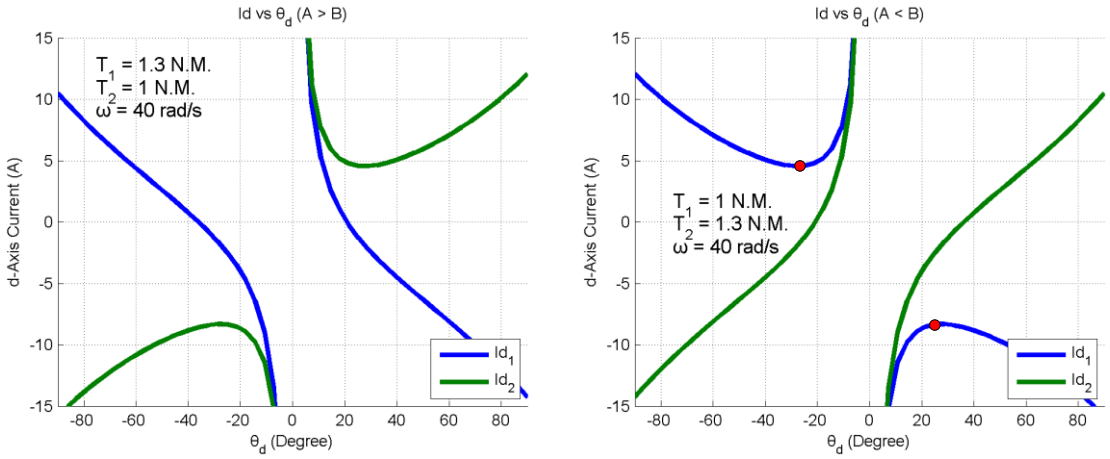

(a) (b)

Figure 3.4 Typical curve of Id response respect to θ_d.

1) $\Delta <$ **0**

This represents the situation in Figure 3.3(a). Under this condition, there is no intersection between the curve and I_{dM_1} axis, (3.24) is always satisfied. This means that steady-state exists for arbitrary I_{dM_1}. This condition is equivalent to A>B, which means M_1 is more loaded. Figure 3.4(a) shows the I_d current response with respect to θ_d when M_1 is more loaded (A>B). It is easy to identify that for a given I_{d1}, there are always two possible θ_d located in the negative plane and the positive plane respectively. For example, if I_{dM_1} is set to 0, the system can only operate at one of two states with θ_d equals to either -35° or 20°.

2) $\Delta \geq$ **0**

This situation regards Figure 3.3(b). When there are two intersections, the value range of I_{dM_1} is:

$$I_{dM_1} \in \left(-\infty, \frac{-C-\sqrt{B^2-A^2}}{Z^2}\right) \cup \left(\frac{-C+\sqrt{B^2-A^2}}{Z^2}, +\infty\right) \tag{3.26}$$

This condition is equivalent to A⩽B, that is M_2 more loaded. Figure 3.4(b) shows the corresponding curve of I_{dM_1} under this condition; it has a hyperbola shape. Obviously, either I_{dM_1} is in the upper or lower plane, there are at most two possible θ_d. The extreme values (shown as red point in Figure 3.4(b)) represents the situation that

$$I_{dM_1} = \frac{-C \mp \sqrt{B^2-A^2}}{Z^2} \tag{3.27}$$

We can insert (3.27) into (3.23) respectively to calculate the corresponding θ_d. In these cases, the term in square root of (3.23) is canceled. Then respect to different I_{dM_1}, we have two solutions which are opposite to each other:

$$k_1 = k_2 = \mp \frac{\sqrt{B^2-A^2}}{B} \tag{3.28}$$

Considering that $k = \sin\theta_d$, we can use $\cos^{-1}\theta_d$ to make the result more compact, which is:

$$\theta_d^{critical} = \pm cos^{-1}\left(\frac{A}{B}\right) \tag{3.29}$$

To summarize, for each given $I^*_{dM_1}$, depending on the torque relationship of the two motors, there are two possible θ_d located in $(-\pi/2, 0)$ and $(0, \pi/2)$ respectively. If I^*_{d1} is in $\left(-\infty, \left(-C - \sqrt{B^2 - A^2}\right)/Z^2\right)$, there are two possible θ_d in $(-\pi/2, -\cos^{-1}(A/B))$ and $(-\cos^{-1}(A/B), 0)$ respectively. Otherwise if I_{d1} is in $\left(\left(-C + \sqrt{B^2 - A^2}\right)/Z^2, +\infty\right)$, the two possibilities would be in $(0, \cos^{-1}(A/B))$ and $(\cos^{-1}(A/B), \pi/2)$. In conclusion, for a given I^*_{d1}, there are at most two corresponding θ_d. When $A > B$, there are always two solutions. When $A < B$, there are two solutions when I_{dM_1} satisfies (3.26).

3.3.2.2 Motor 2's stability region

With the solution condition determined, in the second step, the stability of M_2 must be studied because it operates in open-loop mode. It can only converge to a stable steady state. The proof of stability is based on the conclusion demonstrated in 2.3.3.1. Defining the angle between voltage vector and the back-EMF vector of the slave motor as δ_{M_2}, for a general PMSM its stable region is:

$$-\pi + \alpha < \delta_{M_2} < \alpha \tag{3.30}$$

where $\alpha = \tan^{-1}\frac{\omega_e L_s}{R_s}$ in a forward rotating situation. When δ_{M_2} is defined in $\left(-\frac{\pi}{2}, \frac{\pi}{2}\right)$, it is interesting to compare the tangent values of δ_{M_2} and α directly. Consider the definition of δ_{M_2}, which can be found in Figure 2.11, its tangent can be expressed by (3.31).

$$tan\,\delta_{M_2} = -\frac{V_{dM_2}}{V_{qM_2}} \tag{3.31}$$

Refer to (3.16), we can replace V_{dM_2} and V_{qM_2} with the expression respect to the current, which is:

$$-\frac{V_{dM_2}}{V_{qM_2}} = -\frac{R_s I_{dM_2} - L_s\omega_e I_{qM_2}}{L_s\omega_e I_{dM_2} + R_s I_{qM_2} + \omega_e\varphi_p} < \frac{\omega_e L_s}{R_s} \tag{3.32}$$

Both sides of (3.32) must multiply $V_{qM_2}R_s$ to cancel the fraction. R_s is a positive number. Thus, the value of V_{qM_2} must be specified. Regarding the assumption, V_{qM_2} is always greater than zero, which is equivalent to:

$$I_{dM_2} > -\frac{R_s I_{qM_2} + \omega_e\varphi_p}{L_s\omega_e} \tag{3.33}$$

Taken the precondition (3.33) into consideration, the solution of (3.32) is:

$$I_{dM_2} > -\frac{C}{Z^2} \tag{3.34}$$

The final result is determined by the Intersection of (3.33) and (3.34). They have the same sign so it is necessary to compare the constant term in the right side of them, which is $-\frac{R_s I_{qM_2}+\omega_e \varphi_p}{L_s \omega_e}$ and $-\frac{C}{Z^2}$, to determine the final result. Making subtract between them, the result is:

$$-\frac{R_s I_{qM_2} + \omega_e \varphi_p}{L_s \omega_e} - \left(-\frac{C}{Z^2}\right) = -\frac{\left({R_s}^3 + (\omega_e L_s)^2 R_s\right) I_{qM_2} + {R_s}^2 \omega_e \varphi_p}{L_s \omega_e \left({R_s}^2 + (\omega_e L_s)^2\right)} \tag{3.35}$$

Obviously (3.35) is smaller than zero if the assumptions are taken into account. This means that the constant term in the right side of (3.33) is smaller than (3.34). Thus, the stable region should be (3.34). By replacing I_{dM_2} in (3.34) with the equation in (3.18), the stable region respect to θ_d is determined by (3.36).

$$\frac{A - B\cos\theta_d}{Z^2 \sin\theta_d} > 0 \tag{3.36}$$

Discussion on $\sin\theta_d$ should be made. When $\sin\theta_d > 0$, which corresponds to $\theta_d \in \left(0, \frac{\pi}{2}\right)$, $Z^2 \sin\theta_d$ can be multiplied without changing the sign of (3.36). (3.36) becomes:

$$\cos\theta_d < \frac{A}{B} \tag{3.37}$$

In this situation, relationship between A and B must discussed. The result is shown in (3.38).

$$\begin{cases} \left(\cos^{-1}\left(\frac{A}{B}\right), \frac{\pi}{2}\right) & A < B \\ \left(0, \frac{\pi}{2}\right) & A \geq B \end{cases} \tag{3.38}$$

On the other hand, when $\sin\theta_d < 0$, which corresponds to $\theta_d \in \left(-\frac{\pi}{2}, 0\right)$, (3.36) becomes:

$$\cos\theta_d > \frac{A}{B} \tag{3.39}$$

Its solution is:

$$\begin{cases} \left(-cos^{-1}\left(\frac{A}{B}\right), 0\right) & A < B \\ \emptyset & A \geq B \end{cases} \tag{3.40}$$

Merging (3.38) and (3.40), the stable region of θ_d can be obtained.

$$\begin{cases} \left(-cos^{-1}\left(\frac{A}{B}\right), 0\right) \cup \left(cos^{-1}\left(\frac{A}{B}\right), \frac{\pi}{2}\right) & A < B \\ \left(0, \frac{\pi}{2}\right) & A \geq B \end{cases} \tag{3.41}$$

Figure 3.5(a) shows δ angle of each motor with respect to θ_d when M_1 is more loaded (A>B). The red dotted line represents the critical α angle. If focus is on M_2, its stability is achieved when δ_{M_2} is below the red dotted line. It is represented as the green area in the various figures. This situation is similar with the Master-Slave strategy that a less loaded motor will be advance in the electrical angle ($\theta_d > 0$).

Figure 3.5 (b) shows the curve when M_2 is more loaded (A<B). The intersecting points between δ_{M_2} and α coincide with the extreme points of I_{dM_1} in Figure 3.4. Here we must pay attention to the right part of the stable region. Because in this region, M_1 is open-loop instable. Controller for M_1 must be capable of manipulating the master motor under instable condition. Otherwise, this part must not be considered as a valid stable region.

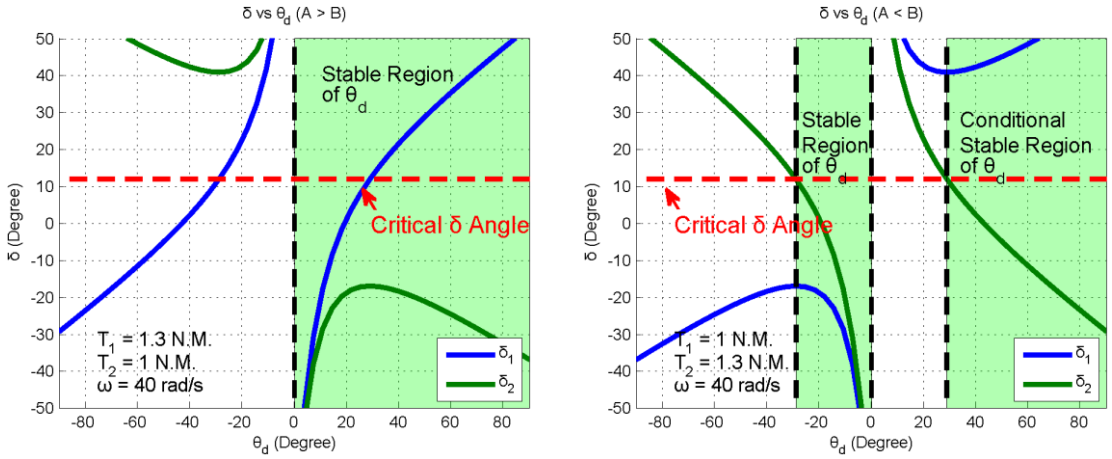

(a) (b)

Figure 3.5 Typical curve of δ response respect to θ_d

3.3.2.3 Conclusion

As a summary, the analysis of the solution condition illustrates that for a given I_{d1}, there are at most two corresponding steady states. And only one of these corresponds to the given state. But if stability is taken into account, only one feasible steady state remains. The conclusion is represented in Figure 3.6. θ_d^1 and θ_d^2 represent the two possible solutions for a given I_{d1} respectively. It is easy to identify that, in each case, only one stable solution is available. It can therefore be concluded that the precondition only holds

true when θ_d^* is in the stable region determined by (3.41). In Figure 3.7 the stable region is drawn respect to the torque ration between two motors.

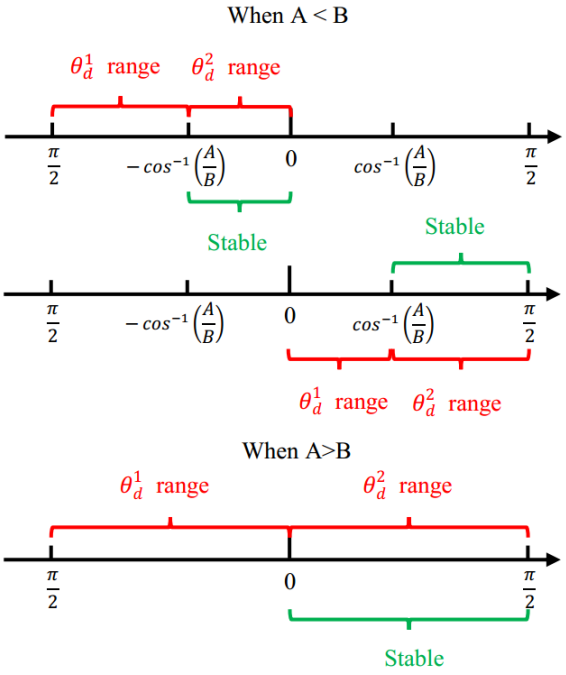

Figure 3.6 Illustration of proof

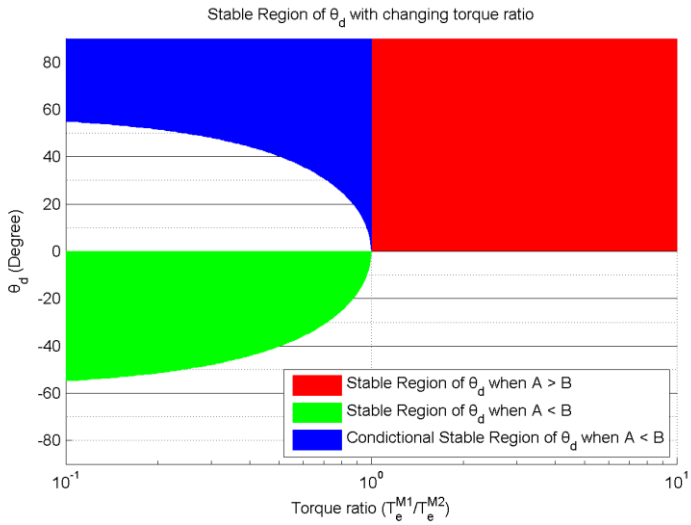

Figure 3.7 Illustration of the stable region of θ_d with changing torque ratio

3.3.3 Efficiency optimization

The efficiency is optimized by minimizing the loss of Joules from the motor. The cost function is the same as in [72], which is (3.6). Insert (3.18) into (3.6), a cost function respect to θ_d is obtained.

$$f(x,y) = \left(\frac{Ay - B}{Z^2 x} - \frac{C}{Z^2}\right)^2 + \left(\frac{A - By}{Z^2 x} - \frac{C}{Z^2}\right)^2 \tag{3.42}$$

θ_d is the only degree of freedom that minimizes this cost function. As $\sin\theta_d = x$ and

$\cos\theta_d = y$, this cost function must be subjected to constraint (3.43).

$$g(x,y) = x^2 + y^2 = 1 \tag{3.43}$$

The analytical solution of the optimal θ_d, which is the extreme point of (3.42), can be obtained using the Lagrange multiplier method.

$$L(x,y,\lambda) = f(x,y) + \lambda(g(x,y) - 1) \tag{3.44}$$

Making partial derivation of (3.44), which is shown below,

$$\frac{\partial L(x,y,\lambda)}{\partial x} = 2\lambda x + 2\left(\frac{C}{Z^2} + \frac{B - Ay}{Z^2 x}\right)\frac{Ay - B}{Z^2 x^2} + 2\left(\frac{C}{Z^2} + \frac{By - A}{Z^2 x}\right)\frac{A - By}{Z^2 x^2} = 0 \tag{3.45}$$

$$\frac{\partial L(x,y,\lambda)}{\partial y} = 2\lambda y - 2A\left(\frac{C}{Z^2} + \frac{B - Ay}{Z^2 x}\right)\frac{1}{Z^2 x} + 2B\left(\frac{C}{Z^2} + \frac{By - A}{Z^2 x}\right)\frac{1}{Z^2 x} = 0 \tag{3.46}$$

$$\frac{\partial L(x,y,\lambda)}{\partial \lambda} = x^2 + y^2 - 1 = 0 \tag{3.47}$$

The optimal θ_d is one of the solutions of the above equation set. To solve this equation set, we can firstly multiply (3.45) by y and (3.46) by x then subtract (3.45) by (3.46). Constraints to x and y must be considered because they cannot equal to zero. It is not a problem in this case because as demonstrated in 2.3.1, $x = 0$ and $y = 0$ represent the singularity points of a MIDPMSM system which it cannot work at. Through this operation, variable λ can be canceled. The arranged equation is:

$$\left(\frac{2A}{Z^2} - 2y\frac{B - Ay}{Z^2 x^2}\right)\left(\frac{C}{Z^2} + \frac{B - Ay}{Z^2 x}\right) + \left(2y\frac{A - By}{Z^2 x^2} + \frac{2B}{Z^2}\right)\left(\frac{C}{Z^2} - \frac{A - By}{Z^2 x}\right) = 0 \tag{3.48}$$

Z^2x^2 can be safely applied to both sides of (3.48). After arrangements, the equation becomes:

$$2(Ax^2 - By - Ay^2)(Cx^2 + Bx - Axy) + 2(Ay - By^2 + Bx^2)(Cx^2 - Ax + Bxy) = 0 \tag{3.49}$$

At this step, one variable amongst x and y should be canceled. Considering that the θ_d is range defined in $\left(-\frac{\pi}{2}, \frac{\pi}{2}\right)$, function $\sin^{-1} x$ is defined in this range. To cancel variable y in (3.49), an equation with form of $y = f(x)$ must be firstly developed. Then it can be inserted into (3.47) to obtain an equation respect to x. For the y term in (3.49) that order higher than 1, (3.47) must be used to transform y^2 into x^2. Otherwise, the maximum order of y will exceed 2 after expansion of (3.49). After that we can get:

$$(2A - 2By)(Cx^2 + Bx - Axy) + (2Ay - 2B)(Cx^2 - Ax + Bxy) = 0 \tag{3.50}$$

Expand (3.50) and transform y^2 into x^2 using (3.47) again, a $y = f(x)$ from equation

is achieved.

$$y = \frac{2AB(2-x^2) + x(AC-BC)}{x(BC-AC) + 2(A^2+B^2)} \tag{3.51}$$

Replacing y in (3.47) with (3.51), finally a quartic equation respect to x is got.

$$x^4 + \alpha x^3 + \beta x^2 + \gamma x - \beta = 0 \tag{3.52}$$

where

$$\begin{cases} \alpha = \dfrac{4C(B^3-A^3)}{4A^2B^2 + (BC-AC)^2} \\ \beta = \dfrac{4(B^2-A^2)^2}{4A^2B^2 + (BC-AC)^2} \\ \gamma = \dfrac{4C(A^3-B^3+A^2B-AB^2)}{4A^2B^2 + (BC-AC)^2} \end{cases} \tag{3.53}$$

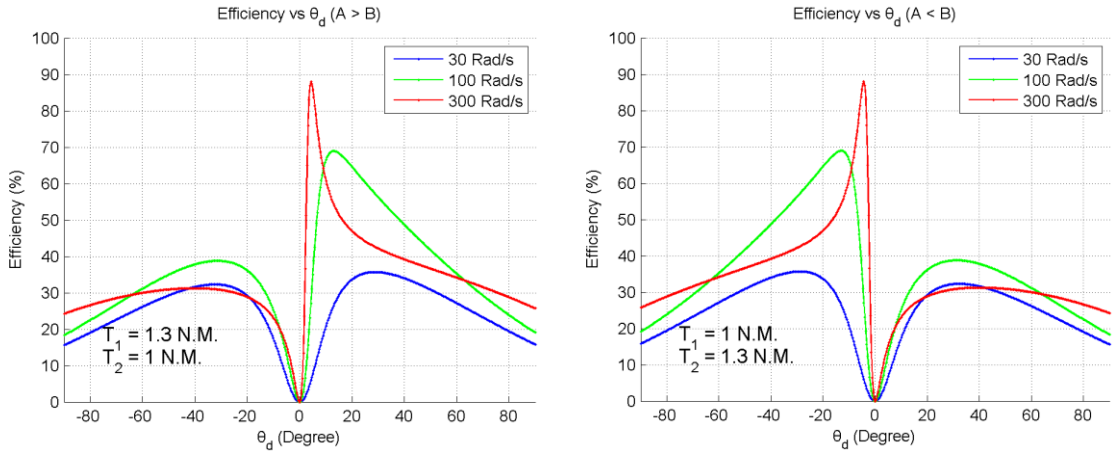

(a) (b)

Figure 3.8 Typical curve of system efficiency respect to θ_d under different speed and torque.

This equation can be solved using the Ferrari method, similar to [75][76]. Figure 3.8 shows a typical curve of system efficiency with respect to θ_d. It illustrates the efficiency of the system at different speeds whilst the torque speed remains constant. Judging from Figure 3.8, there are two extreme points in the left and right panel respectively. They are not coincidence with the $\theta_d^{critical}$ defined in (3.29) because here the $\theta_d^{optimal}$ minimize the sum of $I_{dM_1}{}^2$ and $I_{dM_2}{}^2$ rather than I_{dM_1} or I_{dM_2} individually. It can be concluded that, amongst these four solutions, there are two real solutions and two complex solutions. The real solutions are related to the two extreme points. The optimization procedure is defined as:

7) Calculate A, B, C using (3.19).

8) Calculate α, β, γ using (3.53).

9) Calculate the solutions of (3.52).

10) Ignore the two complex solutions. For the two real solutions, use (3.18) to calculate the corresponding I_d current and compare their cost function value.

11) Set the $\theta_d^{optimal} = \sin^{-1} x$ and verify if it is inside the stable region using (3.41).

12) Set $I_{dM_1}^*$ calculated by (3.20).

3.3.4 Parameter sensitivity

Parameters of a PMSM are subjected to changes during operation. For example, stator winding resistance (R_s) is a temperature sensitive parameter [77]-[79]. When ambient temperature rises or motor is producing high torque, R_s will significantly increase. This situation may also happen to magnet installed on the rotor. The permanent magnetic flux (φ_p) strength will degrade with the rise in temperature [80][81]. In extreme situation, high temperature also can cause irreversible demagnetization of the permanent magnetic.

As demonstrated above, system stability criteria (3.41) and efficiency optimization (3.53) depend heavily on the accuracy of parameters. Therefore, it is necessary to study the impact of parameter variation on system stability to understand how much will be the influence and to find out how to reduce the influence. In this study, only the stator winding resistance (R_s), winding inductance (L_s), and permanent magnetic flux (φ_p) are considered. The variation range of these parameters is inside 50% to 150% respect to their nominal value.

3.3.4.1 Stability influence

(3.41) determines the stability of a MIDPMSM system. When A<B, which means M_1 is less loaded. Its stable region is parameter determined. Thus, when the parameter mismatch exists, the controller cannot guarantee the stability if θ_d^* is close to the boundary of stable region. (3.54) shows the coefficient taken out from the stable region

$$\theta_d^{critical} = f(R_s, L_s, \varphi_p) = -cos^{-1}\left(\frac{A}{B}\right) \tag{3.54}$$

We can also calculate the partial derivative of (3.54) respect to each parameter in order to study the sensitivity of these parameters. These partial derivatives are shown from (3.55) to (3.57).

$$\frac{\partial f(R_s, L_s, \varphi_p)}{\partial R_s} = \frac{B(\omega_e \varphi_p + 2I_{qM_1} R_s) - A(\omega_e \varphi_p + 2I_{qM_2} R_s)}{B\sqrt{(B^2 - A^2)}} \tag{3.55}$$

$$\frac{\partial f(R_s, L_s, \varphi_p)}{\partial L_s} = \frac{2L_s {\omega_e}^2 (BI_{qM_1} - AI_{qM_2})}{B\sqrt{(B^2 - A^2)}} \tag{3.56}$$

$$\frac{\partial f(R_s, L_s, \varphi_p)}{\partial \varphi_p} = \frac{R_s \omega_e (B - A)}{B\sqrt{(B^2 - A^2)}} \tag{3.57}$$

These parameters have different units. If we want to compare the impact on stability region between each other, these partial derivatives must be normalized into the same unit. Introducing three scale factors, k_1, k_2, k_3, parameters in (3.54) can be expressed by the multiplication between the scale factor and their nominal value. The detailed definition is:

$$R_s = k_1 \cdot R_s^{nominal} \tag{3.58}$$

$$L_s = k_2 \cdot L_s^{nominal} \qquad k_1, k_2, k_3 \in [50\%, 150\%] \tag{3.59}$$

$$\varphi_p = k_3 \cdot \varphi_p^{nominal} \tag{3.60}$$

k_1, k_2, k_3 belongs to the region of interest. With this process, (3.54) are normalized to the same unit. And (3.61)~(3.63) show the corresponding partial derivatives.

$$\frac{\partial f(R_s, L_s, \varphi_p)}{\partial k_1} = \frac{\partial f(R_s, L_s, \varphi_p)}{\partial R_s} \frac{\partial R_s}{\partial k_1} = \frac{\omega_e \varphi_p (B - A) + (BI_{qM_1} - AI_{qM_2}) 2k_1 R_s^{nominal}}{B\sqrt{(B^2 - A^2)}} \cdot R_s^{nominal} \tag{3.61}$$

$$\frac{\partial f(R_s, L_s, \varphi_p)}{\partial k_2} = \frac{\partial f(R_s, L_s, \varphi_p)}{\partial L_s} \frac{\partial L_s}{\partial k_2} = \frac{2k_2 L_s^{nominal} {\omega_e}^2 (BI_{qM_1} - AI_{qM_2})}{B\sqrt{(B^2 - A^2)}} \cdot L_s^{nominal} \tag{3.62}$$

$$\frac{\partial f(R_s, L_s, \varphi_p)}{\partial k_3} = \frac{\partial f(R_s, L_s, \varphi_p)}{\partial \varphi_p} \frac{\partial \varphi_p}{\partial k_3} = \frac{R_s \omega_e (B - A)}{B\sqrt{(B^2 - A^2)}} \cdot \varphi_p^{nominal} \tag{3.63}$$

1) R_s Sensitivity

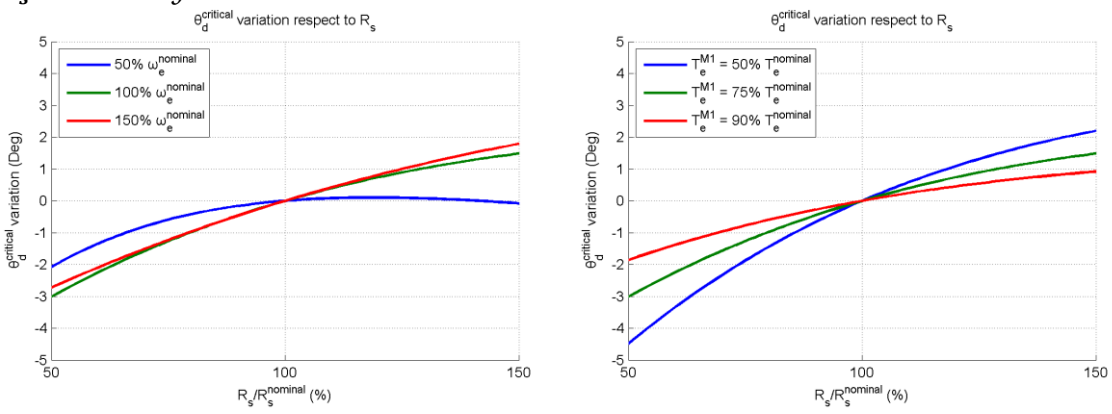

(a) (b)

Figure 3.9 $\theta_d^{critical}$ variation respect to R_s under (a) different speed and (b) different torque load

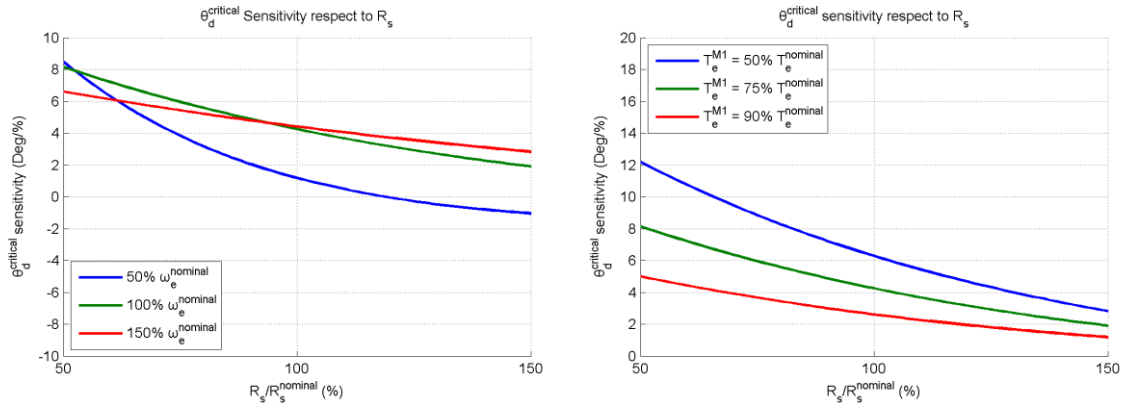

(a) (b)

Figure 3.10 $\theta_d^{critical}$ *sensitivity respect to* R_s *under (a) different speed and (b) different torque load*

Figure 3.9 shows the $\theta_d^{critical}$ variation respect to R_s. The variation means the difference between actual value and ideal value of $\theta_d^{critical}$. Figure 3.10 illustrates the $\theta_d^{critical}$ sensitivity. The higher the value, the more sensitive is the $\theta_d^{critical}$. $\omega_e^{nominal}$ is the nominal electrical angular speed. It equals to $2\pi\frac{4300rpm}{60}N_p = 1800rad/s$. $T_e^{nominal}$ is nominal torque, which is 3.53 N.M.. Usually, R_s increases during motor operation. Overall speaking, in such a condition, the $\theta_d^{critical}$ is not sensitive to R_s. Maximum 2° of variation is visible in both different speed and different torque load condition. From Figure 3.9(b) and Figure 3.10(b) we can found that the influence increase as the unbalanced torques ratio. But this influence is limited.

2) L_s *Sensitivity*

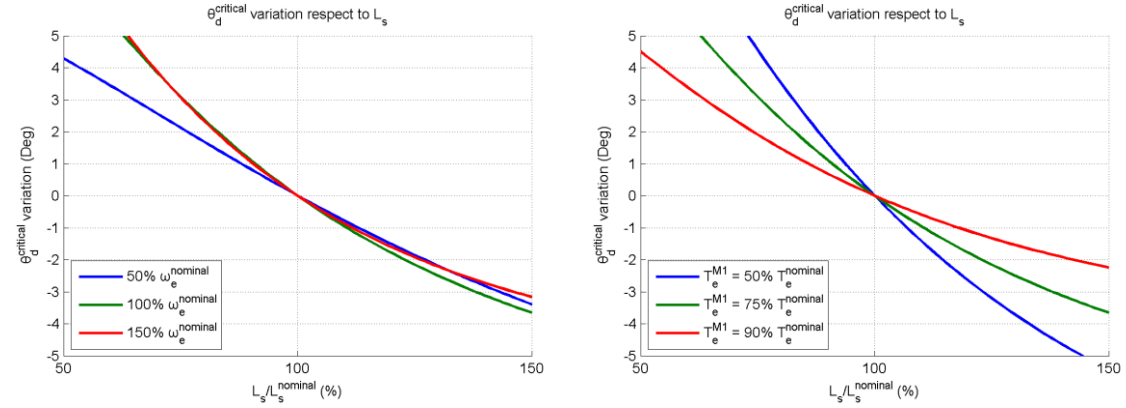

(a) (b)

Figure 3.11 $\theta_d^{critical}$ *variation respect to* L_s *under (a) different speed and (b) different torque load*

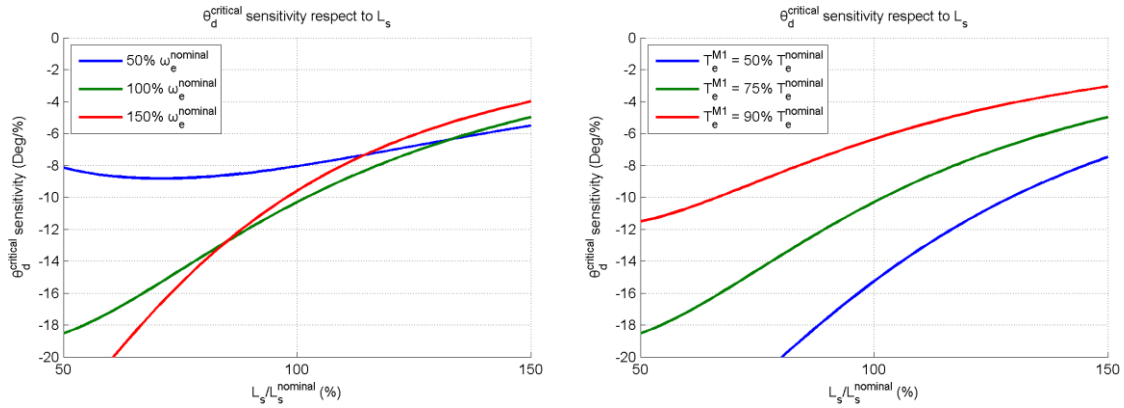

(a) (b)

Figure 3.12 $\theta_d^{critical}$ sensitivity respect to L_s under (a) different speed and (b) different torque load

Figure 3.11 and Figure 3.12 show the variation and sensitivity respect to L_s. It has the same order of magnitude respect to R_s sensitivity. Its sensitivity becomes higher when speed and unbalance ration increase. Especially in unbalance torque condition, maximum 10 ^{o} can be observed.

3) φ_p Sensitivity

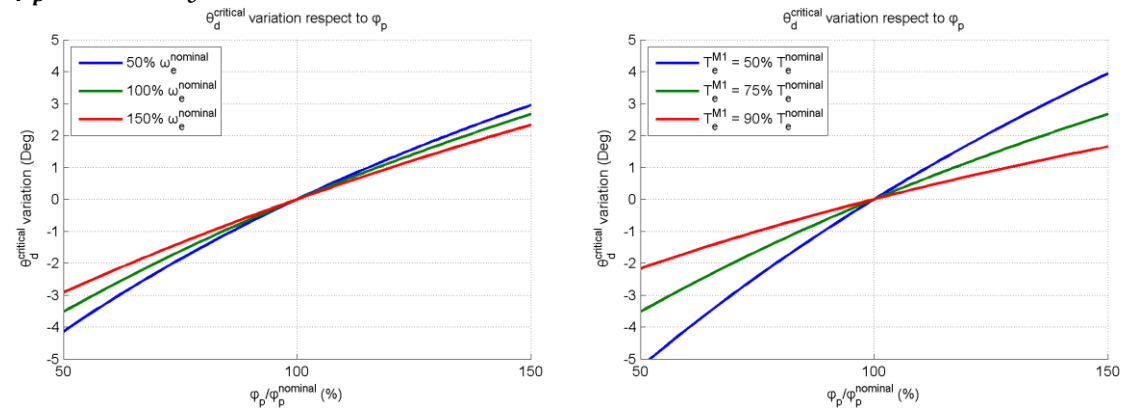

(a) (b)

Figure 3.13 $\theta_d^{critical}$ variation respect to φ_p under (a) different speed and (b) different torque load

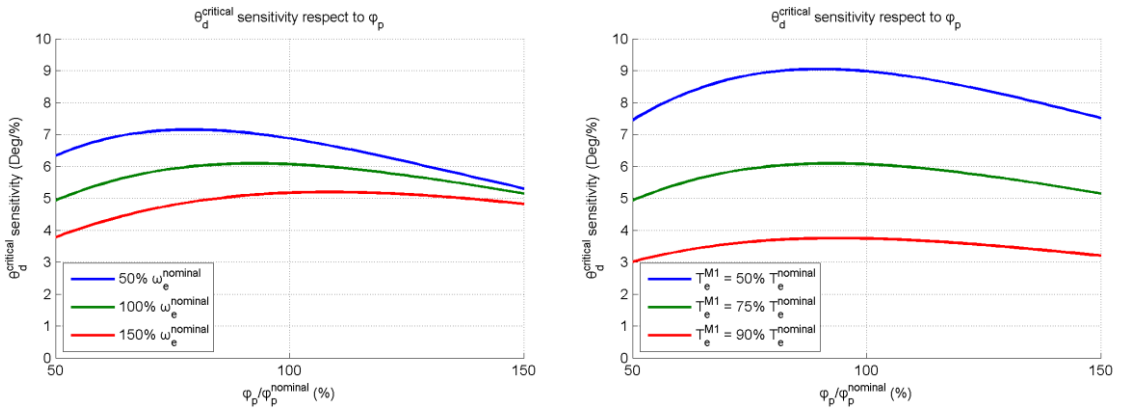

(a) (b)

Figure 3.14 $\theta_d^{critical}$ sensitivity respect to φ_p under (a) different speed and (b) different torque load

Figure 3.13 and Figure 3.14 show the variation and sensitivity respect to φ_p. Its behavior is similar with the previous parameters. It can be concluded that stability boundary is highly sensitive to the parameter variation. Depending on operation state, a 20% changes in parameter may cause 2~3 degrees stability boundary depending on operation state. Moreover, these changes are accumulative. This is very dangerous because if the efficiency optimization procedure gives out a $\theta_d^{optimal}$ close to this boundary, the controller may think it is stable but in fact it isn't. The system will lose stability immediately.

However, there is a simpler approach. Refer to (3.41), the stable region is parameter independent when M_1 is more loaded (A>B). A master-slave mechanism that always select the more loaded motor as M_1 can be introduced. This makes A>B always satisfied and consequently its stably region is always $\left(0, \frac{\pi}{2}\right)$.

3.3.4.2 Efficiency influence

The proposed optimization methods in [72] and in this chapter depend heavily on the parameter accuracy. Thus, it is necessary to see how much the effectiveness of optimization will be influenced. Like the stability influence study, R_s, L_s, φ_p will be changed during the simulation. For example, decrease the actual R_s will also increase the efficiency even in mismatched optimization situation. Thus, in order to quantitively evaluate the influence and to eliminate the impact on the efficiency caused by parameter changes, two optimal θ_ds are calculated based on different system parameters. The first one uses the nominal parameters even when the actual value is moving. This will simulate a mismatched optimization situation. The second one uses actual value (perfect optimization). Their resulted efficiency can be estimated by:

$$\hat{\eta} = \frac{\omega_e \varphi_p \left(I_{qM_1} + I_{qM_2}\right)}{\omega_e \varphi_p \left(I_{qM_1} + I_{qM_2}\right) + R_s \left(\hat{I}_{dM_1}^2 + \hat{I}_{dM_2}^2 + I_{qM_1}^2 + I_{qM_2}^2\right)} \tag{3.64}$$

I_{q1}, I_{q2}, and ω_e are assigned to the same value as there is in stability influence study. R_s, L_s, φ_p use their actual value. $\hat{I}_{d1}$ and $\hat{I}_{d2}$ are estimated by (3.18) respect to a given θ_d. During each simulation, only one of these parameters will be changed. The others equal to their nominal value.

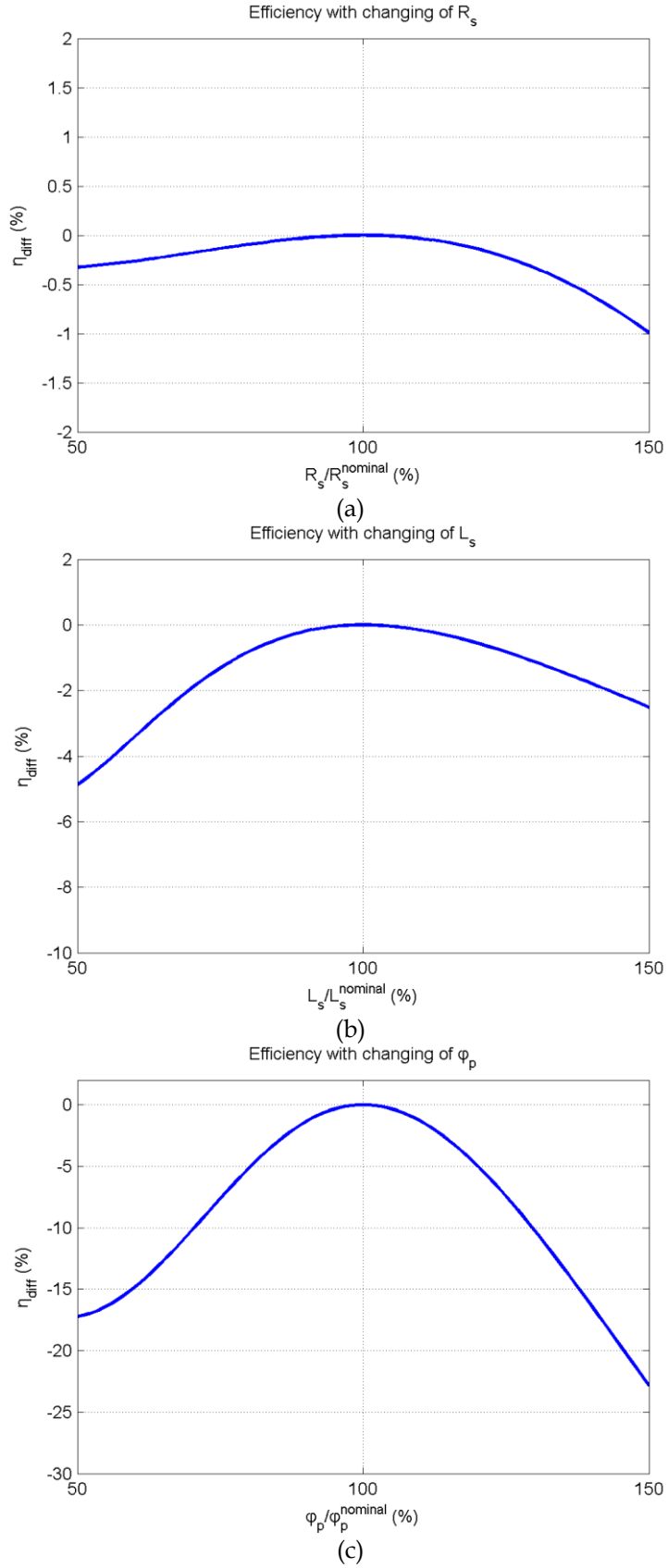

Figure 3.15 Simulation result of parameters influence on efficiency

The simulation result is shown in Figure 3.15. They represent the efficiency difference between mismatched and perfect optimization (η_{diff}). Obviously, when the parameter is

not perfectly matched, the effectiveness of optimization decreases. But the difference varies from parameter to parameter. Figure 3.15(a)-(c) shows the influence of R_s, L_s, and φ_p respectively. For R_s and L_s, their influence is relatively low. A maximum decrease of 4% can be caused for $\pm 50\%$ variation of L_s. But situation changes when it comes to φ_p, 25% efficiency will be lost if it is changed by 50%. Although in practice this extreme situation won't happen, its huge influence cannot be ignored. It is highly recommended to implement a φ_p observer in real application. But we have to consider that the observer is also model and parameter dependent. Its effectiveness cannot be estimated.

3.3.5 Experiment test

An experiment was carried out to verify the feasibility and to illustrate the performance of the proposed controller. The experimental bench has been introduced in chapter 2. To start the motors correctly, the Master-Slave strategy is used, which means that I_{d1} is set to 0 when starting. Once two motors have been started, the optimization process starts execution.

3.3.5.1 Stability demonstration

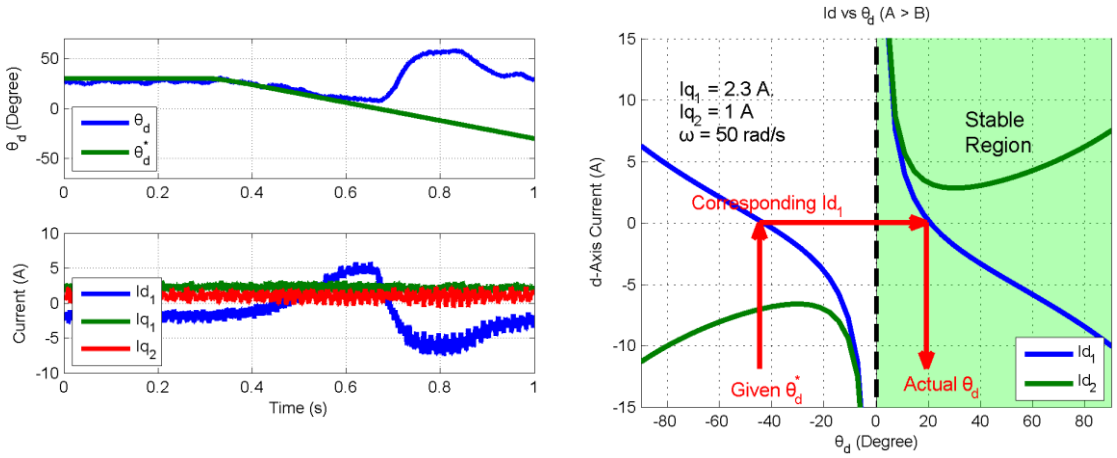

(a) (b)

Figure 3.16 Demonstration of stability conclusion.

Figure 3.16 demonstrates the precondition obtained in section 3.3.2. A ramp-shaped reference θ_d^* changing from $-\frac{\pi}{6}$ to $\frac{\pi}{6}$ is put into the θ_d regulator. Judging from the current response, motor 1 is more loaded (A>B) therefore the stable region is $\left(0, \frac{\pi}{2}\right)$. In Figure 3.16 (a), when θ_d^* is in the stable region, the θ_d response follows. When θ_d^* is in an unstable region, the response remains in the stable region rather than follows the reference. Figure 3.16(b) demonstrates this principle. If a reference in an unstable region is given (indicated as θ_d^*), the θ_d regulator will generate a corresponding I_d^*. But the slave machine will converge to the θ_d in the stable region having the same $I_{dM_1}^*$. This emphasizes the importance of imposing a θ_d^* in the stable region so that the consistency between reference and output is ensured.

3.3.5.2 Efficiency test

Figure 3.18 shows the experiment results of the efficiency test. During the experiment, the two motors were first put in steady speed operation. Then, an external load torque was applied to motor 1 in order to test the system transient, its robustness, and its efficiency in the case of different load torque. Its shape is shown in Figure 3.17. The load torque was not applied to M_2.

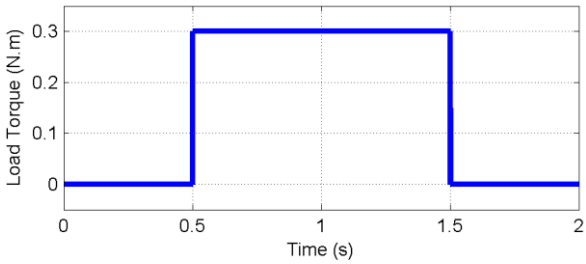

Figure 3.17 Load torque applied to M_1

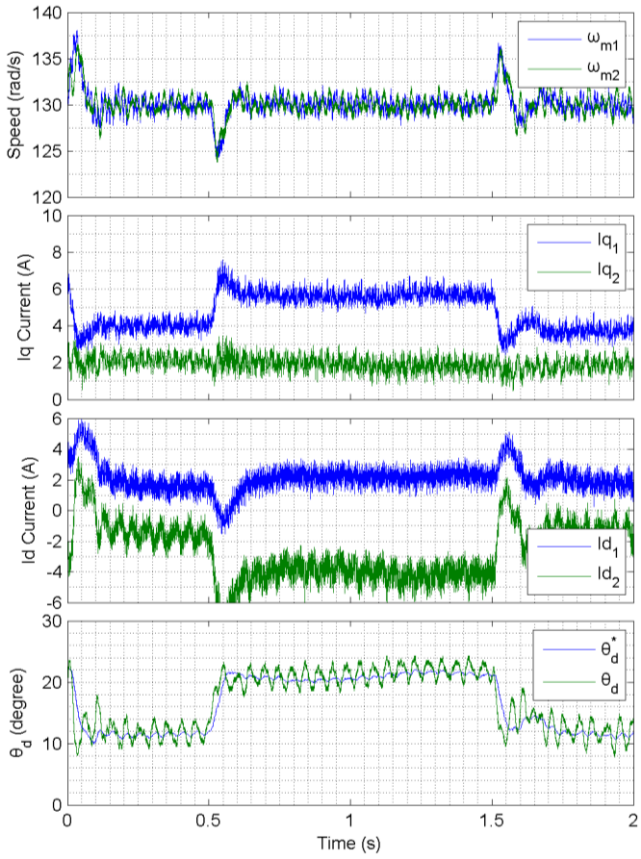

Figure 3.18 Experimental results of efficiency test

Figure 3.18 shows the corresponding θ_d response (green curve). The blue curve is the optimal θ_d realtime calculated during execution. It follows the reference well confirming the effetiveness of the θ_d regulator. The oscillations of θ_d are linked to the mechanical imperfections of the system and in particular to a periodic variation of the friction.

Moreover, as the objective is to optimize efficiency, it is interesting to compare the new proposed control strategy with other strategies. The efficiency is calculated using (3.64).

As tested in the last chapter, master slave is the most efficiency strategy. Now we take this reference to test our new proposal.

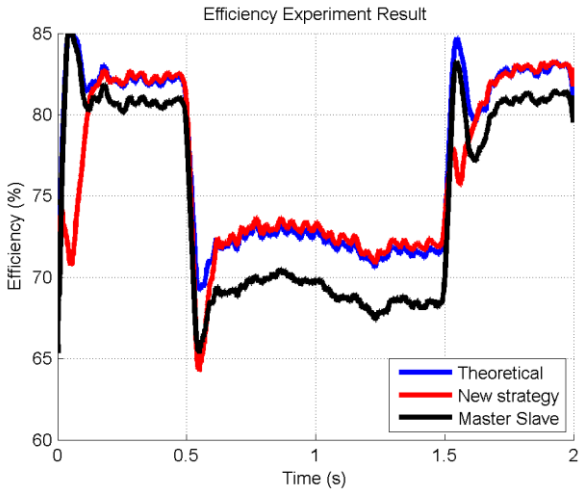

Figure 3.19 Comparison of experimental performance between different controllers

The result is shown in Figure 3.19. The blue curve represents the estimated maximum efficiency obtained by the optimization procedure; it is calculated by the estimated I_{dM_1} and I_{dM_2} through (3.64) based on the calculated optimal θ_d. The red curve shows the efficiency of the new strategy. The black curve is that of the master slave. It can be concluded that the new control strategy provides even higher efficiency, especially in the high torque unbalanced situation. This characteristic can be found in Figure 3.1, the greater the imbalance torque, the greater the difference between new and conventional MTPA trajectory. Meanwhile the efficiency of the new strategy is almost the same as the estimated theoretical efficiency. This proves the correctness of optimization process and parameters matchiness.

3.4 **Conclusion**

In this chapter, an efficiency optimized controller for a MIDPMSM system is proposed and verified by experiment. First, the analysis of system constraints has given out the design guideline to the controller structure. The analysis shows that, apart from the torques and speed, the controller must put one of I_{dM_1}, I_{dM_2} or θ_d under control so that the system is properly defined. This conclusion also explains why there is huge offset between torque reference and response existing in the MPC control strategies for MIDPMSM system.

Second, we have chosen it as an intermediate variable to obtain the stability criteria and optimal efficiency solution. Since the slave motor is open-loop, the validity of the θ_d controller has to be proved as I_{dM_1} is used to indirectly control the θ_d. The state of the entire system is not unique until the stability of the slave motor is taken into account. Therefore, we need to prove this by giving a stable region of θ_d in order to ensure that

the θ_d reference corresponds to the actual response. This conclusion is critical as the foundation of efficiency optimization, which is also the major defects of study [73].

Third，By using Lagrange Multiplier we have obtained the expression of efficiency-optimal θ_d. Through calculating this quartic equation, the optimal θ_d related to torque and speed can be obtained. With this process, the high-computational cost numerical method can be avoided. A look-up table is also a possible solution if lack computing resources.

Forth, we have explored the influence of parameter variation in system stability and efficiency-optimization because our controller depends heavily on the accuracy of the PMSM's parameters. In the aspect of stability region, the three parameters, R_s, L_s, and φ_p, will cause the stability region moves from its expected value. But its influence can be eliminated by using Master-Slave strategy. On the other hand, in the aspect of efficiency optimization, the simulation results have shown that parameter mismatch can cause high efficiency loss under nominal speed condition, especially φ_p. This is also consistent with the conclusion in [82]. Parameter variation is inevitable during normal operation of a motor. They will be influence by multiple aspects such as heat or magnet saturation. Therefore, to obtain a better optimization effect, an observer of φ_p is preferred.

Above all, the controller structure is simple. Regular controllers for a single PMSM system can be easily upgraded to support parallel PMSM just by adding a few blocks without modifying the controller itself. Also, the optimization is computational-cost friendly, in our experiment, it runs at 1kHz without any problem. But, it should be noticed that, the stability region is got based on two assumptions that the motor is rotating positively and they are in motor mode. This limits the adaptation domain of this controller. In the next chapter, we will go deeper into the demonstration so that these assumptions can be eliminated and the resulted controller can work in full range, including the generator mode.

Chapter 4

Control strategies for Mono-Inverter Multiple PMSM system

Table of content

4.1 **Introduction**

In previous chapters, we have discussed in detail the control and efficiency optimization problem of a MIDPMSM system. But the number of the motor is limited to two because we want to simplify the study and the experiment so that we can find out the best point of entry to this special system and verify our conclusions. This limitation is also existing in recent research.

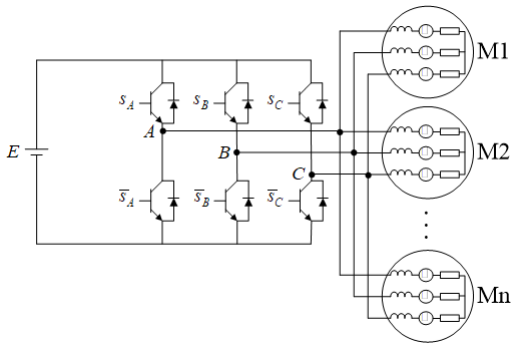

Figure 4.1 A 2-level 3-phase inverter driving N PSMSs in parallel

In Chapter 3, we have analytically designed a controller but it has some insufficient point. First, its stability region is got under two assumptions:

- The rotational speed is positive.
- Operate as motor

And the controller can only support two motors in parallel. In actual application, as presented in Chapter 1, it may happen that more than 2 motors are needed to be connected in parallel. The system structure is shown in Figure 4.1. Therefore, from the application point of view, research in more than two motors in parallel is meaningful. Especially in traction application, it is quite common that an electrical machine changes its role between a motor and generator during operation [83]-[85]. Its aim is obvious that we can use it as an electrical brake to recover energy. Thus, it makes sense that also taking generator mode into account.

These demands give a challenge to the existing conclusion. In this chapter, we will use the same design method proposed in Chapter 3 to extend the conclusion dedicated for dual-motors, including stability criterion, to a Mono-Inverter Multiple-PMSM (MIMPMSM) system. In the derivation, we will remove the two previous assumptions so that the designed controller can operate in full range. Then, the MIDPMSM can be seen as a special case with N=2.

4.2 **System analysis and controller design**

For a PMSM, it is important to control the angle between the stator flux generated by

excitation and the rotor flux imposed by the permanent magnet. But in MIMPMSM system, power supply voltage is common to all motor. Therefore, its stability cannot be guaranteed under different mechanical loads when a regular PMSM controller used. In 2.3.3.1, the open-loop stability leads to a conclusion that the stability of a PMSM is equivalent to its steady-state existence. Once its steady state solution exists, its stability can be subsequently guaranteed thanks to the auto-pilot characteristic of a PMSM. In this chapter, we will start with the constraint analysis proposed in 3.3.1 to prove the feasibility of a MIMPMSM system. Then, the controller can be designed by involving the open-loop stability criterion.

4.2.1 Model of MIMPMSM system

The modelling of a MIMPMSM system is roughly the same as it is for MIDPMSM system. To simplify the analysis, one of these motors is defined as reference motor (M_1) and all the rest motors' voltage is expressed as a transform of M_1's voltage. For motor $M_k \in \mathbb{M}_{slave}$, $\mathbb{M}_{slave} = \mathbb{M} - \{M_1\}$, its steady state model can be expressed as

$$\begin{bmatrix} cos\,\theta_{dM_1,M_k} & sin\,\theta_{dM_1,M_k} \\ -sin\,\theta_{dM_1,M_k} & cos\,\theta_{dM_1,M_k} \end{bmatrix} \begin{bmatrix} V_{dM_1} \\ V_{qM_1} \end{bmatrix} = \begin{bmatrix} R_s & -L_s\omega_e \\ L_s\omega_e & R_s \end{bmatrix} \begin{bmatrix} I_{dM_k} \\ I_{qM_k} \end{bmatrix} + \begin{bmatrix} 0 \\ \omega_e\varphi_f \end{bmatrix} \tag{4.1}$$

where $\theta_{dM_1,M_k} = \theta_{M_k} - \theta_{M_1}$. θ_{M_1} and θ_{M_k} correspond to the electrical angle of M_1 and M_k. It is assumed that all motors have the same parameters and operate at the same speed in steady state. By merging model of M_1~M_N, the steady state model of MIMPMSM system can be obtained (shown in (4.2)).

$$\begin{bmatrix} 1 & 0 \\ 0 & 1 \\ cos\,\theta_{dM_1,M_2} & sin\,\theta_{dM_1,M_2} \\ -sin\,\theta_{dM_1,M_2} & cos\,\theta_{dM_1,M_2} \\ \vdots & \vdots \\ cos\,\theta_{dM_1,M_N} & sin\,\theta_{dM_1,M_N} \\ -sin\,\theta_{dM_1,M_N} & cos\,\theta_{dM_1,M_N} \end{bmatrix}_{2\times 2N} \begin{bmatrix} V_{dM_1} \\ V_{qM_1} \end{bmatrix} = \begin{bmatrix} R_s & -L_s\omega_e & \cdots & 0 & 0 \\ L_s\omega_e & R_s & \cdots & 0 & 0 \\ \vdots & \vdots & \ddots & \vdots & \vdots \\ 0 & 0 & \cdots & R_s & -L_s\omega_e \\ 0 & 0 & \cdots & L_s\omega_e & R_s \end{bmatrix}_{2N\times 2N} \begin{bmatrix} I_{dM_1} \\ I_{qM_1} \\ \vdots \\ I_{dM_N} \\ I_{qM_N} \end{bmatrix}_{1\times 2N} + \begin{bmatrix} 0 \\ \omega_e\varphi_f \\ \vdots \\ 0 \\ \omega_e\varphi_f \end{bmatrix}_{1\times 2N} \tag{4.2}$$

4.2.2 Feasibility demonstration

Refer to the conclusion of 3.3.1, control is feasible when and only when voltage solution exists for desired torque ($I_{qM_1} \dots I_{qM_N}$) and speed (ω_e), which requires more or equal number of unknown variables than constraints. In (4.2) there are 2N + 1 unknown variables including $\underbrace{V_{dM_1}, V_{qM_1}}_{2}$, $\underbrace{I_{dM_1} \dots I_{dM_N}}_{N}$, $\underbrace{\theta_{dM_1,M_2} \dots \theta_{dM_1,M_N}}_{N-1}$. While 2N constraints are provided by (4.2). Thus, absolutely MIMPMSM is feasible from controllability point of view. Similar with the conclusion for 2 motors, to properly constraint the system, the controller must apply an addition constraint on one of $I_{dM_1} \dots I_{dM_N}$ and $\theta_{dM_1,M_2} \dots \theta_{dM_1,M_N}$ so that the solution of (4.2) is finite. Here constraint on I_d is preferred because the advantage of using θ_d here has vanished while the resulted controller structure would be more complex. For example, when θ_{dM_1,M_2} is define as known variables, $\cos\theta_{dM_1,M_2}$ and

$\sin\theta_{dM_1,M_2}$ are still unknown variables. The non-linearity cannot be eliminated.

4.2.3 Controller design

Proceeding with the analysis, constraints on this regulated variable must be discussed because the solution does not necessarily exist under all condition. For example, as the I_{dM_1} is chosen as the constrained variable, the required voltage (V_{dM_1}, V_{qM_1}) is consequently determined. Since all motors are parallel connected to the same inverter, the voltage magnitude is the same. This is the only coupling between each motor. So, our analysis method is that, rather than analyzing the extended model (4.2), it would be more convenient to work with the model of each motor then extend the conclusion to all motors. Speaking in detail, we firstly determine the constraints on I_{dM_1} by discussing each motor's steady state existence. Then, obviously, the solution exists only when I_{dM_1} satisfies all motors' constraints.

(4.3) can be applied between M_1 and M_k $(1 < k \leq N)$.

$$V_{dM_1}{}^2 + V_{qM_1}{}^2 = V_{dM_k}{}^2 + V_{qM_k}{}^2 \tag{4.3}$$

Considering M_k, the only unknown variables in (4.1) is I_{dM_k} and θ_{dM_1,M_k}. (4.4) and (4.5) shows the steady-state model of M_1 and M_k respectively.

$$\begin{cases} V_{dM_1} = R_s I_{dM_1} - L_s \omega_e I_{qM_1} \\ V_{qM_1} = R_s I_{qM_1} + L_s \omega_e I_{dM_1} + \omega_e \varphi_f \end{cases} \tag{4.4}$$

$$\begin{cases} V_{dM_k} = R_s I_{dM_k} - L_s \omega_e I_{qM_k} \\ V_{qM_k} = R_s I_{qM_k} + L_s \omega_e I_{dM_k} + \omega_e \varphi_f \end{cases} \tag{4.5}$$

Replacing V_{dM_1}, V_{qM_1}, V_{dM_k} and V_{qM_k} in (4.3) with the right side of (4.4) and (4.5), the expression of I_{dM_k} can be got.

$$Z^2 I_{dM_k}{}^2 + \alpha I_{dM_k} + \beta = 0 \tag{4.6}$$

where

$$\begin{cases} Z = \sqrt{R_s{}^2 + (\omega_e L_s)^2} \\ \alpha = 2 L_s \omega_e{}^2 \varphi_f \\ \beta = \left(\omega_e L_s I_{qM_k}\right)^2 + \left(R_s I_{qM_k} + \omega_e \varphi_f\right)^2 - \left(R_s I_{dM_1} - L_s \omega_e I_{qM_1}\right)^2 - \left(R_s I_{qM_1} + L_s \omega_e I_{dM_1} + \omega_e \varphi_f\right)^2 \end{cases} \tag{4.7}$$

It is not necessary to consider the existence problem of θ_{dM_1,M_k}. Because if θ_{dM_1,M_k} is define in $\left(-\frac{\pi}{2}, \frac{\pi}{2}\right)$, its expression is:

$$\theta_{dM_1,M_k} = sin^{-1}\left[\frac{V_{qM_1}\left(R_s I_{dM_k} - \omega_e L_s I_{qM_k}\right) - V_{dM_1}\left(R_s I_{qM_k} + \omega_e L_s I_{dM_k} + \omega_e \varphi_f\right)}{V_{qM_1}{}^2 + V_{dM_1}{}^2}\right] \tag{4.8}$$

From (4.8) we can find that θ_{dM_1,M_k} always exists once I_{dM_k} is real. Thus, here we only

need to discuss the real solution existence problem of I_{dM_k}. (4.6) can be seen a quadratic equation with I_{dM_1} as a parameter, which means that the existence criterion of each motor relay on I_{dM_1} only. Its constraint can be calculated by analyzing the discriminant (4.6). (4.6) has two real solutions when and only when

$$\Delta_1 = \left(2Z^2 I_{dM_1} + \alpha\right)^2 + 4Z^4 \left(f\left(I_{qM_1}, \omega_e\right) - f\left(I_{qM_k}, \omega_e\right)\right) \geq 0 \tag{4.9}$$

where

$$f\left(I_q, \omega_e\right) = {I_q}^2 + \frac{2R_s \omega_e \varphi_p}{Z^2} I_q \tag{4.10}$$

Each motor in $\mathbb{M}_1$ must satisfy (4.9) so that the steady state solution for entire system exists. Similar with the study in 3.3.2, as the coefficient before ${I_{dM_1}}^2$ is always positive, the solution of (4.9) can be divided into two cases depending on the discriminant of (4.9).

$$\Delta_2 = -64Z^8 \left(f\left(I_{qM_1}, \omega_e\right) - f\left(I_{qM_k}, \omega_e\right)\right) \tag{4.11}$$

(4.11) is equivalent to (3.25) when discussing the solution existence problem of a MIDPMSM system. But now we can eliminate the assumptions that M_k is working as a motor and positive rotating. But here the definition of the generator mode is more than a negative torque. We will precise this definition later.

1) $\Delta_2 < 0$

In the first case, when $\Delta_2 < 0$, which means:

$$f\left(I_{qM_1}, \omega_e\right) \geq f\left(I_{qM_k}, \omega_e\right) \tag{4.12}$$

This says that Δ_1 is always satisfied despite the value of I_{dM_1}. The value range of I_{dM_1} is consequently define as:

$$(-\infty, +\infty) \tag{4.13}$$

2) $\Delta_2 \geq 0$

In the second case, when

$$f\left(I_{qM_1}, \omega_e\right) < f\left(I_{qM_k}, \omega_e\right) \tag{4.14}$$

The solution of (4.9) is

$$(-\infty, -\frac{\alpha}{2Z^2} - \sqrt{f\left(I_{qM_k}, \omega_e\right) - f\left(I_{qM_1}, \omega_e\right)}\Big] \cup \Big[-\frac{\alpha}{2Z^2} + \sqrt{f\left(I_{qM_k}, \omega_e\right) - f\left(I_{qM_1}, \omega_e\right)}, +\infty) \tag{4.15}$$

(4.15) gives an explicit value range of I_{dM_1} when $f\left(I_{qM_1}\right)$ is less than $f\left(I_{qM_k}\right)$. Define

set $\mathbb{I}_{M_k}$, as expressed in (4.16),

$$\mathbb{I}_{M_k} = \begin{cases} (-\infty, -\frac{\alpha}{2Z^2} - \sqrt{f(I_{qM_k}, \omega_e) - f(I_{qM_1}, \omega_e)}] \cup [-\frac{\alpha}{2Z^2} + \sqrt{f(I_{qM_k}, \omega_e) - f(I_{qM_1}, \omega_e)}, +\infty) & f(I_{qM_k}, \omega_e) \geq f(I_{qM_1}, \omega_e) \\ (-\infty, +\infty) & f(I_{qM_k}, \omega_e) < f(I_{qM_1}, \omega_e) \end{cases} \quad (4.16)$$

which represents the constrained range of I_{dM_1} determined by M_k. Thus, for the entire system composed by N motors, I_{dM_1} must be regulated in the range determined by $\mathbb{I} = \mathbb{I}_{M_2} \cap \ldots \cap \mathbb{I}_{M_N}$. This constraint on I_{dM_1} leads to two different control strategies. Their control schemes are shown in Figure 4.2 and Figure 4.3.

1) Non-master selection

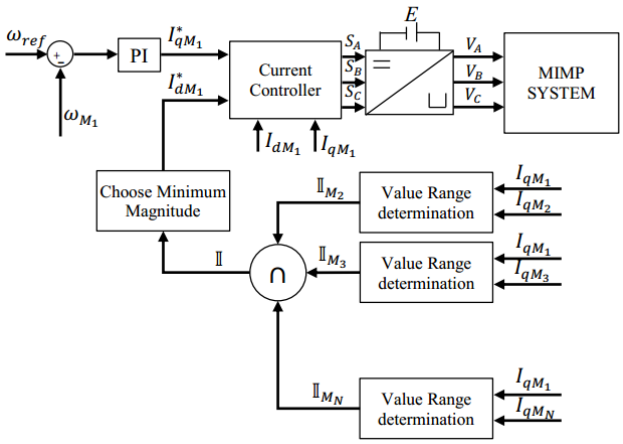

Figure 4.2 Block diagram of Non-master selection controller

The controller structure is similar to Master-Slave, but compared to Master-Slave strategy, the master selection part is replaced with a dedicated block that is responsible for calculating appreciate reference of I_{dM_1}. At each instant, it will evaluate $f(I_{qM_1}, \omega_e)$ and $f(I_{qM_k}, \omega_e)$ then calculate $\mathbb{I}_{M_k}$ by (4.16). In final $\mathbb{I}$ can be obtained. $I^*_{dM_1}$ is set to the minimal magnitude value in $\mathbb{I}$ under the Maximum Torque Per Ampere (MTPA) law. It should be noticed that if $\mathbb{I} = (-\infty, +\infty)$, $I^*_{dM_1}$ is set to 0. The motor under control remains unchanged.

2) Master selection

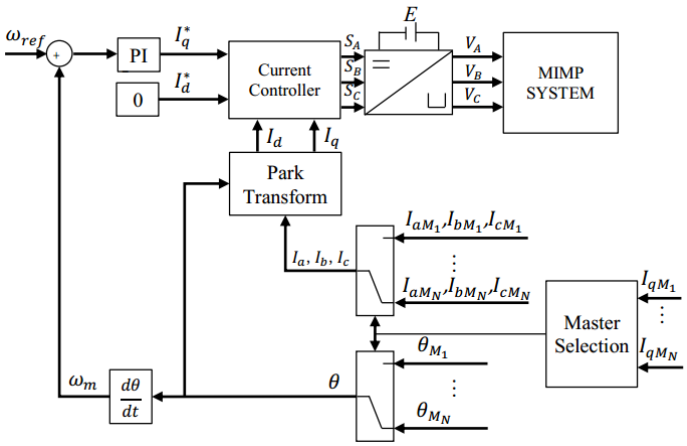

Figure 4.3 Block diagram of master selection controller

On the other hand, it is possible that not only regulate I_{dM_1} passively under the constraints but also choose the motor as M_1 which satisfies $f(I_{qM_1}, \omega_e) > f(I_{qM_k}, \omega_e)$, $M_k \in \mathbb{M}_1$. Therefore, the constraint range $\mathbb{I}$ is always $(-\infty, +\infty)$ in such case. $I_{dM_1}^*$ can be arbitrary. This strategy is similar with the Master-Slave strategy oriented for MIDPMSM system. Their difference will be discussed in the following section.

4.2.3.1 Extension of Master-Slave strategy

There is a difference between the master-selection strategy here and the conventional Master-Slave strategy introduced in section 2.3.3. The conventional strategy compares the electrical angle of both machines to determine the master machine based on the relationship (4.17).

$$\theta_{eM_1} < \theta_{eM_1} \Leftrightarrow \delta_{M_1} > \delta_{M_2} \Leftrightarrow T_{eM_1} > T_{eM_2} \Leftrightarrow I_{qM_1} > I_{qM_2} \tag{4.17}$$

When $\theta_{eM_1} < \theta_{eM_1}$, which resulted in $I_{qM_1} > I_{qM_2}$, M_1 is selected as the master, and vice versa. But in (4.16), we have used the value calculated by (4.10) that relatives to not only the torque but also the speed and machine parameters to determine the master machine. This is because there are the conventional master criteria is oriented for motor mode (generate torque). When one or both of the two motors become a generator, this criterion is no longer valid.

If define

$$I_q^{critical} = -\frac{R_s \omega_e \varphi_p}{Z^2} \tag{4.18}$$

The curve shape of (4.10) when motors are rotating in positive direction ($\omega_e > 0$) are shown in Figure 4.4. The curve can be divided into three regions:

(4.19)

$$\begin{cases} I_q \in \left(-\infty, -I_q^{critical}\right) & (4.20) \\ I_q \in \left[-I_q^{critical}, 0\right] & \\ I_q \in (0, +\infty) & (4.21) \end{cases}$$

They can be identified with red, green and blue curve correspondingly in Figure 4.4. Their explanations are:

a) Blue region: Machines working as motors. $I_{qM_1} > I_{qM_k} \Leftrightarrow f(I_{qM_1} I_{qM_k}, \omega_e) > f(I_{qM_k} I_{qM_k}, \omega_e)$.

b) Green region: Machines working as generators. $I_{qM_1} > I_{qM_k} \Leftrightarrow f(I_{qM_1} I_{qM_k}, \omega_e) > f(I_{qM_k} I_{qM_k}, \omega_e)$.

c) Red region: Machines working as generators. $I_{qM_1} > I_{qM_k} \Leftrightarrow f(I_{qM_1} I_{qM_k}, \omega_e) < f(I_{qM_k} I_{qM_k}, \omega_e)$.

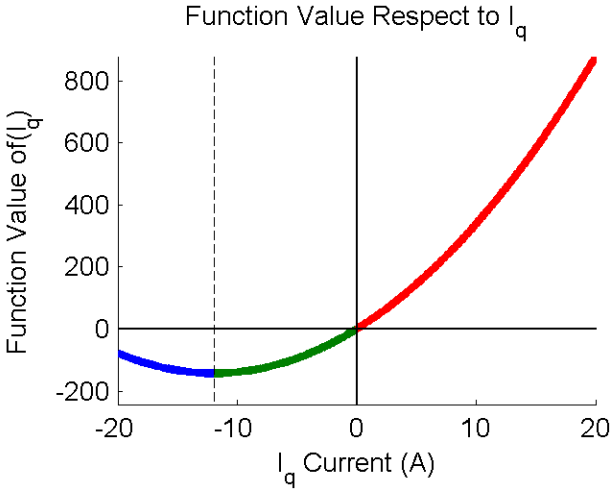

Figure 4.4 Curve shape of f(x) when machine is rotating in the positive direction

As a summary, the relationship between I_q current and function value is symmetric to $I_q^{critical}$, in the region

$$\Phi_A = \left[-\frac{R_s \omega_e \varphi_p}{Z^2}, +\infty\right] \quad (4.22)$$

$I_{qM_1} > I_{qM_k} \Leftrightarrow f(I_{qM_1}, \omega_e) > f(I_{qM_k}, \omega_e)$, while in the region

$$\Phi_B = \left[-\infty, -\frac{R_s \omega_e \varphi_p}{Z^2},\right] \quad (4.23)$$

$I_{qM_1} < I_{qM_k} \Leftrightarrow f(I_{qM_1}, \omega_e) > f(I_{qM_k}, \omega_e)$. It would be easier to understand this conclusion if we draw the torque-δ curve described in (2.44) respect to different voltage amplitude. Here we use the I_q current to represent the torque directly. The term $N_p \varphi_p$ in (2.44) should be taken out so that the current term is left. We can found that the sine shape torque curve is also symmetric to $I_q^{critical}$. As only the master motor is under control, the current

regulator will adapt the voltage amplitude consequently the amplitude of the curve to meet its torque requirement.

In fact, $I_q^{critical}$ corresponds to the stator current when zero voltage is applied. In such a condition, the three-phase terminations are connected in short circuit. We can easily obtain this result by setting the voltage equals to zero

$$\begin{bmatrix}0\\0\end{bmatrix} = \begin{bmatrix}R_s & -L_s\omega_e\\ L_s\omega_e & R_s\end{bmatrix}\begin{bmatrix}I_d\\I_q\end{bmatrix} + \begin{bmatrix}0\\ \omega_e\varphi_p\end{bmatrix} \tag{4.24}$$

The corresponding currents are:

$$\begin{cases} I_d = -\dfrac{L_s{\omega_e}^2\varphi_p}{Z^2} \\ I_q = -\dfrac{R_s\omega_e\varphi_p}{Z^2} \end{cases} \tag{4.25}$$

The output power can be calculated as:

$$\vec{V}_{dq}\cdot\vec{I}_{dq} = \left|\vec{V}_{dq}\right|\left|\vec{I}_{dq}\right| cos\,\varphi = R_s\left({I_d}^2 + {I_q}^2\right) + \omega_e\varphi_p I_q \tag{4.26}$$

where $\cos\varphi$ is the power factor. (4.26) equals to zero if we insert (4.25) into (4.26). This means that all mechanical power is absorbed by stator resistance. When (4.26) becomes positive, $\cos\varphi > 0$, this means that torque above (4.18) needs external energy input. While (4.26) becomes negative, $\cos\varphi < 0$, torque below (4.18) needs external energy consumer. Thus, in this chapter, the definition of a motor or generator is relative to its energy direction.

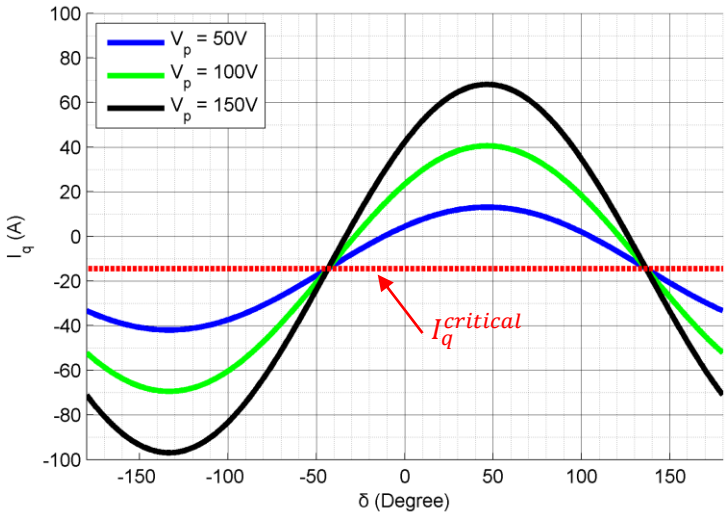

Figure 4.5 Torque-δ curve respect to different voltage amplitude

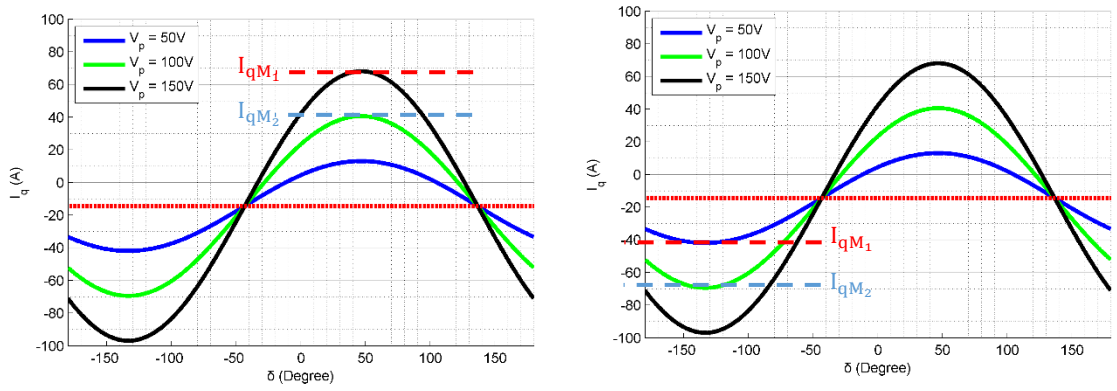

Figure 4.6 Demonstration of stability conclusion.

In the conventional master-slave strategy, as the more loaded motor is controlled, the torque requirement of the slave motor is thought to be also satisfied in such a condition. We can judge it from Figure 4.7(a). If the torque requirement of the master motor is I_{qM_1}(represented as red dash line), the current controller will generate the voltage around black curve. Meanwhile, the torque requirement of the slave motor (represented as blue dash line) is also satisfied. But in Figure 4.7(b), when two machines are in generator mode, the conventional Master-Slave will still choose M_1 as the master machine due to $\theta_{eM_1} < \theta_{eM_1} \Leftrightarrow I_{qM_1} > I_{qM_2}$. But obviously the generated voltage cannot support the torque requirement of M_2. It will loss stability immediately. Thus, the conventional master-slave strategy only works when $I_{qM_1} \in \Phi_A$ and $I_{qM_2} \in \Phi_A$. To ensure the stability in the entire operation range, the value of function (4.10) rather than the torque must be used as the master criteria.

4.3 **Simulation**

Due to the limitation that there are only two motors available in our experiment bench. We have to use a simulation conducted in MATLAB/Simulink to verify the controller proposed in this chapter. A regular FOC controller is responsible for controlling the current of the master machine. In order to approach the real experiment environment, the screw tracks used in our experiment bench are modeled and imported into Simulink.

During the simulation, the system is assigned with four motors. The first motor has the highest friction parameter because it is connected to another screw track apart from its own track. After simulation started, all motors are brought to steady speed operation condition. The two control strategies proposed here depends heavily on torque relationship determination. The non-master-selection strategy must use the torque relationship of each motor to determine the value range of I_{dM_1}. The Master-selection strategy must use it to determine the master motor. The shape of applied torque is shown in Figure 4.7. Thus, we can have relationship transition of each motor during the test.

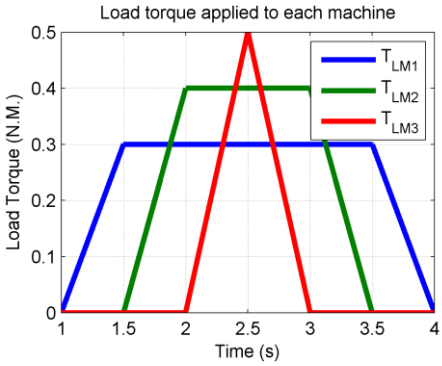

Figure 4.7 Load Torque applied to each machine

4.3.1 Demonstration of non-master selection strategy

Figure 4.8 has shown the simulation results of non-master selection strategy. Figure 4.8(a) shows the speed response while Figure 4.8(b) shows the current response. It can be identified that when there is no external load applied, M_1 is the most loaded motor. Refer to (4.16), the value range of I_{dM_1} is $(-\infty, +\infty)$. Thus, in such condition, I_{dM_1} (green curve) is regulated as 0. The system's stability is kept.

Around 1.4s, the load torque of M_2 becomes larger than the torque of M_1. M_2 becomes the most loaded machine. At this instant, the controller increases I_{dM_1} to preserve the system stability following the constraint applied by (4.16). The same transition happens to M_3 and M_4 as their applied torque increase. The system is still stable even there is no master-selection. This validates the conclusion of open-loop stability that the stability is equivalent to the steady-state existence. Meanwhile, because there is no state change inside the controller, speed response of all three motors is relatively steady. No jitter can be observed.

4.3.2 Demonstration of master selection strategy

Figure 4.9 illustrates the result of the master-selection strategy. The simulation configuration is the same as it is for non-master selection strategy. When there is no external load applied, its behavior looks similar with non-master selection strategy. I_{dM_1} is also regulated as 0 respect to MTPA law.

In 1.4s, as soon as the torque of M_2 exceed M_1, M_2 is chosen as the control object and I_{dM_2} becomes 0. The same transition happens to M_3 and M_4 as their applied torque increase.

4.3.3 Demonstration of extend master-slave strategy

The extend master-slave strategy is different with the conventional one because it compares the value of (4.10) rather than their torque directly. This extension enables the master-slave strategy also works in generator mode. Thus, it is necessary to verify its correctness. To reduce the simulation complexity, we have used only two machines to

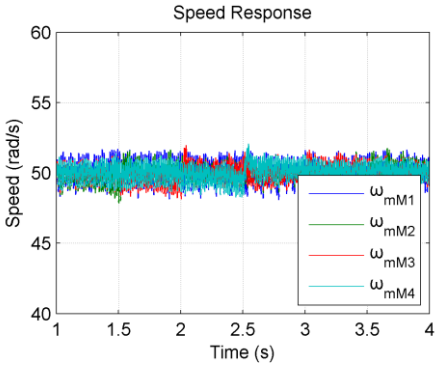

(a)

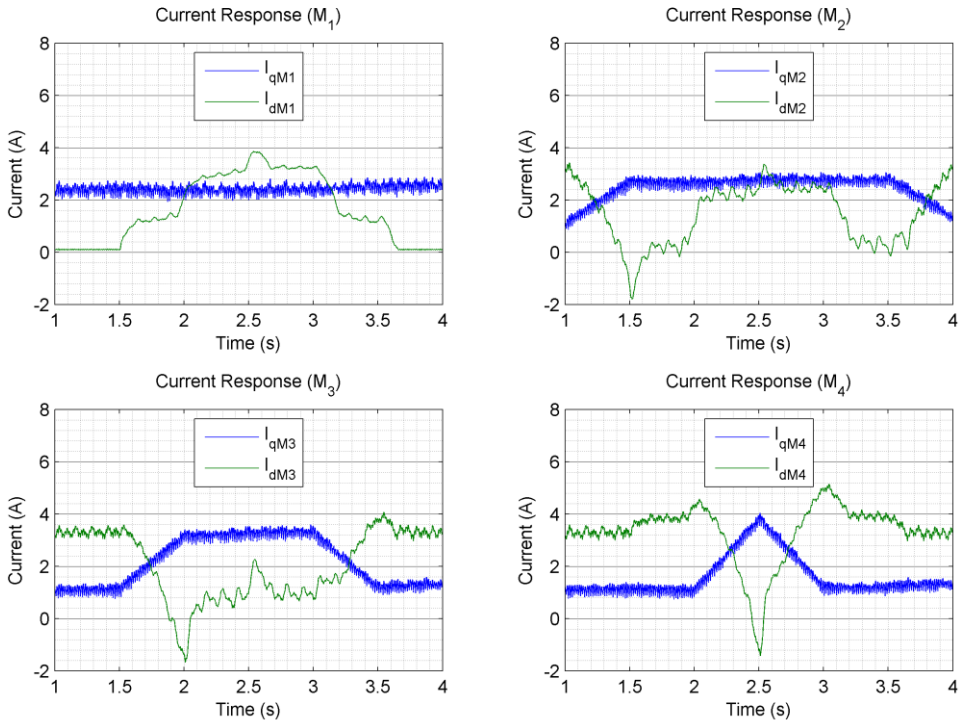

(b)

Figure 4.8 Simulation result of non-master selection strategy

conduct the test. The number of the machine won't change the conclusion of the simulation. The interested region is defined in (4.20) where master-selection strategy has an inverse relationship respect to the torque. We must first calculate this region depending on the simulation parameters.

In the simulation, the mechanical speed is 50rad/s. The critical torque consequently is:

$$T_e^{critical} = -\frac{N_p R_s \omega_e {\varphi_p}^2}{Z^2} \approx -1.36N.M. \tag{4.27}$$

The corresponding $I_q^{critical}$ is around -7.1A. So our simulation region is:

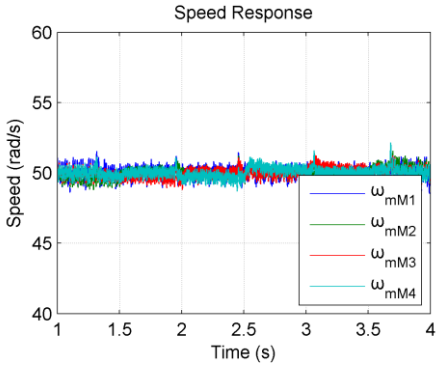

(a)

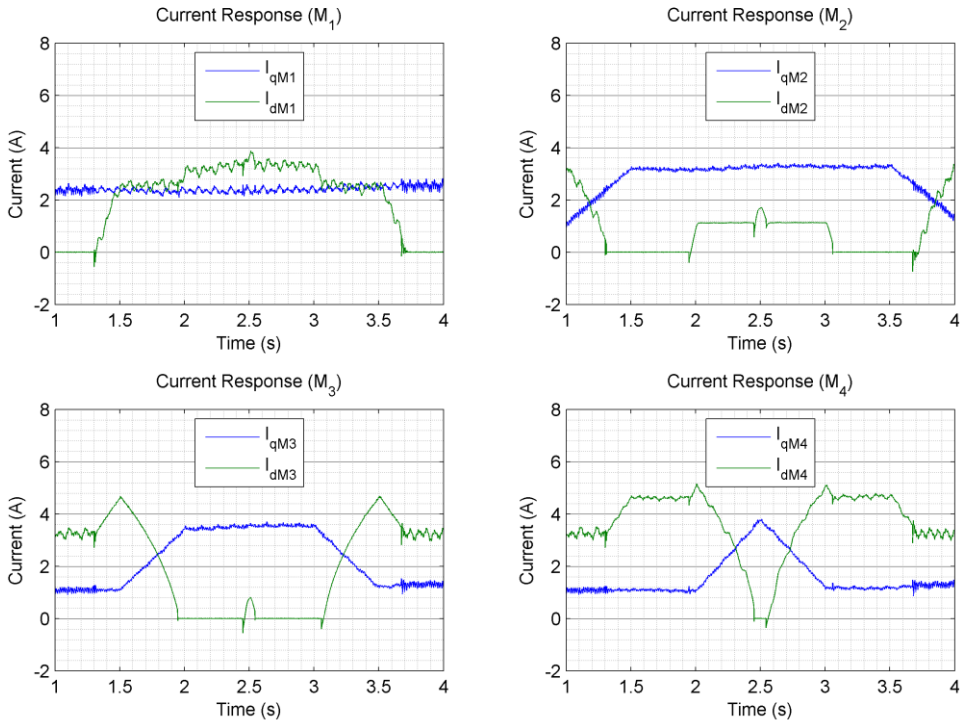

(b)

Figure 4.9 Simulation result of master selection strategy

$$(-\infty, -7.1) \tag{4.28}$$

External load torques are configured to both two motors to bring them to the region (4.28). They are illustrated in Figure 4.10. Meanwhile, with such torques applied, we can keep I_{qM_1} always greater than I_{qM_2} so that the difference between two strategies can be observed.

The simulation results are shown in Figure 4.11. Figure 4.11(a) shows the results of the extended master-slave strategy. We can conclude from them that even high speed-jitter exist when control object transit, the two machines are kept stable operation. On the

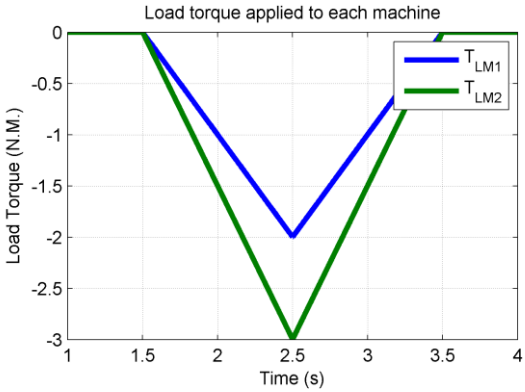

Figure 4.10 Torque load applied to two motors during simulation

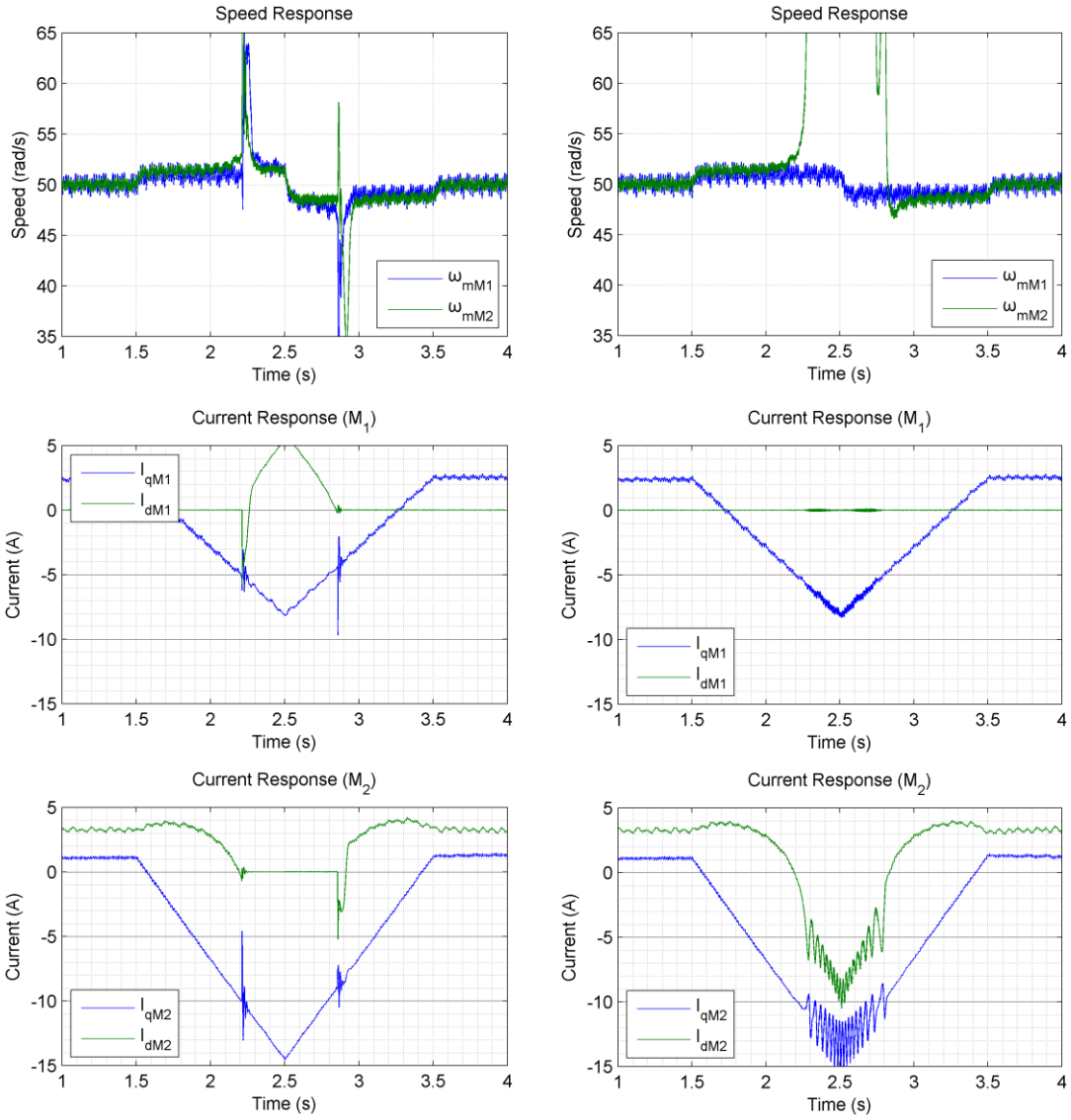

(a) (b)

Figure 4.11 Demonstration of (a) extend Master-Slave strategy. (b) Conventional Master-Slave strategy

contrary, in Figure 4.11(b), although I_{qM_1} is always greater than I_{qM_2}, when the torque of M_2 exceed certain value, it lost stability immediately.

4.4 **Conclusion**

In this chapter, we have adapted the design method introduced in the previous chapter to a MIMPMSM system. By using the constraint analysis method proposed in the previous section, it is proved that the MIMPMSM system is feasible. Similar to the MIDPMSM system, the controller must and can only control one extra variable to make the system fully constrained. Considering that the advantage of using θ_d for a MIMPMSM system more than 2 machines has vanished while the resulted controller structure would be more complex, I_{dM_1} is used as this constrained variable.

According to the previous derivation, in the case of open-loop operation, PMSM's stability is equivalent to the existence of steady-state solution. Therefore, we derive the existence criterion of the steady-state solution of each motor with respect to the constraint variable. And according to this criterion, two control strategies are designed. Both of them only control one machine among all machines. The first strategy, called non-master-selection, regulates I_{dM_1} passively under the constraints to assure the system stability. On the other hand, the master-selection strategy we calculate the value of function (4.10) and choose the machine with highest value as the master. This strategy extends the conventional master-slave strategy to generator mode which makes sense in traction applications such as an electric vehicle.

Meanwhile, the controller for MIDPMSM system obtained in Chapter 3 can also be extended to generator mode using the conclusion here. The efficiency optimization method isn't based on these assumptions, it can be used directly. The controller itself can be replaced by either the non master-selection strategy or extend master-selection strategy. In the case of non master-selection strategy, the output of the θ_d regulator, which is I_{dM_1}, is the reference value set to the current controller if it is inside the stable region defined by (4.16). On the other hand, in the case of master-selection, it can be set to the controller directly.

Finally, we have verified these control strategies in a simulation involving 4 machines conducted in MATLAB/Simulink. The simulation results verify that both control strategies are operational and stable even highly unbalanced torques applied to the machines.

Conclusion and perspective

In the thesis, we have designed two different types of controller for MIDPMSM system and MIMPMSM system. Their common point is that they have used the same design method. Rather than control all machine concurrently, we just put one of these machines closed-loop controlled with existing controller for single PMSM and let the rest of the motor operate open-loop. Then, the I_d current of the master machine is used to implement our control strategy taking stability and efficiency into account. For the stability, the steady-state existence together with the characteristic of the open-loop stability are our breakthrough. The optimization process that minimizing the copper loss of the system calculates the optimal system state. Simulation and experiment show that the design method can effectively guarantee the stability of multiple machines system.

In chapter II, we tested four different control strategies based on model predictive control, including different cost functions, optimization and modulation methods. The test shows that the modulation method has the greatest impact on current ripple. Increasing the number of voltage vector can greatly improve this performance. But small number of voltage vector can reduce the switching losses of inverter. In practice, these two aspects need to be coordinated. Meanwhile the experimental results have also shown that the efficiency of a unique cost function is lower than that of a master-slave. The analysis has shown that it is due to the over-constrained situation. This inspired us to design the controller from a steady-state model.

Chapter III mainly describes how to design an efficiency-optimal controller for MIDPMSM system. Through analyzing the solution existence problem of the steady-state model, we can obtain the structure of the controller and prove the system controllability. Then, Lagrange multiplier is used to calculate the efficiency-optimal state. The analytical solution of this optimal-state is given. The experiment test has proved the effectiveness of the controller both in stability and efficiency. Moreover, this design method is also proved to be effective.

In chapter IV, we have tried to extend the design method to a MIMPMSM system. It resulted in two different control strategies. The first strategy, called non-master-selection, regulates I_{dM_1} based on the speed and torque of each motor. The second strategy, called master-selection strategy, proposed to choose the master machine by comparing the value of a function of each machine. On the one hand, we extended the controller to control more than two machines. On the other hand, both strategies can support not only the motor mode but also the generator mode. Especially in the master-selection strategy, we extended the Master-Slave strategy to achieve this goal. MIMPMSM systems then can be used in some traction applications, such as electric vehicles, which requires the machines to switch between motor and generator mode during operation. Multiple generators application can even be adapted.

For a multi-PMSM system, especially the parallel structure, its control problem is more complex than a general PMSM system due to the limited control input and strong coupling between each machine. It brings a lot of problems and this thesis only tried to solve a small part of them. There are still a lot of unknowns in front of us, such as:

- Transient performance

Although the design method proposed in this thesis can effectively ensure the stability and controllability of the system, optimal-efficiency of the system can even be guaranteed under the two motors. However, due to the design method that uses only steady-state model, it is deficient in transient response performance. In our controller, all machines except the master machine are operating in open-loop. This makes the transient responses of these machines to be completely uncontrolled. Oscillation and large overshoot may occur during operation, which is unacceptable in practice. Therefore, it is necessary to strengthen the research in this respect.

- Efficiency optimization taking more machines and other types of loss into account

Although in Chapter 3 we have come to an analytical solution of the optimal efficiency state of two machines. For more than two motor case, this part of the study is basically blank. The same calculation method can be used in this case, but the existence of analytical solutions still needs to be studied. The efficiency optimization only takes copper loss into account. In the thesis, we have studied the controller influence on different type of loss, such as inverter loss. In the future, it is interesting to put them into consideration.

- Sensor reduction and sensorless

As the number of motors increases, the number of corresponding sensors also increases linearly. If we can use technology to reduce the overall number of sensors, such as measuring the current at the inverter output rather than each motor's own current, then the complexity of the system can be even more reduced. At the same time, in the case of PMSM sensorless control, their position estimation will be more complicated in parallel.

- Motors with different parameters

The problem of control and efficiency optimization when machines have different parameters. This problem involves two aspects, first, we can use different types of machines to build a multi-PMSM system. Second, due to the operation status of the machine and the production process, the parameters of each machine may be different even they are the same type. In this thesis, we have obtained these results based on the assumption that all machines are identical. Obviously, it cannot be true in practice. In the third chapter, we have already understood that parameter variations have a great impact on system stability and efficiency optimization. This problem has to be solved in the future.

Reference

[1] Kelecy, P.M.; Lorenz, R.D., "Control methodology for single inverter, parallel connected dual induction motor drives for electric vehicles," in Power Electronics Specialists Conference, PESC '94 Record., 25th Annual IEEE, pp.987-991 vol.2, 20-25 Jun 1994.

[2] Bouscayrol, A.; Pietrzak-David, M.; Delarue, P.; Pena-Eguiluz, R.; Vidal, P.-E.; Kestelyn, X., "Weighted Control of Traction Drives With Parallel-Connected AC Machines," in Industrial Electronics, IEEE Transactions on , vol.53, no.6, pp.1799-1806, Dec. 2006.

[3] T. M. Jahns, "Torque Production in Permanent-Magnet Synchronous Motor Drives with Rectangular Current Excitation," in IEEE Transactions on Industry Applications, vol. IA-20, no. 4, pp. 803-813, July 1984.

[4] T. Y. Lee, M. K. Seo, Y. J. Kim and S. Y. Jung, "Motor Design and Characteristics Comparison of Outer-Rotor-Type BLDC Motor and BLAC Motor Based on Numerical Analysis," in IEEE Transactions on Applied Superconductivity, vol. 26, no. 4, pp. 1-6.

[5] Z. Q. Zhu and D. Howe, "Electrical Machines and Drives for Electric, Hybrid, and Fuel Cell Vehicles," in Proceedings of the IEEE, vol. 95, no. 4, pp. 746-765, April 2007.

[6] M. Zeraoulia, M. E. H. Benbouzid and D. Diallo, "Electric Motor Drive Selection Issues for HEV Propulsion Systems: A Comparative Study," in IEEE Transactions on Vehicular Technology, vol. 55, no. 6, pp. 1756-1764, Nov. 2006.

[7] A. Akrad, M. Hilairet and D. Diallo, "Design of a Fault-Tolerant Controller Based on Observers for a PMSM Drive," in IEEE Transactions on Industrial Electronics, vol. 58, no. 4, pp. 1416-1427, April 2011.

[8] T. M. Jahns, G. B. Kliman and T. W. Neumann, "Interior Permanent-Magnet Synchronous Motors for Adjustable-Speed Drives," in IEEE Transactions on Industry Applications, vol. IA-22, no. 4, pp. 738-747, July 1986.

[9] K. Li, F. C. Chou and J. Y. Yen, "Real-Time, Energy-Efficient Traction Allocation Strategy for the Compound Electric Propulsion System," in IEEE/ASME Transactions on Mechatronics, vol. 22, no. 3, pp. 1371-1380, June 2017.

[10] Raj Kumar K, Nithin K and Vinay Kumar. T, "Reduction of torque ripples in 3-level inverter fed PMSM drive based on instantaneous voltage control technique," 2016 International Conference on Electrical Power and Energy Systems (ICEPES), Bhopal, 2016, pp. 145-150.

[11] M. Siami, D. A. Khaburi, M. Rivera and J. Rodríguez, "A Computationally Efficient Lookup Table Based FCS-MPC for PMSM Drives Fed by Matrix Converters," in IEEE Transactions on Industrial Electronics, vol. 64, no. 10, pp. 7645-7654, Oct. 2017.

[12] P. Ghani, M. Arasteh and H. R. Tayebi, "Analysis of electromechanical model of traction system with single inverter dual induction motor," 2016 7th Power Electronics and Drive Systems Technologies Conference (PEDSTC), Tehran, 2016, pp. 99-104.

[13] J.Chiasson, Danbing Seto, Fanping Sun, A. Stankovic and S. Bortoff, "Independent control of two PM motors using a single inverter: application to elevator doors," Proceedings of the 2002 American Control Conference (IEEE Cat. No.CH37301), Anchorage, AK, USA, 2002, pp. 3093-3098 vol.4.

[14] J. Germishuizen, A. Jockel, T. Hoffmann, M. Teichmann, L. Lowenstein and F. v. Wangelin, "SyntegraTM - next generation traction drive system, total integration of traction, bogie and braking technology," International Symposium on Power Electronics, Electrical Drives, Automation and Motion, 2006. SPEEDAM 2006., Taormina, 2006, pp. 1073-1077.

[15] Jöckel, A.; Knaak, H.-J.: INTRA ICE – A Novel Direct Drive System for Future High-Speed Trains. International Conference on Electrical Machines ICEM 2002, Brugge, September 2002.

[16] B. Sarlioglu and C. T. Morris, "More Electric Aircraft: Review, Challenges, and Opportunities for Commercial Transport Aircraft," in IEEE Transactions on Transportation Electrification, vol. 1, no. 1, pp. 54-64, June 2015.

[17] A. R. Behbahani and K. J. Semega, "Control strategy for electromechanical actuators versus hydraulic actuation systems for aerospace applications," SAE Tech. Pap. 2010-01-1747, 2010.

[18] Mengmeng Liu and Yuanjun Zhou, "The reliability prediction of an Electro-Mechanical Actuator of aircraft with the hybrid redundant structure," 2008 IEEE Vehicle Power and Propulsion Conference, Harbin, 2008, pp. 1-5.

[19] D. Briere and P. Traverse, "AIRBUS A320/A330/A340 electrical flight controls - A family of fault-tolerant systems," FTCS-23 The Twenty-Third International Symposium on Fault-Tolerant Computing, Toulouse, France, 1993, pp. 616-623.

[20] S. Siala, “Motorisation asynchrone d’un robot mobile, Observation et régulation du flux, Contrôle d’alimentation pour le suivi de trajectoire”, Doctoral Thesis, INP Toulouse, 1992.

[21] J. M. Lazi, Z. Ibrahim, M. Sulaiman and R. Mustafa, "Performance investigation for independent speed sensorless control of Dual-PMSM drives," International Multi-Conference on Systems, Sygnals & Devices, Chemnitz, 2012, pp. 1-6.

[22] BOUSCAYROL A., “Structures d'alimentation et strategies de commande pour des systemes multimachines asynchrones — Application a la motorisation d’un robot mobile”, Doctoral Thesis, INP Toulouse, 1995.

[23] Atsushi Furuya, Kazuo Oka and Kouki Matsuse, "A characteristic analysis of four-leg inverter in two AC motor drives with independent vector control," 2007 International Conference on Electrical Machines and Systems (ICEMS), Seoul, 2007, pp. 619-624.

[24] D. Bidart, M. Pietrzak-David, P. Maussion and M. Fadel, "Mono inverter multi-parallel permanent magnet synchronous motor: structure and control strategy," in IET Electric Power Applications, vol. 5, no. 3, pp. 288-294, March 2011.

[25] E. Foch, G. Bisson, P. Maussion, M. Pietrzak-David and M. Fadel, “Power system comprising several synchronous machines synchronously self-controlled by a converter and control method for such a system, ” US Patent, US 2007/0273310 A1, November 2007.

[26] J. M. Lazi, Z. Ibrahim, M. H. N. Talib and R. Mustafa, "Dual motor drives for PMSM using average phase current technique," 2010 IEEE International Conference on Power and Energy, Kuala Lumpur, 2010, pp. 786-790.

[27] J. M. Lazi, Z. Ibrahim, M. Sulaiman, I. W. Jamaludin and M. Y. Lada, "Performance comparison of SVPWM and Hysteresis Current Control for Dual motor drives," 2011 IEEE Applied Power Electronics Colloquium (IAPEC), Johor Bahru, 2011, pp. 75-80.

[28] A. Asri, D. Ishak, S. Iqbal and M. Kamarol, "A speed sensorless field oriented control of parallel- connected dual PMSM," 2011 IEEE International

Conference on Control System, Computing and Engineering, Penang, 2011, pp. 567-570.

[29] Ahmad Asri Abd Samat, D. Ishak, P. Saedin and S. Iqbal, "Speed- sensorless control of parallel- connected PMSM fed by a single inverter using MRAS," 2012 IEEE International Power Engineering and Optimization Conference Melaka, Malaysia, Melaka, 2012, pp. 35-39.

[30] M. S. D. Acampa, A. Del Pizzo, D. Iannuzzi and I. Spina, "Predictive control technique of single inverter dual motor AC-brushless drives," 2008 18th International Conference on Electrical Machines, Vilamoura, 2008, pp. 1-6.

[31] M. S. D. Acampa, A. Del Pizzo and D. Iannuzzi, "Optimized control technique of single inverter dual motor AC-brushless drives," 2008 43rd International Universities Power Engineering Conference, Padova, 2008, pp. 1-6.

[32] A. Del Pizzo, D. Iannuzzi and I. Spina, "High performance control technique for unbalanced operations of single-vsi dual-PM brushles motor drives," 2010 IEEE International Symposium on Industrial Electronics, Bari, 2010, pp. 1302-1307.

[33] Jiangbo Wang, Yue Wang, Zhaoan Wang, Jun Yang, Yunqing Pei and Qiang Dong, "Comparative Study of Vector Control Schemes for Parallel-Connected Induction Motors," 2005 IEEE 36th Power Electronics Specialists Conference, Recife, 2005, pp. 1264-1270.

[34] M. Taniguchi, T. Yoshinaga and K. Matsuse, "A speed-sensorless vector control of parallel-connected multiple induction motor drives with adaptive rotor flux observers," 2006 37th IEEE Power Electronics Specialists Conference, Jeju, 2006, pp. 1-5.

[35] M. Fadel, N. L. Nguyen and A. Llor, "Direct Torque Control — A solution for mono inverter-dual parallel PMSM system," 21st Mediterranean Conference on Control and Automation, Chania, 2013, pp. 1477-1483.

[36] N. L. Nguyen, M. Fadel and A. Llor, "Predictive Torque Control - A solution for mono inverter-dual parallel PMSM system," 2011 IEEE International Symposium on Industrial Electronics, Gdansk, 2011, pp. 697-702.

[37] N. L. Nguyen, M. Fadel and A. Llor, "A new approach to Predictive Torque Control with Dual Parallel PMSM system," Industrial Technology (ICIT), 2013 IEEE International Conference on, Cape Town, 2013, pp. 1806-1811.

[38] A. Bouarfa, M. Fadel, "Optimal Predictive Torque Control of Two PMSM supplied in Parallel on a Single Inverte," in 9th IFAC Symposium on Control of Power and Energy Systems (CPES), New Delhi, 2015, vol.48, Issue 30, pp. 84-89.

[39] J. Rodriguez and P. Cotes, "Model Predictive Control" in *Predictive Control of Power Converters and Electrical Drives*, New York: Wiley-IEEE Press, USA, 2012.

[40] F. Zhang, L. Zhu, S. Jin, W. Cao, D. Wang and J. L. Kirtley, "Developing a New SVPWM Control Strategy for Open-Winding Brushless Doubly Fed Reluctance Generators," in *IEEE Transactions on Industry Applications*, vol. 51, no. 6, pp. 4567-4574, Nov.-Dec. 2015.

[41] T. Liu and M. Fadel, "Performance comparison of control strategies for mono-inverter Dual-PMSM system," 2016 IEEE International Power Electronics and Motion Control Conference (PEMC), Varna, 2016, pp. 637-642.

[42] T. Liu and M. Fadel, "Comparative study of different predictive torque control strategies for mono-inverter dual-PMSM system," 2016 18th Mediterranean Electrotechnical Conference (MELECON), Lemesos, 2016, pp. 1-6.

[43] P. Correa, M. Pacas and J. Rodriguez, "Predictive Torque Control for Inverter-Fed Induction Machines," in IEEE Transactions on Industrial Electronics, vol. 54, no. 2, pp. 1073-1079, April 2007.

[44] J. Rodriguez, J. Kolar, J. Espinoza, M. Rivera and C. Rojas, "Predictive torque and flux control of an induction machine fed by an indirect matrix converter with reactive power minimization," 2010 IEEE International Symposium on Industrial Electronics, Bari, 2010, pp. 3177-3183.

[45] Z. Zhou, C. Xia, Y. Yan, Z. Wang and T. Shi, "Torque Ripple Minimization of Predictive Torque Control for PMSM With Extended Control Set," in IEEE Transactions on Industrial Electronics, vol. 64, no. 9, pp. 6930-6939, Sept. 2017.

[46] Q. Liu and K. Hameyer, "Torque Ripple Minimization for Direct Torque Control of PMSM With Modified FCSMPC," in IEEE Transactions on Industry Applications, vol. 52, no. 6, pp. 4855-4864, Nov.-Dec. 2016.

[47] M. J. Lesani, H. Mahmoudi, M. Ebrahim, S. Varzali and D. Arab khaburi, "Predictive torque control of induction motor based on improved fuzzy control method," 2013 13th Iranian Conference on Fuzzy Systems (IFSC), Qazvin, 2013, pp. 1-5.

[48] L. Springob and J. Holtz, "High-bandwidth current control for torque-ripple compensation in PM synchronous machines," in IEEE Transactions on Industrial Electronics, vol. 45, no. 5, pp. 713-721, Oct 1998.

[49] M. Yang, X. Lang, J. Long and D. Xu, "Flux Immunity Robust Predictive Current Control With Incremental Model and Extended State Observer for PMSM Drive," in IEEE Transactions on Power Electronics, vol. 32, no. 12, pp. 9267-9279, Dec. 2017.

[50] T. Türker, U. Buyukkeles and A. F. Bakan, "A Robust Predictive Current Controller for PMSM Drives," in IEEE Transactions on Industrial Electronics, vol. 63, no. 6, pp. 3906-3914, June 2016.

[51] M. Fadel, N. L. Nguyen and A. Llor, "Different solutions of predictive control for two synchronous machines in parallel," 2013 IEEE International Symposium on Sensorless Control for Electrical Drives and Predictive Control of Electrical Drives and Power Electronics (SLED/PRECEDE), Munich, 2013, pp. 1-7.

[52] Ngoc Linh NGUYEN, “Command Predictive de deux Machines Synchrones alimentees en parallele par um Onduleur de Tension Triphase”, Doctoral Thesis, INP Toulouse, 2013.

[53] Damien Bidart, “Commande Cooperative des Systemes Monoconvertisseurs Multimachines Synchrones”, Doctoral Thesis, INP Toulouse, 2011.

[54] dSPACE. DS1103 PPC Controller Board, 2003

[55] Y. Zhang, J. Zhu and W. Xu, "Predictive torque control of permanent magnet synchronous motor drive with reduced switching frequency," *Electrical Machines and Systems (ICEMS), 2010 International Conference on*, Incheon, 2010, pp. 798-803.

[56] Hyung-Tae Moon and Myung-Joong Youn, "Predictive current control for PMSM with consideration of calculation delay," in *Electronics Letters*, vol. 37, no. 24, pp. 1488-1489, 22 Nov 2001.

[57] J. Kim and C. D. Scott, "Kernel Classification via Integrated Squared Error," *2007 IEEE/SP 14th Workshop on Statistical Signal Processing*, Madison, WI, USA, 2007, pp. 783-787.

[58] Z. Kowalczuk and J. Kozlowski, "Integrated squared error and integrated absolute error in recursive identification of continuous-time plants," Control

'98. UKACC International Conference on (Conf. Publ. No. 455), Swansea, 1998, pp. 693-698 vol.1.

[59] H. Ge, B. Bilgin and A. Emadi, "Global loss minimization control of PMSM considering cross-coupling and saturation," *2015 IEEE Energy Conversion Congress and Exposition (ECCE)*, Montreal, QC, 2015, pp. 6139-6144.

[60] D. M. Ionel, M. Popescu, M. I. McGilp, T. J. E. Miller, S. J. Dellinger and R. J. Heideman, "Computation of Core Losses in Electrical Machines Using Improved Models for Laminated Steel," in *IEEE Transactions on Industry Applications*, vol. 43, no. 6, pp. 1554-1564, Nov.-dec. 2007.

[61] Y. Ying, Z. Jianguo, and G. Youguang, "A permanent magnet synchronous motor model with core loss," Japanese Soc. Appl. Electromagn. Mech., vol. 15, pp. 147–150, 2007.

[62] Chunting Mi, G. R. Slemon and R. Bonert, "Modeling of iron losses of permanent-magnet synchronous motors," in *IEEE Transactions on Industry Applications*, vol. 39, no. 3, pp. 734-742, May-June 2003.

[63] C. Mademlis and N. Margaris, "Loss minimization in vector-controlled interior permanent-magnet synchronous motor drives," in *IEEE Transactions on Industrial Electronics*, vol. 49, no. 6, pp. 1344-1347, Dec 2002.

[64] Drofenik, Uwe, and Johann W. Kolar. "A general scheme for calculating switching-and conduction-losses of power semiconductors in numerical circuit simulations of power electronic systems." Proceedings of the 2005 International Power Electronics Conference (IPEC'05), Niigata, Japan, April. 2005.

[65] Bai Baodong and Chen Dezhi, "Inverter IGBT loss analysis and calculation," 2013 IEEE International Conference on Industrial Technology (ICIT), Cape Town, 2013, pp. 563-569.

[66] B. Kaku, I. Miyashita and S. Sone, "Switching loss minimised space vector PWM method for IGBT three-level inverter," in IEE Proceedings - Electric Power Applications, vol. 144, no. 3, pp. 182-190, May 1997.

[67] J. I. Itoh, N. Nomura and H. Ohsawa, "A comparison between V/f control and position-sensorless vector control for the permanent magnet synchronous motor," Proceedings of the Power Conversion Conference-Osaka 2002 (Cat. No.02TH8579), Osaka, 2002, pp. 1310-1315 vol.3.

[68] R. Ancuti, I. Boldea and G. D. Andreescu, "Sensorless V/f control of high-speed surface permanent magnet synchronous motor drives with two novel stabilising loops for fast dynamics and robustness," in IET Electric Power Applications, vol. 4, no. 3, pp. 149-157, March 2010.

[69] Q. Liu and K. Hameyer, "High-Performance Adaptive Torque Control for an IPMSM With Real-Time MTPA Operation," in IEEE Transactions on Energy Conversion, vol. 32, no. 2, pp. 571-581, June 2017.

[70] N. Bedetti, S. Calligaro, C. Olsen and R. Petrella, "Automatic MTPA Tracking in IPMSM Drives: Loop Dynamics, Design, and Auto-Tuning," in IEEE Transactions on Industry Applications, vol. 53, no. 5, pp. 4547-4558, Sept.-Oct. 2017.

[71] G. Brando, L. Piegari and I. Spina, "Simplified Optimum Control Method for Mono-inverter Dual Parallel PMSM Drive," in IEEE Transactions on Industrial Electronics, vol. PP, no. 99, pp. 1-1.

[72] Yongjae Lee and J. I. Ha, "Minimization of stator currents for mono inverter dual parallel PMSM drive system," 2014 International Power Electronics Conference (IPEC-Hiroshima 2014 - ECCE ASIA), Hiroshima, 2014, pp. 3140-3144.

[73] Y. Lee and J. I. Ha, "Control Method for Mono Inverter Dual Parallel Surface-Mounted Permanent-Magnet Synchronous Machine Drive System," in *IEEE Transactions on Industrial Electronics*, vol. 62, no. 10, pp. 6096-6107, Oct. 2015.

[74] Y. Lee and J. I. Ha, "Control Method of Monoinverter Dual Parallel Drive System With Interior Permanent Magnet Synchronous Machines," in IEEE Transactions on Power Electronics, vol. 31, no. 10, pp. 7077-7086, Oct. 2016.

[75] S. Y. Jung, J. Hong and K. Nam, "Current Minimizing Torque Control of the IPMSM Using Ferrari's Method," in IEEE Transactions on Power Electronics, vol. 28, no. 12, pp. 5603-5617, Dec. 2013.

[76] I. Jeong, B. G. Gu, J. Kim, K. Nam and Y. Kim, "Inductance Estimation of Electrically Excited Synchronous Motor via Polynomial Approximations by Least Square Method," in IEEE Transactions on Industry Applications, vol. 51, no. 2, pp. 1526-1537, March-April 2015.

[77] I. Takahashi and Y. Ohmori, "High-performance direct torque control of an induction motor," in IEEE Transactions on Industry Applications, vol. 25, no. 2, pp. 257-264, Mar/Apr 1989.

[78] M. F. Rahman, L. Zhong, W. Y. Hu, K. W. Lim and M. A. Rahman, "A direct torque controller for permanent magnet synchronous motor drives," 1997 IEEE International Electric Machines and Drives Conference Record, Milwaukee, WI, 1997, pp. TD1/2.1-TD1/2.3.

[79] F. Zidani, D. Diallo, M. E. H. Benbouzid and R. Nait-Said, "Direct torque control of induction motor with fuzzy stator resistance adaptation," in IEEE Transactions on Energy Conversion, vol. 21, no. 2, pp. 619-621, June 2006.

[80] D. Fernandez; D. Hyun; Y. Park; D. Diaz; S. B. Lee; D. M. Lee; F. Briz, "Permanent Magnet Temperature Estimation in PM Synchronous Motors Using Low Cost Hall Effect Sensors," in IEEE Transactions on Industry Applications , vol.PP, no.99, pp.1-1.

[81] G. Feng, C. Lai and N. C. Kar, "Expectation-Maximization Particle-Filter- and Kalman-Filter-Based Permanent Magnet Temperature Estimation for PMSM Condition Monitoring Using High-Frequency Signal Injection," in IEEE Transactions on Industrial Informatics, vol. 13, no. 3, pp. 1261-1270, June 2017.

[82] Y. Lee and J. I. Ha, "Analysis of parameter variations on mono inverter dual parallel SPMSM drive system," 2015 9th International Conference on Power Electronics and ECCE Asia (ICPE-ECCE Asia), Seoul, 2015, pp. 1875-1880.

[83] Yuan-Chih Chang, Jui-Teng Chan, Jian-Cheng Chen and Jeng-Gung Yang, "Development of permanent magnet synchronous generator drive in electrical vehicle power system," 2012 IEEE Vehicle Power and Propulsion Conference, Seoul, 2012, pp. 115-118.

[84] L. Vido, M. Ruellan, Y. Amara, H. Ben Ahmed and G. Mohamed, "PMSM optimal parameters for a specification sheet including motor and generator operation," The XIX International Conference on Electrical Machines - ICEM 2010, Rome, 2010, pp. 1-6.

[85] A. N. Reshetnikov and S. V. Klassen, "PMSM analysis in dq axis at generator mode as the part of ISG," 2016 17th International Conference of Young Specialists on Micro/Nanotechnologies and Electron Devices (EDM), Erlagol, 2016, pp. 536-538.

Appendix A

Ferrari's method

The *Ferrari method* is a method for reducing the solution of an equation of degree 4 over the complex numbers to the solution of one cubic and two quadratic equations; it was discovered by L. Ferrari (published in 1545).

For a general quartic equation:

$$y^4 + ay^3 + by^2 + cy + d = 0 \tag{A.1}$$

By the substitution

$$y = x - \frac{a}{4} \tag{A.2}$$

(A.1) can be reduced to a equation whose cubic term is canceled. It is shown in (A.3).

$$x^4 + px^2 + qx + r = 0 \tag{A.3}$$

where

$$\begin{cases} p = -\dfrac{3a^2}{8} + b \\ q = \dfrac{a^3}{8} - \dfrac{ab}{2} + c \\ r = -\dfrac{3a^4}{256} + \dfrac{a^2 b}{16} - \dfrac{ac}{4} + d \end{cases} \tag{A.4}$$

Here we introduce an auxiliary parameter ε, the left-hand side of (A.3) can be written as:

$$\left(x^2 + \frac{p}{2} + \varepsilon\right)^2 - \left[2\varepsilon x^2 - qx + \left(\varepsilon^2 + p\varepsilon + \frac{p^2}{4} - r\right)\right] = 0 \tag{A.5}$$

Then ε must be chosen a value such that the quadratic trinomial in the square bracket is a perfect square. For this the discriminant of the quadratic trinomial must vanish.

$$\left(x^2 + \frac{p}{2} + \varepsilon\right)^2 - \left[2\varepsilon x^2 - qx + \left(\varepsilon^2 + p\varepsilon + \frac{p^2}{4} - r\right)\right] = 0 \tag{A.6}$$

This gives a cubic equation for ε:

$$q^2 - 4 \cdot 2\varepsilon\left(\varepsilon^2 + p\varepsilon + \frac{p^2}{4} - r\right) = 0 \tag{A.7}$$

Let ε_0 be one of the roots of (A.7), the polynomial in square brackets in (A.5) has one

double root:

$$x_0 = \frac{q}{4\varepsilon_0} \tag{A.8}$$

which leads to the equation:

$$\left(x^2 + \frac{p}{2} + \varepsilon\right)^2 - 2\alpha_0(x - x_0)^2 = 0 \tag{A.9}$$

This equation of degree 4 splits into two quadratic equations. The roots of these equations are also the roots of (A.1).

Appendix B

Lagrange multiplier

Optimization problem is one of the most common problems in calculus. It usually comes to find the maximum or minimum of a function. However, it is often difficult to find explicit expressions for extreme functions, especially when functions have prerequisites or constraints. the *Lagrange multiplier* (named by mathematician Joseph Lagrange) is a systematic method to find the extremum of a multivariate function under one or more constraints. This method turns an optimization problem consisted of *n* variable s and *k* constraints into solving *n*+*k* equations. The introduced *k* unknown variables are called *Lagrange multiplier*. The extreme points obtained by the Lagrange multiplier method will include all extreme points of the original function, but it is not guaranteed that each extreme point is the extreme point of the original problem.

An example is given to express the usage of *Lagrange multiplier*. If we want to calculate the extreme points of a function:

$$f(x_1, \cdots, x_n) = 0 \tag{B.1}$$

which contains *n* unknown variables. Meanwhile it is also constrained by *k* constraints:

$$\begin{cases} g_1(x_1, \cdots, x_n) = c_1 \\ \vdots \\ g_k(x_1, \cdots, x_n) = c_k \end{cases} \tag{B.2}$$

Introducing the *Lagrange multiplier* $\lambda_1 \sim \lambda_k$, the candidate extreme points of $f(x_1, \cdots, x_n)$ is included in the extreme points of a union equation represented in (B.3).

$$\mathcal{L}(x_1, \cdots, x_n, \lambda_1, \cdots, \lambda_n) = f(x_1, \cdots, x_n) + \sum_{i=1}^{n} \lambda_i \left(g_i(x_1, \cdots, x_n) - c_i\right) \tag{B.3}$$

Making partial derivative of (B.3) respect to $x_1 \sim x_n$ and $\lambda_1 \sim \lambda_n$. The solution of (B.4) is the candidate extreme points of (B.1).

$$\begin{cases} \dfrac{\partial \mathcal{L}(x_1, \cdots, x_n, \lambda_1, \cdots, \lambda_k)}{\partial x_1} = 0 \\ \vdots \\ \dfrac{\partial \mathcal{L}(x_1, \cdots, x_n, \lambda_1, \cdots, \lambda_k)}{\partial x_n} = 0 \\ \dfrac{\partial \mathcal{L}(x_1, \cdots, x_n, \lambda_1, \cdots, \lambda_k)}{\partial \lambda_1} = 0 \\ \vdots \\ \dfrac{\partial \mathcal{L}(x_1, \cdots, x_n, \lambda_1, \cdots, \lambda_k)}{\partial \lambda_k} = 0 \end{cases} \tag{B.4}$$

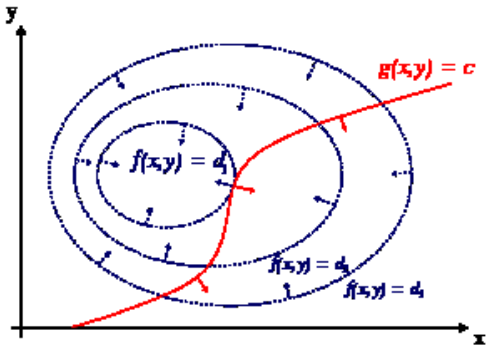

Figure B.1 Simulation result of non-master selection strategy

Here we use a figure to give an intuitive understanding. In Figure B.1, for the case of only one constraint ($g(x, y) = c$) and only two variables (x, y), the red line shows the constraint $g(x, y) = c$. The blue lines are contours of $f(x, y)$. The point where the red line tangentially touches a blue contour is the maximum of $f(x, y)$, since $d_1 > d_2$